



HIGH-ASPECT-RATIO NANO-MATERIALS FOR BIOMEDICAL APPLICATIONS

Hui Li

Master of Medicine

Thesis submitted to obtain the degree of Doctor in Pharmaceutical Sciences

2018

Promoter:

Prof. Dr. Ir. Bruno G. De Geest

Department of Pharmaceutics

Ghent University

The author and the promoter give the authorization to consult and to copy part of this thesis for personal use only. Any other use is limited by the Laws of Copyright, especially concerning the obligation to refer to the source whenever results are cited from this thesis.

Ghent, May 17th, 2018

The Promoter

Prof. Dr. Ir. Bruno G. De Geest

The Author

Hui Li

Acknowledgements

ACKNOWLEDGEMENTS

ACKNOWLEDGEMENTS

After a wonderful period of four and half years, today is the day to write this note of thanks as the beginning of my dissertation. It has been a period of learning for me, not only in the scientific arena, but also on a personal level. On the road to completing my dissertation I received help, words of encouragement and inspiration from many people, and I would like to take this opportunity to sincerely thank them.

Foremost, I would like to express my sincere gratitude to my promoter **Prof. Dr. Ir. Bruno De Geest** for providing me the opportunity to be a PhD student in the laboratory of pharmaceutical technology and continuous support of my Ph.D study and research, for his patience, motivation, enthusiasm, and immense knowledge. His guidance helped me in all the time of research and writing of this thesis. Furthermore, I also would like to thank you for your care and concern in my private life, including giving me some advices for my tooth surgery in 2014, helping to buy my second-handed car and giving enough patience during my pregnancy. THANK YOU!

Following, I would like to thank Prof. Jean Paul Remon and Prof. Chris Vervaeet from Department of Pharmaceutics, and Prof. Thomas De Beer from Department of Pharmaceutical analysis. Thank you for creating such friendly work atmosphere and effective cooperation in both research and life.

My sincere thanks also goes to my fellow labmates I had the privilege to work with, André Antunes, Marijke Dierendonck, Lutz Nuhn, Zhiyue Zhang, Nane Vanparijs, Lien Lybaert, Benoit Louage, Ruben De Coen, Sabah Kasmi, Simon Van Herck, Alexandra Van Driessche, Jana De Vrieze, Annemiek Uvyn and Fien Gysens. I could never have achieved all of this without you. Thanks for the nice atmosphere, the interesting discussions, the sharing of frustrations, the support and all the fun we have had in the last four years. I wish you all the best of luck with your future research carrier and life. I also want to appreciate all my colleagues in the laboratory of Pharmaceutical Technology. Thank you for sharing your life and lab equipments, and helping me. Thanks a lot for all of you to organize the great lab activities like Christmas dinner and team building. I also want to thank my previous and current officemates, Sabah Kasmi, Kaat De Clercq, Glenn Verstraete, Jana De Vrieze. You always create cordial and friendly working atmosphere. Thanks, our wonderful secretaries, Ms. Ilse Dupon and Ms.

ACKNOWLEDGEMENTS

Katharine Wullaert, and our technician, Christine for helping a lot not only on official documents, but also on private issues.

I gratefully acknowledge the Chinese Scholarship Council for my PhD scholarship and Ghent University for BOF co-funding.

Here I thank my friends, we were not only able to support each other by deliberating over our problems and findings, but also happily by talking about things other than just our papers. Without you, I would lose a lot of funny and happy in my life.

I would like to thank my family: my parents and parents-in-law for supporting and loving me spiritually throughout writing this thesis and my life in general. You are always there for me. After being a new mother, I could understand more of your love.

我想要感谢我的家人：我的父母和公公婆婆，一直以来在精神和生活上给与我的支持和关爱。你们永远在我身边。在成为一个新手妈妈之后，我可以更多地了解你们的爱。

I am very grateful to my most important colleague and also my husband **Zhiyue Zhang**, thank you for introducing me to our kind promotor Prof. Dr. Ir. Bruno De Geest, thank you for your support and concern for my research and life, thank you for your love, thank you for sharing a lot of wonderful time with me in the last 12 years, thank you for being you. I also would like to thank our son, Leo Zhang, who brings so much happiness to my life. The happiest thing for me is to accompany with you and watch you growing up day by day.

Finally, I would thank the jury members for examination of the thesis and their insightful comments and encouragement, and also for providing valuable suggestions which incited me to widen my research from various perspectives.

HUI LI

2018, GHENT, BELGIUM

Table of Contents

List of Abbreviations and Symbols.....	1
Aim and Outline of the Thesis.....	7
PART I General Introduction.....	11
PART II Carbon-Derived Multi-Dimensional Nanomaterials.....	53
Chapter 1 The Role of Tannic Acid for Intracellular Protein Delivery by Carbon Nanotubes.....	55
Chapter 2 Spontaneous Protein Adsorption on Graphene Oxide Nanosheets Allows Straightforward Intracellular Vaccine Protein Delivery.....	87
PART III Polymer-Modified Inorganic Nanomaterials --- The Gold NR/PolyHPMA –Glycolamide.....	123
Chapter 3 A Synthetic Transiently Thermoresponsive Homopolymer with UCST Behavior within a Physiologically Relevant Window.....	125
Broader International Context, Relevance and Future Perspectives.....	153
Summary and General Conclusions.....	171
Samenvatting en Algemene Conclusies.....	175
Curriculum Vitae.....	179

TABLE OF CONTENTS

List of Abbreviations and Symbols

Å	angstrom, 10^{-10} metre or 0.1 nanometre
ACN	acetonitrile
AFM	atomic force microscopy
AF488	Alexa Fluor 488
AIBN	2,2'-azobisisobutyronitrile
ATR-FTIR	attenuated total reflection fourier transform infrared spectroscopy
Au	gold
AuNRs	gold nanorods
AuNPs	gold nanoparticles
BCE	before the common era
BSA	bovine serum albumin
C	carbon
C ₆₀	buckyballs
CD	circular dichroism spectrum
CD4 T cells	T helper cells
CD8 T cells	cytolytic T cells
CDI	1,1'-carbonyldiimidazole
CFSE	carboxyfluorescein succinimidyl ester
CNTs	carbon nanotubes
CNTs-COOH	carboxylic acid functionalized carbon nanotubes
CNTs-1	multi-wall CNTs with a length of 1-10 μ m

LIST OF ABBREVIATIONS AND SYMBOLS

CNTs-2	single-wall CNTs with a diameter of 1.5nm and a length of 1-5um
CNTs-3	multi-wall CNTs with a diameter of 9.5 nm and a length of 1.5um
CNT-(OVA-AF488)	CNTs adsorbed with OVA-AF488
CNT-protein	CNTs adsorbed with proteins
CNTs-TA	CNTs which were pretreated by tannic acid
CNTs-sonication	CNTs which were pretreated by ultra-sonication
-COOH	carboxylic acids functional group
CTA	chain transfer agent
CTB-AF555	AlexaFluor555-labeled cholera toxin subunit B
CTAB	cetyl trimethyl ammonium bromide
CTLs	cytotoxic T cells
DC	dendritic cell
DCM	dichloromethane
Demi Water (DI)	deionized water
DLS	dynamic light scattering
DMAc	<i>N,N</i> -dimethylacetamide
DMF	dimethylformamide
DMSO	dimethylsulfoxide
DNA	deoxyribonucleic acid
DP	degree of polymerization
EDC-HCl	<i>N</i> -(3-Dimethylaminopropyl)- <i>N'</i> -ethylcarbodiimide hydrochloride
ESI	electrospray ionization
ESI-MS	electron spray ionization-mass spectroscopy
FA	formic acid
FACS	fluorescent-activated cell sorting
FBS	fetal bovine serum
FCM	flow cytometry
FITC	fluorescein isothiocyanate

LIST OF ABBREVIATIONS AND SYMBOLS

FITC-BSA	albumin–fluorescein isothiocyanate conjugate
FL1-A+	the area under the fluorescence intensity curve by the first channel, FITC channel
g-C3N4	graphitic carbon nitride
GOx	graphene oxide
GOx~OVA	graphene oxide coupling with OVA
H	hydrogen
h	hour
HAuCl ₄	chloroauric acid
h-BN	hexagonal boron nitride
HIV	human immunodeficiency virus
HPLC	high performance liquid chromatography
HPMA	<i>N</i> -(2-hydroxypropyl)methacrylamide
HPMA-CI	<i>N</i> -(2-hydroxypropyl)methacrylamide- carbonylimidazole
HPMA-GA	<i>N</i> -(2-hydroxypropyl)methacrylamide-glycolamide
HSQC	heteronuclear singular quantum correlation
IFN γ	interferon gamma
IL13	interleukin 13
IL17	interleukin 17
K	lysine
LC-MS/MS	liquid chromatography–mass spectrometry / mass spectrometry
LCST	lower critical solution temperature
LEDs	light-emitting diodes
LYS	lysozyme
[M]	monomer
M-GOx	modified graphene oxide
MHCI	major histocompatibility complex class I molecules
MHCII	major histocompatibility complex class II molecules
MIP	maximum intensity projection
MPLA	mouse specific peripheral lymphocyte antigen

LIST OF ABBREVIATIONS AND SYMBOLS

MRI	magnetic resonance imaging
MW-CNTs	multi-wall carbon nanotubes
N ₂	nitrogen
NGO-PEG	PEGylated nano graphene oxide
NIR	near infrared
NMR	nuclear magnetic resonance
NPs	nanoparticles
-OH	hydroxyls functional group
OT-I	OVA-specific T-cell receptor transgenic CD8+ T cells
OVA	ovalbumin
OVA-AF488	AlexaFluor488 conjugated ovalbumin
PAGE	polyacrylamide
PBS	phosphate buffered saline
PEG	polyethylene-glycol
PMMA	polymethylmethacrylate
PSS	poly(4-styrenesulfonic acid) sodium salt
PVP	polyvinyl pyrrolidone
R	arginine
RAFT	reversible addition-fragmentation chain transfer
R-GOx	reduced graphene oxide
RID	refractive index detector
RNA	ribonucleic acid
RT	room temperature
SEC	size exclusion chromatography
SEM	scanning electron microscope
SERS	surface-enhanced raman scattering
SPR	surface plasmon resonance
SW-CNTs	single-wall carbon nanotubes
TA	tannic acid
TEM	transmission electron microscope
TMDs	transition metal dichalcogenides

LIST OF ABBREVIATIONS AND SYMBOLS

UV-Vis	ultraviolet-visible
0D	zero dimensional
1D	one dimensional
2D	two dimensional
3D	three dimensional

Aim and Outline of the Thesis

The overall aim of this thesis is to investigate the potential biomedical applications of multi-dimensional high-aspect ratio nanomaterials.

Part I

General Introduction

In the first part, the thesis provides a general introduction on the importance of materials science to our daily life. Particular attention is devoted to the biomedical applications of high-aspect ratio nanomaterials such as carbon-derived multi-dimensional nanomaterials (fullerene, zero-dimension; carbon nanotubes, one-dimension; graphene and graphene oxide, two-dimension; graphite and diamond, three-dimension) and polymer-modified inorganic metal nanoparticles, i.e. gold nanorods.

Part II

The second part includes two chapters that deal with protein adsorption to high-aspect ratio carbon-derived nanomaterials, including **One-Dimensional Carbon Nanotubes** and **Two-Dimensional Graphene Oxide Nanosheets**.

Part II - chapter 1

In the first chapter, carboxylic acid functionalized carbon nanotubes (CNTs-COOH) from different commercial sources will be evaluated. Ultra-sonication and tannic acid as a low toxicity dispersant will be tested to obtain stable CNT suspension that can further be used for protein adsorption.

Part II - chapter 2

The second chapter aims at the synthesis of water-soluble graphene derivative, i.e. graphene oxide nanosheets (GOx), that combines high-aspect ratio dimensions with hydrophilic functional groups such as hydroxyl and carboxyl groups. These GOx nanosheets will be investigated for their ability to adsorb the model protein antigens. Finally, we will investigate the interaction between antigen-adsorbed GOx nanosheets and dendritic cells *in vitro*.

Part III - chapter 3

Part III of this thesis will investigate another type of high-aspect ratio nanomaterials, i.e. gold nanorods, that can be combined as an external light trigger to generate heat and induce phase transformation of a transiently thermo-responsive polymer. For this purpose, a synthetic bio-degradable polymer with upper critical solution temperature (UCST) behavior will be developed.

In addition to the research chapters, this doctoral dissertation provides a prominent section to discuss the scientific findings in view of the broader international context of the conducted research and the future developments to be expected in this field. Additionally, this thesis will be concluded with a section that summarizes the overall findings.

PART I

General Introduction

Nano-materials

Today, with the steady increase of our material life, from the basic necessities to the study of science and technology, we have become inseparable from materials and materials science. Even for the major historical periods of our society, we assorted them as stone age, bronze age, steel age (the industrial revolution) and polymer age, etc.. As the 21st century unfolds, we are not only striving to understand and modify the world around us but also looking forward to a better understanding, optimizing and application of advanced materials.

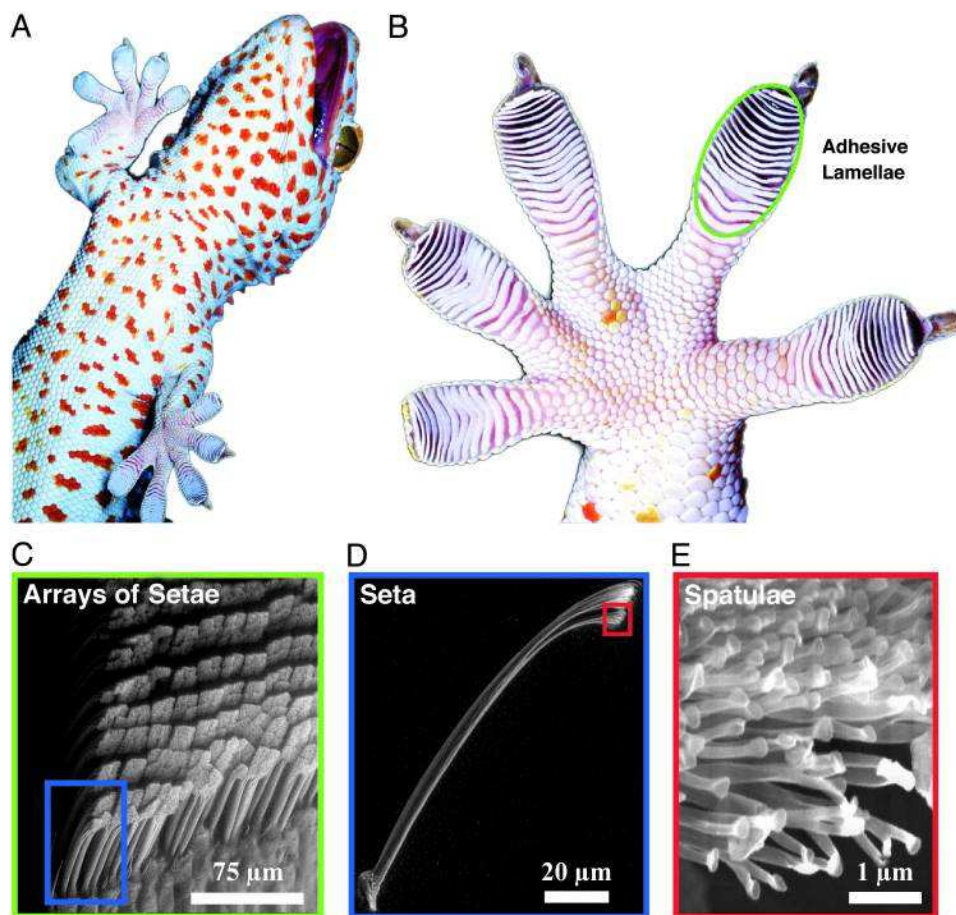


Figure 1. Structural hierarchy of the gecko adhesive system. From macrostructure (A,B) to microstructure (C,D, and E). ^[1]

By suggesting the development of molecular machines, the seminal idea of “nanotechnology” was first proposed by Richard Feynman at the meeting of the American Physical Society in 1959.^[2] The concept of “Nano” was then widespread used in most of the modern sciences. Decreasing the size into the nanoscale or assembling materials at nanoscale lead to a dramatic increase in the surface area, surface roughness and surface area to volume ratios which are important parameters that instigate material bulk properties.^[3] Also in nature, many existing materials are nano-scaled such as cells, bacteria and viruses. Even some seem smooth materials to the naked eye, have intricate structures at the nanoscale, as shown in **Figure 1**.^[1] The term “nanotechnology” was first used in a scientific publication “On the Basic Concept of 'Nano-Technology” authored by Norio Taniguchi in 1974.^[4] Thereafter, in parallel with the emergence of nanotechnology, the research on nanomaterials has also grown exponentially in the fields of materials science, biological and chemical science, biomedicine and drug delivery, etc..

Nanomaterials, in principle can have any shape (e.g. nanoparticles, nanotubes, quantum dots, nanowires, nanofibers or nano-rods) and at least one dimension, including internal structure or surface structure, sized below 1000nm.^[5] Although this field was in its relative infancy decades ago, at present, nanomaterials have already been used in a wide range of products such as sunscreens, composites, catalysts and medical devices.

Comparing to the same material without nanoscale features, nanomaterials are developed to exhibit particular size and shape dependent properties such as unique optical, chemical reactivity, electronic conductivity and mechanical properties which are primary caused by surface and quantum effects.^[6, 7] As nanomaterials are sufficiently small to confine their electrons and produce quantum effects, they often possess unexpected visual properties. For instance, different sizes gold nanoparticles appear deep red to black in solution.^[8, 9] In the meantime, nanomaterials are also considered to be a bridge between bulk materials and atomic or molecular structures.^[10] Today, we can easily synthesize a large amount of pure single composition nanomaterials but the ones that are found in nature are often agglomerated and with various compositions. Depending on the size of the agglomerate which is often occurred between the nanoscale materials, nanoparticles may behave as larger

entities.^[11, 12]

In the past, the general tendency was to consider all nanoparticles as being spherical in shape. However, since the advent of fibre toxicology of asbestos,^[13] high-aspect ratio nanomaterials with a length many times of their width have attracted widespread attention by nanomaterial scientists. These fiber-like nanostructure can induce toxicity by causing lysosomal damage.^[14] As a growth area in nanotechnology, elongated materials with nanometer length scales such as nanorods, nanowires, and nanotubes often result in inherent chemical, electrical, optical and magnetic anisotropy which make them attractive for biomedical applications.^[13, 15, 16]

Given their unique elongated shape, high-aspect ratio nanomaterials could interact with cells and biomolecules in fundamentally new ways.^[17] By introducing multiple targeting units on their surface, one could enable multivalent interactions with receptors to enhance cellular internalization.^[18, 19] Additionally, due to the magnetic anisotropy, high-aspect ratio nanomaterials could be used as improved contrast agents compared to their spherical analogues for the magnetic resonance imaging (MRI) applications.^[20, 21] Both the length as well as aspect ratio of high-aspect ratio nanomaterials play significant roles in their biological reactivity. Zhaoxia Ji and coworkers found that at lengths >200 nm and aspect ratios ≥ 22 , CeO₂ nanorods induced progressive pro-inflammatory effects and cytotoxicity *in vitro*.^[14] In comparison, small nanorods or nanowires diameters (6-10 nm) with relatively low “critical” length and aspect ratio often possess strong van der Waals and dipole-dipole attractions which result in the formation of stacking bundles. The two main synthetic strategies for the preparation of the high-aspect ratio nanomaterials are often classified as direct synthesis and assembly method.^[22-24] For the former route, tuning the reaction conditions or using templates could induced anisotropic growth. While, for the later assembly method, the anisotropy is achieved by assembly from individual building blocks.

However, it is worth to point out that each material has its own advantages and disadvantages. Nanomaterials can offer exceptional new properties while also show signs of toxicity. Due to their small size, smaller than most of the cells and cellular organelles, they are clearly associated with health risks, some happened to be toxic to biological systems, some are relatively benign, while others confer health benefits.^[5, 25-28] However, these toxic

properties of nanoparticles may be beneficial for medical diagnostics and treatment, as they are thereby able to fight disease at the cellular level, and hold potential of altering the interaction between therapeutic molecules and target cells or tissues to destroy cancerous cells. For example, chemical-functionalized fullerene can act as antioxidants^[29, 30]. Carbon nanotubes and gold nanorods, the best known and studied of high-aspect ratio nanomaterials, owing to their fibrous shape with different nano-sized diameters, have the potential for human inhalation exposure.^[14, 31, 32]

Therefore, to limit the adverse health impacts of nanomaterials and drive their safety as well as utility to be better used in our biomedical applications, particular intelligent design and development of nanomaterials are urgently needed. Bearing this in mind, this thesis is focused on the biomedical applications of some high-aspect ratio nanomaterials such as carbon-derived multi-dimensional nanomaterials and polymer-modified inorganic gold-nanorods.

Carbon-Derived Multi-Dimensional Nanomaterials

Carbon, a very common element which comes from the Latin *carbo* for “coal and charcoal”,^[33] is almost present everywhere in our universe such as atmosphere, crust and living organisms. By mass, it is the fourth most abundant element after hydrogen, helium, and oxygen in the universe and the second in our human body (about 18.5%) after oxygen.^[34] Carbon has long been known and used, the earliest human civilizations known of carbon was in the forms of soot and charcoal in prehistory. In 1789, Antoine Lavoisier listed carbon as a chemical element with symbol C in the Periodic table of elements IV A.^[35, 36] This element can form bonds by itself and has the ability to arrange and rearrange its atoms in chains and rings. The different ways carbon atoms arrange leads the different carbon substances.^[37, 38] The use of carbon is almost unlimited for it is capable to be very soft as graphite or very hard as diamond.^[39, 40] Therefore, the utilizing of carbon and its allotropes (the material is made of a pure substance or element with a few differences in atom formation) has grown exponentially in almost all of the industrial and academic fields.^[41-43]

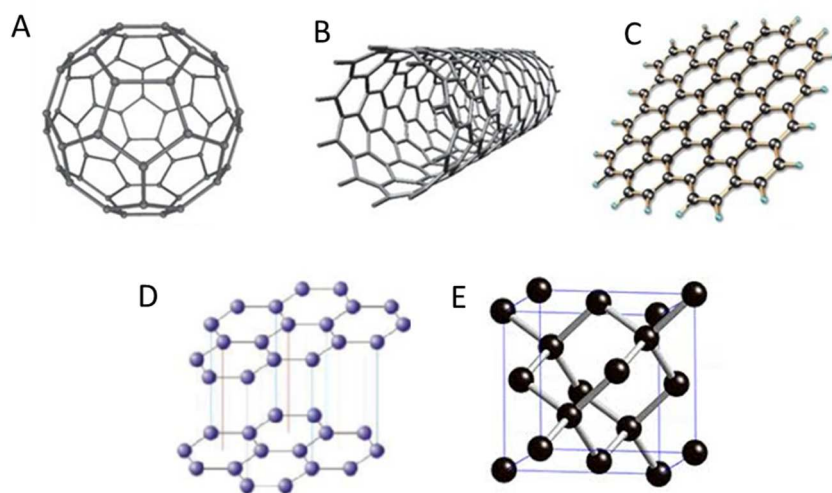


Figure 2. Schematic structures of zero-dimensional material (0D), Fullerene(A); one-dimensional material (1D), Carbon Nanotube(B); two-dimensional material(2D), Graphene (C); and three-dimensional materials(3D), Graphite(D) and Diamond(E).

In the 20th century, a series of exciting carbon-based nanomaterials are arising. Taking the number of their dimensions into account, carbon-derived nanomaterials could be classified, as shown in **Figure 2.**, from zero-dimensional materials (0D) like fullerene to one-dimensional materials (1D) (including carbon nanowires, nanotubes and nanofibers), two-dimensional materials (2D) such as graphene and graphene oxide and three-dimensional materials (3D) which are rich in nanostructures but exceed the nanoscopic size in all of the three dimensions.^[39] Their nano-level size and unique structures result in excellent mechanical strength, electrical and thermal conductivity, and optical properties. All of these advantageous properties have attracted tremendous attention and much of the research efforts have been focused on their utilizing. Additionally, due to their multi-functional nature, carbon-derived nanomaterials are regarded as highly attractive biomaterials for biomedical applications and breakthroughs.

Zero-dimensional (0D) carbon-derived nanomaterials.

Zero-dimension (0D) starts from a point which is viewed as a geometric point. It has no size, no time and no dimension. Materials which are nano-scaled in all three dimensions are considered **zero-dimensional (0D) nanomaterials** including atomic-scale porosity, colloids, and free nanoparticles with various morphologies.

Fullerenes, as their sphere structure, caged molecules and nanometer-scale diameter 0.7 nm, are classified as zero-dimensional (0D) carbon-derived nanomaterials.^[39] The first fullerene molecule C_{60} was discovered by serendipity during laser spectroscopy experiments in 1985^[44] and the discoverers Robert Curl, Harold Kroto and Richard Smalley received the Nobel Prize in Chemistry “for their discovery of fullerenes” in 1996.^[45] These convex polyhedrons are composed of pentagonal and hexagonal surfaces. The discovery of fullerenes greatly expanded the number of known carbon allotropes include hollow sphere, ellipsoid, tube, and many other shapes such as buckyballs (C_{60}) and buckytubes (carbon nanotubes).^[44, 46, 47] Fullerenes have been found not only in nature but also in the outer space.^[48, 49] The smallest fullerene is a regular dodecahedron molecule C_{20} .^[50] In the last two decades, a lot of research groups have contributed to this field to produce fullerenes and their derivatives in a mild and mass yielded method.^[47, 51-56]

Buckyball (C_{60}) and its derivatives, owing to their lower cost and easy purification, are the most common and compelling zero-dimensional (0D) nanomaterials in the field of research and applications.^[59-61] Fullerenes have been the subject of intense research for their unique chemistry and technological applications, especially in materials field, electronics, and nanotechnology.

Fullerenes are chemical stable and sparingly soluble in many solvents such as toluene and chlorobenzene, but not totally unreactive. A chemical reaction to which they are often subjected is electrophilic addition at 6,6-double bonds, which reduces angle strain by changing sp^2 -hybridized carbons (120°) into sp^3 -hybridized ones (109.5°). Some fullerenes (e.g. C_{76} , C_{78} , C_{80} , and C_{84}) are inherently chiral for their D_2 -symmetric and research efforts have been devoted to the development of specific sensors for enantiomers.^[57, 58]

Haddon and coworkers found that alkali-doped C_{60} exhibit superconductivity.^[59] For example, in 1991, the potassium-doped C_{60} superconducting behavior at 18K was the highest molecular superconducting temperature to be found. Since then, a large amount of metal-doped fullerene superconductors have been identified. The superconducting conversion temperature will rise with the increase of the unit cell volume of alkali-doped fullerenes.

Fullerenes have also been extensively used for biomedical applications such as the design of high-performance MRI and X-Ray imaging contrast agents, photodynamic therapy, drug and gene delivery.^[60] Although cancer radiotherapy has been used for many years in the clinic,^[61-65] photodynamic therapy is gaining increase popularity.

The solubility of fullerenes can be increased by functionalization with L-phenylalanine, folic acid, and L-arginine.^[62, 63] When internalized by cancer cells and exposed to light radiation, C_{60} -derivatives can transform molecular oxygen into reactive oxygen which could trigger apoptosis of these cancer cells and minimize the damage to surrounding tissues. Once the light radiation treatment is finished, the fullerenes will reabsorb the free radicals to prevent damage of other tissues.^[65]

One-dimensional (1D) carbon-derived nanomaterials.

One-dimension (1D) space is like a line between two points which only has length but no width or depth. **One-dimensional (1D) nanomaterials** are materials with two dimensions in the nanometer scale, including nanowires, nanotubes, nanobelts and nanorods which have a high-aspect ratio and large surface area.^[66]

Carbon nanotubes (CNTs) are cylindrical fullerenes, a new more deliberately fabricated "one-dimensional" type of crystalline carbon nanoparticles that can be envisioned as rolled graphene.^[67] The first important discovery of carbon nanotubes (CNTs) which brought them into the awareness of the scientific community was in 1991 by Iijima.^[68] Since then, CNTs represent a new class of technological nanomaterial with innovative and unique electrical, optical and mechanical properties including their large surface areas and superior bundle strength^[69-71] which make them suitable for many applications in biomedicine and pharmacology. To date, CNTs are still one of the most powerful one-dimensional nanomaterials in the world. In the meantime, CNTs possess a broad field of applications, including energy conversion, quantum nanowires, catalyst supports, etc..

Depending on the number of graphene layers, CNTs are classified as single-wall carbon nanotubes (SW-CNTs)^[72-76] and multi-wall carbon nanotubes (MW-CNTs).^[68, 77, 78] Additionally, based on the morphology, there are also some other types of CNTs such as end-closed and end-opened carbon nanotubes, carbon nanobuds, carbon peapod, graphenated carbon nanotubes and extreme carbon nanotubes which could improve the composite's mechanical or chemical properties.^[79-86]

As be envisioned as rolled graphene, CNT) could have different properties by the different rolling angles and curvatures.^[87, 88] But unlike graphene being semimetal, CNTs are either semiconducting or metallic along the tubular axis.^[89] CNT are only few nanometers wide, but in length can range from micrometers to millimeters. Measured for their tensile strength and elastic modulus, CNT are the strongest and stiffest materials,^[90-92] but by Young's modulus, they are in fact very soft in the radial direction.^[93-95] CNTs are good thermal conductors along the tube but insulators lateral to the tube axis. Additionally, the quality of CNTs can be

changed by numerous synthesis parameters intentionally or unintentionally which could be characterized by their absorption, photoluminescence (fluorescence), and Raman spectroscopy properties. Related to the typical nanomaterials, all of the properties of CNTs are anisotropic (directionally dependent) and tunable which are favorable for various applications.

CNTs can be functionalized to equip them with specific properties. Covalent reactions and non-covalent coating are the two main methods for CNTs functionalization.^[77, 96-102] CNTs are hydrophobic and trend to agglomerate and sediment in water due to strong Van der Waals interaction forces along their length axis.^[90, 91, 96, 103-105] The bundles or aggregates of CNTs can reduce the final composite's mechanical performance. Also the CNT surface can be modified to reduce the hydrophobicity and improve interfacial adhesion. ^[106, 107]

The quality of CNT can be quickly and non-destructively characterized by its special absorption, photoluminescence (fluorescence), and Raman spectroscopy properties.^[108-110] Furthermore, based on the CNT anisotropic (directionally dependent) and tunable properties, they are potentially useful in optics and photonics, especially for light-emitting diodes (LEDs)^[111, 112] and photo-detectors.^[113] Their narrow selectivity in the wavelength of emission and detection of light have already been used in bolometer and optoelectronic memory devices.^[114, 115] Compared to copper which is well known for its good thermal conductivity (transmits $385 \text{ W}\cdot\text{m}^{-1}\cdot\text{K}^{-1}$), CNTs have a higher room-temperature thermal conductivity along its axis (transmits $3500 \text{ W}\cdot\text{m}^{-1}\cdot\text{K}^{-1}$).^[116]

Thanks to the high surface area^[17, 87, 103, 117] and rich electronic poly-aromatic structure, CNTs are able to adsorb or conjugate to a wide variety of therapeutic and diagnostic agents (drugs, genes, DNA, enzymes, vaccines, antibodies, biosensors, etc.).^[97, 118-121] Furthermore, they have been explored as a vehicle for drug delivery by directly penetrating the cells membrane or even nuclear membrane,^[122-124] and keeping the drug intact during transport. Compared to traditional methods, agents linked to CNTs can be delivered more safely into cells which open a new way for drug formulation.^[67, 125]

The state-of-art progress on the potential applications of CNT have excited the interest of scientists in fields of pharmacy and medicine, not only for drug and gene therapies^[126, 127] but also for immunotherapy, tissue regeneration, catalyst supports, enantiomer separation of chiral drugs and diagnosis of different ailments.^[67, 128-130]

By the high Van der Waals interaction forces along the length axis, CNTs are hydrophobic and trend to agglomerate and sediment in water.^[125, 131] Therefore, CNTs must be functionalized (covalent reactions and non-covalent coating by amphiphilic molecules) to afford water solubility and biocompatibility in view of biomedical applications. Addition of dispersants such as sodium dodecyl sulfate (SDS), Triton X-100 and polyvinyl pyrrolidone (PVP)^[127, 132] could help to stabilize CNTs suspensions but if the excess of stabilizing molecules are removed these carbon nanotubes will aggregate and deposit. The ideal CNT for biomedical applications should have high water solubility, good biocompatibility, stable nanotube structure and functional groups for further bio-conjugations.^[77] Given their unique structural features and outstanding properties, in the near future, CNTs will find broad applicability in a wide variety of disciplines both for industry and academic.

Two-dimensional (2D) carbon-derived nanomaterials.

If we draw a rectangle on paper, the inside of this rectangle will look like a two-dimensional (2D) space. The objects in two-dimensional space have a width and a length, but no depth.

Two-dimensional (2D) nanomaterials have only one dimension in the nano-scale such as ultrathin 2D nano-films and surface coatings. The lateral size of these sheet-like structures is larger than 100 nm while the thickness is only single- or few-atoms thick, so called monolayers. In the past decade, given their unique structural features, the research area of ultrathin 2D nanomaterials has led to an emerging class of nanomaterials and has grown exponentially in the fields of condensed matter physics, material science, chemistry, and nanotechnology.

Graphene and Graphene oxide (GOx)

As one of the most famous ultrathin two-dimensional (2D) carbon-derived nanomaterials in the 21st century, **graphene**,^[39, 133] a two-dimensional single layer of carbon atoms like hexagonal lattice, is named by Hanns-Peter Boehm as a combination of "graphite" and the suffix 'ene' in 1962.^[134, 135] It was originally observed on metal surfaces by electron microscopy. Graphene was discovered by Andre Geim and Konstantin Novoselov in 2004 at the University of Manchester^[136] and awarded the 2010 Nobel Prize in Physics.^[137, 138]

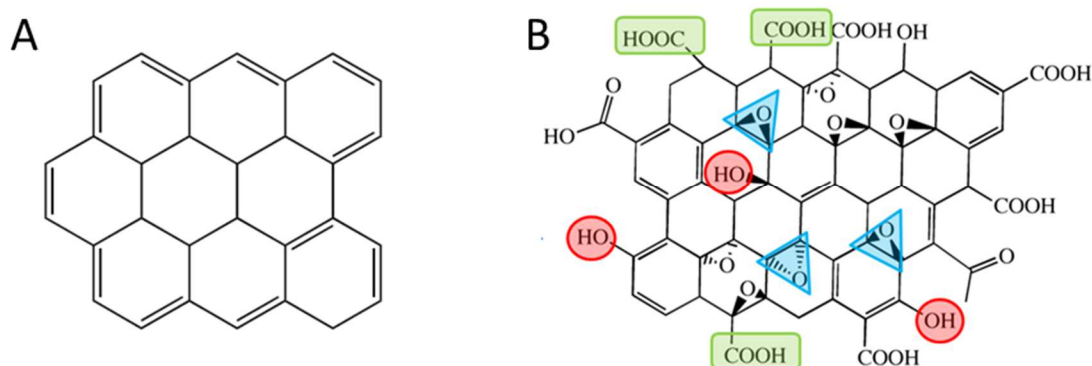


Figure 3. Schematic structures of Graphene (A) and Graphene oxide (B).

Graphene can be considered as a flat "infinite alternant" polycyclic aromatic hydrocarbon composed of six-member carbon rings. Due to its tightly packed carbon atoms and the sp^2 orbital hybridization, graphene has several exciting chemical and mechanical properties.^[139-142] For example, it is a semi-metallic or zero-gap semi-conductor.^[143] Although the theoretical thickness of graphene is only 0.335 nm and it is nearly transparent to visible light, it is about 200 times stronger than the strongest steel.^[144, 145] Furthermore, graphene can be modified with oxygen- and nitrogen-containing functional groups.

The research into its applications includes solar cells, light-emitting diodes (LED), the touch sensor in touch panels and smart windows or phones.^[146, 147] In addition, graphene and modified graphene have also been applied in the biomedical field as they could pierce the cell membranes via sharp and jagged points.^[148] Meanwhile, the shape, size, purity and the dose of administration or exposure times of graphene determines its toxicity.^[149, 150]

Moving on from the graphene, its oxidation derivative, the water-soluble graphene derivative **graphene oxide (GOx)**^[151-153] has also been explored for a wide range of potential applications. **Figure 3.** shows the schematic structures of graphene and graphene oxide.

Graphene oxide (GOx) is the single-layer form of graphite oxide which was first prepared by Oxford chemist Benjamin C. Brodie in 1859.^[154] And then in 1957, the famous Hummers' method, a much safer, quicker, and more efficient process was developed by Hummers and Offeman.^[151] Graphite powder was reacted with the strong oxidizing agents potassium permanganate ($KMnO_4$), concentrated sulfuric acid (H_2SO_4) and sodium nitrate ($NaNO_3$). Exactly, "oxide" is an incorrect but historically established name. GOx is known for its particularly high-aspect ratio and surface area which is almost 10-fold of other nanomaterials and favorable for various applications. This planar structure, with a 2D atomic layer composed of crumpled sheets of sp^2 - and sp^3 - hybridized carbon atoms,^[155-158] is enriched with epoxides, hydroxyls (-OH) and carboxylic acids (-COOH) functional groups.^[159-162] The thickness of GOx layers are about 1.1 ± 0.2 nm but the detailed structures are still unclear due to the strong disorder and irregular packing of the layers.^[163, 164]

Owing to all of the aforementioned unique structures and functional groups, GOx is hydrophilic.^[165] It can be easily dispersed in water and other organic solvents, and it is a good surfactant material to stabilize various emulsion systems. Once removing most of the functional oxygen groups, the reduced graphene oxide (R-GOx) is tended to aggregate and more difficult to disperse.^[166, 167]

For a long time, graphite oxide, i.e. multilayered GOx, has attracted much interest as a possible route for the large-scale production and manipulation of graphene at a low cost. Being hydrophilic, graphite oxide can be easily dispersed in water, breaking up into macroscopic flakes, mostly one layer thick GOx. The reported interlayer distance in dried state of graphite oxide is about 6-7 Å while in water it increases to about 11-13 Å at room temperature. However, it is difficult to mass produce graphene sheets with the same quality by mechanical exfoliation.^[168] Different qualities of the precursor, GOx, and different chemical reductions may lead to graphene sheets of different qualities.^[169-173] In the future, if this issue could be overcome, we can expect a much more widely used of graphene in medical, commercial and industrial applications.

The first reports on biomedical applications of graphene and GOx as nanocarrier for drug delivery have emerged in 2008 by Dai and co-workers.^[174] They functionalized GOx nanosheets with branched polyethylene-glycol (PEG) to obtain a biocompatible GOx-PEG conjugate which is stable in various biological solutions and could be used for attaching hydrophobic aromatic molecules. Since then, a lot of work has been carried out to explore the use of graphene and GOx in the biomedical field, from drug/gene delivery, antibacterial materials, biological sensing and imaging to cancer therapy, and biocompatible scaffolds for cell culture.^[175-178] For example, GOx with a size of a few hundreds of nanometers in the planar direction, can destabilize the membrane of bacteria^[122, 123, 148] which could render GOx an attractive nano-carrier for intracellular delivery of therapeutic molecules.^[179, 180] Utilizing the intrinsic near-infrared (NIR) optical absorbance, the GOx can be applied photothermally for antitumor treatment.^[181, 182]

In addition, the theoretical load of GOx is up to 200%, for both sides of it have aromatic structures and oxygen-containing functional groups that can be used for covalent and non-

covalent modification by van der Waals force, π - π conjugation, hydrophobic effects, hydrogen bonding and electrostatic interaction.^[155-157]

GOx can be fundamentally changed by functionalization and used for multiple applications.^[153, 183, 184] For example, introduction of amines could increase its dispersibility in organic solvents. GOx nanosheets can spontaneously adsorb proteins by a combination of interactions without the requirement of additional reagents.^[165] After that, the GOx nanosheets adsorbed proteins could efficiently destabilize the lipid membranes and be internalized by dendritic cells then promote antigen cross-presentation to CD8 T cells^[122, 148, 165] which is a hallmark in the induction of potent cellular antigen-specific immune responses against intracellular pathogens and cancer.

Without a doubt, the current research on two-dimensional (2D) nanomaterials has prompted several exciting developments, but most still remain to be explored in more depth and far from the criteria which are required for industry or commercialization, especially those beyond Graphene and Graphene oxide(GOx) such as Hexagonal Boron Nitride(h-BN),^[185-187] Graphitic Carbon Nitride(g-C₃N₄)^[188] and Transition Metal Dichalcogenides(TMDs)^[189, 190].

Three-dimensional (3D) carbon-derived nanomaterials.

The space which we all live in, with length, width and height, is the three-dimensional (3D) space. In another word, bending the two-dimensional space, we could get a three-dimensional space.

Owing to the different array of carbon in each matter, carbon could produce the softest material (**Graphite**) and the hardest substance (**Diamond**).

Graphite is an allotrope of carbon aside from diamond and amorphous carbon which means it is one of carbon's pure forms with its atoms arranged in big sheets of hexagonal rings.^[191, 192] This block form of graphene, has a layered, planar structure and can be easily broken down.^[191] Under standard conditions, graphite is the most stable form of crystalline of carbon.

Diamond, is one of the highest hardness and oldest materials found on earth.^[193, 194] The natural diamond is irregular in shape and its formation requires very specific conditions like high temperature (900 to 1,300 °C), high pressure (45 to 60 kilo bars) and at depths of 140 to 190 kilometers in the Earth's mantle.^[195] Because of the strength and directionality of sp³ hybrid carbon bonding, diamond is the hardest natural substance so to speak.^[196, 197] The element carbon arranged in a tetrahedral crystalline fashion, each carbon atom is surrounding with four neighboring carbon atoms with strong covalent bonding between them which is a fancy way of describing the state of covalent bonding in carbon.^[198, 199]

Polymer Modified Inorganic Metal Nanomaterials

--- The gold nanorods with Poly(HPMA-Glycolamide)

Gold (with symbol Au in the periodic table), is one of the most inert chemical elements and a transition metal element.^[200] To date, gold is still a popular noble metal^[201, 202] and precious material used for money, jewelry^[203, 204] and arts,^[205-207] due to its relatively scarce, unique color and corrosion resistance.^[208, 209] Given all of the aforementioned unique properties, gold has mainly been utilized as corrosion-resistant electronic connectors in all types of electronic equipment.^[210] Additionally, it is also developed to shield infrared, produce colored glass and gold foil.^[211] In medicine, gold is often used to repair teeth, and some gold salts can be exploited as anti-inflammatory agent.^[212-215] The properties of colloidal gold, i.e. suspensions of gold nanoparticles (1 to 100 nm), strongly depend on both nanoparticles size and shape.^[216] High-aspect ratio (length divided by width) gold nanoparticles, in particular **gold nanorods (AuNRs)**, are attractive for a range of biomedical applications, due to their modular functionality and anisotropic structural, optical, electronic, magnetic and catalytic properties.^[217-221]

Fabrication of AuNPs is dated back to 1857 by Faraday while the synthesis of colloidal AuNRs emerged only during the past decade.^[222, 223] Several strategies for AuNR synthesis have been reported and comprise both bottom-up and top-down approaches.^[229, 254-256] To date, the one-step seedless method and the seed-mediated growth method are two of the most simple and reproducible bottom-up techniques.

In the one-step seedless method, sodium borate is directly added to the growth solution in the presence of ascorbic acid, cetyltrimethyl ammonium bromide (CTAB) as surfactant and silver ions to initiate particle nucleation and growth.^[224] Changing the amount of sodium borate or adjusting the reaction temperature can control the aspect ratio of the obtained nanorods. In the meantime, the seed-mediated growth method is originated in 2001 by Jana

et al.^[221] AuNRs were prepared by the addition of citrate-capped small gold nanospheres to a bulk HAuCl_2 growth solution which was obtained by the reduction of HAuCl_4 with ascorbic acid in the presence of CTAB as surfactant and ions.^[225] The introducing of silver ions (lower reduction potential than gold) to the growth solution could help ascorbic acid to reduce gold ions into metallic gold as a catalyst for the reduction reaction. Furthermore, a three-step procedure in the absence of silver nitrate was proposed by the same group for the synthesis of AuNRs with an aspect ratio of 25.^[221, 225-227] In this typical procedure, first-stage AuNRs were used as seeds for second growth, and sequentially be used as seeds for the next growth. Finally, simple centrifugation can be used to stop the overgrowth and remove the free CTAB.

With slight modifications in the preparation conditions (eg. carefully control of the solutions temperature, stirring speed, ratio of seed to metal salt, etc...), the aspect ratio of the AuNRs can be tuned. In the growth solution, the amount of ascorbic acid mainly influences how many gold ions will be reduced, and the number of seeds determine how to divide the intrinsic growth rate in width and length.

Alongside, CTAB can promote the growth of gold seeds in one dimension to produce rods and provide their surface with a positive surface charge which prevents the aggregation in water via electrostatic repulsion.^[228-230] Due to the affinity of thiols for gold, CTAB can also be ion-exchanged with other sulfur-containing compounds. The growth at the ends of AuNRs can be further tuned by changing the amount of silver nitrate or the reaction temperature. Silver ions do not directly influence rod length or width.^[231] However, freshly prepared silver nitrate and ascorbic acid solutions are also important for good yield and high shape purity mono-dispersity of AuNRs.^[232]

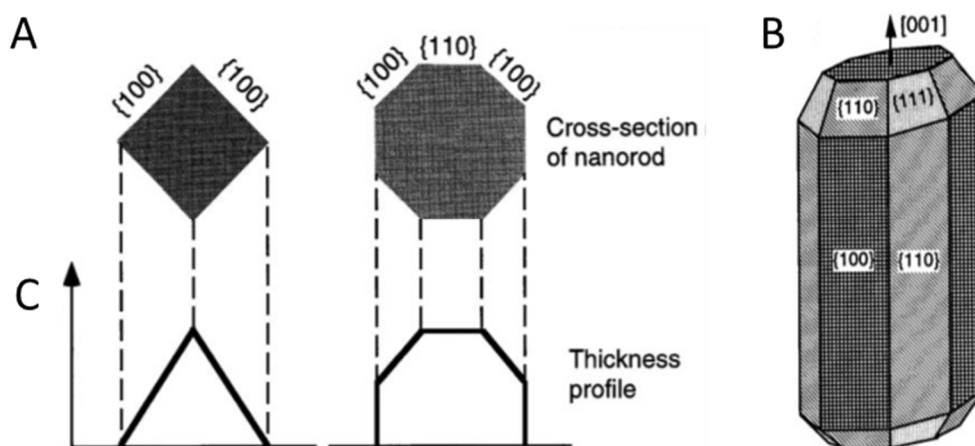


Figure 4. Schematic structures of AuNRs. (A, B) Two possible cross-sections of the AuNRs and the corresponding profiles of crystal thickness variation across the rods. (C) A structural model of AuNRs. Reproduced from ref. ^[233]

As shown in **Figure 4.**, prismatic-structured gold nanoparticles could have (111), (100) and (110) facets. The different growth rates of different faces and the different facets' combination will form different shapes of nanocrystals. Short AuNRs are dominated by (110) and (100) facets, long AuNRs are dominated by (110) and (111) facets, and spherical gold nanoparticles with equivalent mass to the short rods are dominated by (100) and (111) facets with shapes of truncated octahedra, icosahedra and decahedra. Furthermore, the unique (110) facets of AuNRs are expected to have particular surface properties.^[233]

Due to their exceptional radiative and nonradiative properties, the strong plasmonic properties of AuNRs and their tunability have prompted their application in the biomedical field (such as biosensing, biomedical imaging, gene and drug delivery, disease detection, diagnosis, and therapy).^[9, 200, 234] To date, surface plasmon resonance (SPR) is the most appealing optical feature of metallic nanoparticles which consists of a collective oscillation of the conduction electrons.^[235-237] In addition, the SPR in gold nanoparticles enhances locally the light electric field several orders of magnitude. For spherical gold nanoparticles, their SPRs lead to a light absorption in the visible range of the spectrum (~ 525 nm) which overlaps with

some biological tissues and molecules such as hemoglobin in the bloodstream. Since the optical spectrum is directly correlated to the aspect ratio of the particles, the above-mentioned limitation can be overcome by the synthesis of non-spherical AuNRs which possess two SPR bands. One associated with their cross-section, falls approximately in the same area of spherical nanoparticles, and the other with the excited longitudinal rod axis, shifts its perpendicular SPR to higher wavelengths (i.e. 750-1200 nm) into the near-infrared region (NIR) where biological tissues and blood scarcely absorb.^[238]

Given that, standard UV–vis–NIR spectroscopy can easily monitor the formation of different aspect ratios AuNRs in solution. As the absorbance band changes with the refractive index of local material, AuNRs are considered excellent candidates for biological sensing and allow for extremely accurate sensing.^[7] For example, the red-shift in the spectrum has been used to detect antigen by antibody functionalized AuNRs.^[239, 240]

AuNRs are electron dense and can be directly visualized by transmission electron microscopy (TEM) without the need of staining.^[224, 241-244] The photothermal properties of AuNRs can be used to either directly kill cancer cells upon illumination or promote the release of therapeutic agents.^[242, 245, 246] To prevent desorption and reduce toxicity, the surface of CTAB-coated AuNRs can be modified by replacing or covering with biocompatible compounds. For example, a thiolated DNA can be used to ‘displace’ the CTAB bilayer to form DNA-modified AuNRs.^[247] In addition, the CTAB bilayer can also be replaced first by a nonionic surfactant, and then exchanged with a cationic phospholipids. RNA can then further be associated to AuNRs through electrostatic complexation.^[248]

AuNRs can also be coated with a thermo-sensitive shell, for example based on poly (N-isopropylacrylamide)^[224, 249] that exhibits lower critical solution temperature (LCST)^[250-253] or upper critical solution temperature (UCST) behaviour^[254, 255]. Irradiating these gold nanorods with NIR light can generate heat and induce a phase transition to release the entrapped drug molecules. Meanwhile, the generated heat can also increase the efficacy of the released drug.

REFERENCES

1. Hansen, W.R. and K. Autumn, *Evidence for self-cleaning in gecko setae*. Proceedings of the National Academy of Sciences of the United States of America, 2005. **102**(2): p. 385-389.
2. Feynman, R.P., (*The transcript of a talk in 1959 at the annual meeting of the American Physical Society (APS)*). IEEE J. Microelectromech. Syst., 1992. **1**.
3. Zhang, L. and T.J. Webster, *Nanotechnology and nanomaterials: promises for improved tissue regeneration*. Nano today, 2009. **4**(1): p. 66-80.
4. Taniguchi, N. *On the basic concept of nano-technology*. in *Proc. Intl. Conf. Prod. London, 1974*. 1974. British Society of Precision Engineering.
5. Buzea, C., I.I. Pacheco, and K. Robbie, *Nanomaterials and nanoparticles: Sources and toxicity*. Biointerphases, 2007. **2**(4): p. MR17-MR71.
6. Jain, P.K., et al., *Noble metals on the nanoscale: optical and photothermal properties and some applications in imaging, sensing, biology, and medicine*. Accounts of chemical research, 2008. **41**(12): p. 1578-1586.
7. Ray, P.C., *Size and shape dependent second order nonlinear optical properties of nanomaterials and their application in biological and chemical sensing*. Chemical reviews, 2010. **110**(9): p. 5332-5365.
8. Chithrani, B.D., A.A. Ghazani, and W.C. Chan, *Determining the size and shape dependence of gold nanoparticle uptake into mammalian cells*. Nano lett, 2006. **6**(4): p. 662-668.
9. Jain, P.K., et al., *Calculated absorption and scattering properties of gold nanoparticles of different size, shape, and composition: applications in biological imaging and biomedicine*. J. Phys. Chem. B, 2006. **110**(14): p. 7238-7248.
10. Raffaini, G. and F. Ganazzoli, *Understanding the performance of biomaterials through molecular modeling: crossing the bridge between their intrinsic properties and the surface adsorption of proteins*. Macromolecular bioscience, 2007. **7**(5): p. 552-566.
11. Nel, A., et al., *Toxic potential of materials at the nanolevel*. science, 2006. **311**(5761): p. 622-627.
12. Limbach, L.K., et al., *Oxide nanoparticle uptake in human lung fibroblasts: effects of particle size, agglomeration, and diffusion at low concentrations*. Environmental science & technology, 2005. **39**(23): p. 9370-9376.

13. Oberdörster, G., V. Stone, and K. Donaldson, *Toxicology of nanoparticles: a historical perspective*. *Nanotoxicology*, 2007. **1**(1): p. 2-25.
14. Ji, Z., et al., *Designed synthesis of CeO₂ nanorods and nanowires for studying toxicological effects of high aspect ratio nanomaterials*. *ACS nano*, 2012. **6**(6): p. 5366-5380.
15. Meng, H., et al., *Aspect ratio determines the quantity of mesoporous silica nanoparticle uptake by a small GTPase-dependent macropinocytosis mechanism*. *ACS nano*, 2011. **5**(6): p. 4434-4447.
16. Poland, C.A., et al., *Carbon nanotubes introduced into the abdominal cavity of mice show asbestos-like pathogenicity in a pilot study*. *Nature nanotechnology*, 2008. **3**(7): p. 423-428.
17. Bauer, L.A., N.S. Birenbaum, and G.J. Meyer, *Biological applications of high aspect ratio nanoparticles*. *Journal of Materials Chemistry*, 2004. **14**(4): p. 517-526.
18. Chou, L.Y., K. Ming, and W.C. Chan, *Strategies for the intracellular delivery of nanoparticles*. *Chemical Society Reviews*, 2011. **40**(1): p. 233-245.
19. Wang, J., et al., *The complex role of multivalency in nanoparticles targeting the transferrin receptor for cancer therapies*. *Journal of the American Chemical Society*, 2010. **132**(32): p. 11306-11313.
20. Jun, Y.-w., J.-w. Seo, and J. Cheon, *Nanoscaling laws of magnetic nanoparticles and their applicabilities in biomedical sciences*. *Accounts of chemical research*, 2008. **41**(2): p. 179-189.
21. Laurent, S., et al., *Magnetic iron oxide nanoparticles: synthesis, stabilization, vectorization, physicochemical characterizations, and biological applications*. *Chemical reviews*, 2008. **108**(6): p. 2064-2110.
22. Wu, H.-Y., W.-L. Huang, and M.H. Huang, *Direct high-yield synthesis of high aspect ratio gold nanorods*. *Crystal Growth & Design*, 2007. **7**(4): p. 831-835.
23. Lazzari, M., et al., *Self-assembly: a minimalist route to the fabrication of nanomaterials*. *Journal of nanoscience and nanotechnology*, 2006. **6**(4): p. 892-905.
24. Treguer-Delapierre, M., et al., *Synthesis of non-spherical gold nanoparticles*. *Gold Bull*, 2008. **41**(2): p. 195-207.
25. Howard, J., *Current intelligence bulletin 65: occupational exposure to carbon nanotubes and nanofibers*. DHHS (NIOSH) Publication, 2013(2013-145).

26. Hodson, L., M. Methner, and R.D. Zumwalde, *Approaches to safe nanotechnology; managing the health and safety concerns associated with engineered nanomaterials*. 2009.
 27. Schaefer, S., *Let's Stop Worrying and Learn to Love Transparency: Food and Technology in the Information Age*. *J. Food L. & Pol'y*, 2014. **10**: p. 233.
 28. Turkevich, L.A., et al., *Potential explosion hazard of carbonaceous nanoparticles: screening of allotropes*. *Combustion and flame*, 2016. **167**: p. 218-227.
 29. Constantin, C., et al., *Fullerene–porphyrin nanostructures in photodynamic therapy*. *Nanomedicine*, 2010. **5**(2): p. 307-317.
 30. Wang, Z., et al., *Syntheses, structures and antioxidant activities of fullerenols: knowledge learned at the atomistic level*. *Journal of Cluster Science*, 2015. **26**(2): p. 375-388.
 31. Donaldson, K., et al., *Identifying the pulmonary hazard of high aspect ratio nanoparticles to enable their safety-by-design*. *Nanomedicine*, 2011. **6**(1): p. 143-156.
 32. Sharifi, S., et al., *Toxicity of nanomaterials*. *Chemical Society Reviews*, 2012. **41**(6): p. 2323-2343.
 33. Dictionary, O.E., *Oxford English Dictionary*. 2003, JSTOR.
 34. Reece, J.B., et al., *Campbell biology*. 2013: Pearson Higher Ed.
 35. Wieser, M.E., et al., *Atomic weights of the elements 2011 (IUPAC Technical Report)*. *Pure and Applied Chemistry*, 2013. **85**(5): p. 1047-1078.
 36. Meija, J., et al., *Atomic weights of the elements 2013 (IUPAC Technical Report)*. *Pure and Applied Chemistry*, 2016. **88**(3): p. 265-291.
 37. Demming, A., *King of the elements?* *Nanotechnology*, 2010. **21**(30): p. 300201.
 38. Irifune, T., et al., *Materials: Ultrahard polycrystalline diamond from graphite*. *Nature*, 2003. **421**(6923): p. 599-600.
 39. Mostofizadeh, A., et al., *Synthesis, properties, and applications of low-dimensional carbon-related nanomaterials*. *Journal of nanomaterials*, 2011. **2011**: p. 16.
 40. Itzhaki, L., et al., *Harder than Diamond: Determining the Cross-Sectional Area and Young's Modulus of Molecular Rods*. *Angewandte Chemie International Edition*, 2005. **44**(45): p. 7432-7435.
-

41. Cantwell, W. and J. Morton, *The impact resistance of composite materials—a review*. composites, 1991. **22**(5): p. 347-362.
42. Coelho, R., et al., *The application of polycrystalline diamond (PCD) tool materials when drilling and reaming aluminium based alloys including MMC*. International Journal of Machine Tools and Manufacture, 1995. **35**(5): p. 761-774.
43. Harris, D.C., *Materials for infrared windows and domes: properties and performance*. Vol. 70. 1999: SPIE press.
44. Kroto, H., JR Heath. SC O'Brien. RF Curl. and RE Smalley. *Astrophys. J*, 1987. **314**: p. 352-355.
45. Curl, R., H.W. Kroto, and R.E. Smalley, *Nobel prize in chemistry for 1996*. South African Journal of Chemistry-Suid-Afrikaanse Tydskrif Vir Chemie, 1997. **50**: p. 102-5.
46. Krätschmer, W., K. Fostiropoulos, and D.R. Huffman, *The infrared and ultraviolet absorption spectra of laboratory-produced carbon dust: evidence for the presence of the C₆₀ molecule*. Chemical Physics Letters, 1990. **170**(2-3): p. 167-170.
47. Alekseyev, N. and G. Dyuzhev, *Fullerene formation in an arc discharge*. Carbon, 2003. **41**(7): p. 1343-1348.
48. Cami, J., et al., *Detection of C₆₀ and C₇₀ in a young planetary nebula*. Science, 2010. **329**(5996): p. 1180-1182.
49. Atkinson, N., *Buckyballs Could Be Plentiful in the Universe*. Universe Today. <http://www.universetoday.com/76732/buckyballs-could-be-plentiful-in-the-universe>. Retrieved, 2010: p. 10-28.
50. Bankehsaz, M., *Investigating mechanical and physical properties of nanostructures*. 2010: Rice University.
51. Howard, J.B., et al., *Fullerenes C₆₀ and C₇₀ in flames*. Nature, 1991. **352**(6331): p. 139-141.
52. Howard, J.B., et al., *Fullerenes synthesis in combustion*. Carbon, 1992. **30**(8): p. 1183-1201.
53. Xie, S.-y., et al., *Microwave synthesis of fullerenes from chloroform*. Applied physics letters, 1999. **75**(18): p. 2764-2766.
54. Taylor, R., et al., *Formation of C₆₀ by pyrolysis of naphthalene*. Nature, 1993. **366**(6457): p. 728-731.

55. Richter, H., et al., *Fullerene formation in acetylene/oxygen/argon/chlorine flames*. Carbon, 1996. **34**(6): p. 797-803.
 56. Scott, L.T., *Methods for the chemical synthesis of fullerenes*. Angewandte Chemie International Edition, 2004. **43**(38): p. 4994-5007.
 57. BUSECK, P., S. TSIPURSKY, and R. Hettich, *Fullerenes from the geological environment*. Science, 1992. **257**(5067): p. 215-217.
 58. Prato, M., *[60] Fullerene chemistry for materials science applications*. Journal of Materials Chemistry, 1997. **7**(7): p. 1097-1109.
 59. Duclos, S., et al., *Raman studies of alkali-metal doped AxC60 films (A= Na, K, Rb, and Cs; x= 0, 3, and 6)*. Science, 1991. **254**(5038): p. 1625-1627.
 60. LALWANI, G. and B. SITHARAMAN, *Multifunctional fullerene-and metallofullerene-based nanobiomaterials*. Nano Life, 2013. **3**(03): p. 1342003.
 61. Brown, S.B., E.A. Brown, and I. Walker, *The present and future role of photodynamic therapy in cancer treatment*. The lancet oncology, 2004. **5**(8): p. 497-508.
 62. Mroz, P., et al., *Functionalized fullerenes mediate photodynamic killing of cancer cells: Type I versus Type II photochemical mechanism*. Free Radical Biology and Medicine, 2007. **43**(5): p. 711-719.
 63. Ganapathy, V., M. Thangaraju, and P.D. Prasad, *Nutrient transporters in cancer: relevance to Warburg hypothesis and beyond*. Pharmacology & therapeutics, 2009. **121**(1): p. 29-40.
 64. Hu, Z., et al., *Photodynamic anticancer activities of water-soluble C 60 derivatives and their biological consequences in a HeLa cell line*. Chemico-biological interactions, 2012. **195**(1): p. 86-94.
 65. Markovic, Z. and V. Trajkovic, *Biomedical potential of the reactive oxygen species generation and quenching by fullerenes (C 60)*. Biomaterials, 2008. **29**(26): p. 3561-3573.
 66. Kuchibhatla, S.V., et al., *One dimensional nanostructured materials*. Progress in materials science, 2007. **52**(5): p. 699-913.
 67. He, H., et al., *Carbon nanotubes: applications in pharmacy and medicine*. BioMed research international, 2013. **2013**.
 68. Iijima, S., *Helical microtubules of graphitic carbon*. nature, 1991. **354**(6348): p. 56-58.
-

69. Jia, W., B. Tang, and P. Wu, *Novel Composite PEM with Long-Range Ionic Nanochannels Induced by Carbon Nanotube/Graphene Oxide Nanoribbon Composites*. ACS applied materials & interfaces, 2016. **8**(42): p. 28955-28963.
70. Lambin, P., et al., *Atomic structure and electronic properties of a bent carbon nanotube*. Synthetic metals, 1996. **77**(1-3): p. 249-252.
71. Bera, B., *A Review on Polymer, Graphene and Carbon Nanotube: Properties, Synthesis and Applications*. Imperial Journal of Interdisciplinary Research, 2017. **3**(10).
72. Ziegler, K.J., et al., *Controlled oxidative cutting of single-walled carbon nanotubes*. Journal of the American Chemical Society, 2005. **127**(5): p. 1541-1547.
73. Wong, E.W., P.E. Sheehan, and C.M. Lieber, *Nanobeam mechanics: elasticity, strength, and toughness of nanorods and nanotubes*. science, 1997. **277**(5334): p. 1971-1975.
74. Dekker, C., et al., *Individual single-wall carbon nanotubes as quantum wires*. Nature 386 (6624), 474-477.(1997), 1997.
75. Iijima, S. and T. Ichihashi, *Single-shell carbon nanotubes of 1-nm diameter*. nature, 1993. **363**(6430): p. 603-605.
76. Bethune, D., et al., *Cobalt-catalysed growth of carbon nanotubes with single-atomic-layer walls*. Nature, 1993. **363**(6430): p. 605-607.
77. Liu, Z., et al., *Preparation of carbon nanotube bioconjugates for biomedical applications*. Nature protocols, 2009. **4**(9): p. 1372-1381.
78. Ebbesen, T. and P. Ajayan, *Large-scale synthesis of carbon nanotubes*. Nature, 1992. **358**(6383): p. 358220a0.
79. Smith, B.W., M. Monthieux, and D.E. Luzzi, *Encapsulated C60 in carbon nanotubes*. Nature, 1998. **396**: p. 323-324.
80. Smith, B.W. and D.E. Luzzi, *Formation mechanism of fullerene peapods and coaxial tubes: a path to large scale synthesis*. Chemical Physics Letters, 2000. **321**(1): p. 169-174.
81. Su, H., W.A. Goddard III, and Y. Zhao, *Dynamic friction force in a carbon peapod oscillator*. Nanotechnology, 2006. **17**(22): p. 5691.
82. Wang, M. and C.M. Li, *An oscillator in a carbon peapod controllable by an external electric field: A molecular dynamics study*. Nanotechnology, 2009. **21**(3): p. 035704.
83. Liu, L., et al., *Colossal paramagnetic moments in metallic carbon nanotubes*. Physical review letters, 2002. **88**(21): p. 217206.

84. Huhtala, M., A. Kuronen, and K. Kaski, *Carbon nanotube structures: molecular dynamics simulation at realistic limit*. Computer Physics Communications, 2002. **146**(1): p. 30-37.
 85. Parker, C.B., et al., *Three-dimensional arrays of graphenated carbon nanotubes*. Journal of Materials Research, 2012. **27**(7): p. 1046-1053.
 86. Liu, Q., et al., *Semiconducting properties of cup-stacked carbon nanotubes*. Carbon, 2009. **47**(3): p. 731-736.
 87. Wang, X., et al., *Fabrication of ultralong and electrically uniform single-walled carbon nanotubes on clean substrates*. Nano letters, 2009. **9**(9): p. 3137-3141.
 88. Zhang, R., et al., *Growth of half-meter long carbon nanotubes based on Schulz–Flory distribution*. Acs Nano, 2013. **7**(7): p. 6156-6161.
 89. Lu, X. and Z. Chen, *Curved pi-conjugation, aromaticity, and the related chemistry of small fullerenes*. Chemical Reviews, 2005. **105**(10): p. 3643-3696.
 90. Yu, M.-F., et al., *Strength and breaking mechanism of multiwalled carbon nanotubes under tensile load*. Science, 2000. **287**(5453): p. 637-640.
 91. Peng, B., et al., *Measurements of near-ultimate strength for multiwalled carbon nanotubes and irradiation-induced crosslinking improvements*. Nature nanotechnology, 2008. **3**(10): p. 626-631.
 92. Collins, P.G. and P. Avouris, *Nanotubes for Electronics—Scientific American*. 2000, December.
 93. Yakobson, B.I. and P. Avouris, *Mechanical properties of carbon nanotubes*, in *Carbon nanotubes*. 2001, Springer. p. 287-327.
 94. Gupta, S., K. Dharamvir, and V. Jindal, *Elastic moduli of single-walled carbon nanotubes and their ropes*. Physical Review B, 2005. **72**(16): p. 165428.
 95. Pampaloni, F. and E.-L. Florin, *Microtubule architecture: inspiration for novel carbon nanotube-based biomimetic materials*. Trends in biotechnology, 2008. **26**(6): p. 302-310.
 96. Boyer, P.D., et al., *Delivering Single-Walled Carbon Nanotubes to the Nucleus Using Engineered Nuclear Protein Domains*. ACS applied materials & interfaces, 2016. **8**(5): p. 3524-3534.
 97. Cheng, J., et al., *Reversible accumulation of PEGylated single-walled carbon nanotubes in the mammalian nucleus*. ACS nano, 2008. **2**(10): p. 2085-2094.
-

98. Battigelli, A., et al., *Endowing carbon nanotubes with biological and biomedical properties by chemical modifications*. *Advanced drug delivery reviews*, 2013. **65**(15): p. 1899-1920.
 99. Pantarotto, D., et al., *Translocation of bioactive peptides across cell membranes by carbon nanotubes*. *Chemical Communications*, 2004(1): p. 16-17.
 100. Britz, D.A. and A.N. Khlobystov, *Noncovalent interactions of molecules with single walled carbon nanotubes*. *Chemical Society Reviews*, 2006. **35**(7): p. 637-659.
 101. Adeli, M., et al., *Carbon nanotubes in cancer therapy: a more precise look at the role of carbon nanotube-polymer interactions*. *Chemical Society Reviews*, 2013. **42**(12): p. 5231-5256.
 102. Karajanagi, S.S., et al., *Protein-assisted solubilization of single-walled carbon nanotubes*. *Langmuir*, 2006. **22**(4): p. 1392-1395.
 103. Jensen, K., et al., *Buckling and kinking force measurements on individual multiwalled carbon nanotubes*. *Physical Review B*, 2007. **76**(19): p. 195436.
 104. Filleter, T., et al., *Ultra-high strength and stiffness in cross-linked hierarchical carbon nanotube bundles*. *Advanced Materials*, 2011. **23**(25): p. 2855-2860.
 105. Kaiser, J.-P., et al., *Single walled carbon nanotubes (SWCNT) affect cell physiology and cell architecture*. *Journal of Materials Science: Materials in Medicine*, 2008. **19**(4): p. 1523-1527.
 106. Mu, Q., D.L. Broughton, and B. Yan, *Endosomal leakage and nuclear translocation of multiwalled carbon nanotubes: developing a model for cell uptake*. *Nano letters*, 2009. **9**(12): p. 4370-4375.
 107. Li, X., et al., *Carboxyl-modified single-walled carbon nanotubes selectively induce human telomeric i-motif formation*. *Proceedings of the National Academy of Sciences*, 2006. **103**(52): p. 19658-19663.
 108. Fantini, C., et al., *Optical transition energies for carbon nanotubes from resonant Raman spectroscopy: Environment and temperature effects*. *Physical review letters*, 2004. **93**(14): p. 147406.
 109. Iakoubovskii, K., et al., *IR-extended photoluminescence mapping of single-wall and double-wall carbon nanotubes*. *The Journal of Physical Chemistry B*, 2006. **110**(35): p. 17420-17424.
 110. Miyauchi, Y., M. Oba, and S. Maruyama, *Cross-polarized optical absorption of single-walled nanotubes by polarized photoluminescence excitation spectroscopy*. *Physical Review B*, 2006. **74**(20): p. 205440.
-

111. Misewich, J., et al., *Electrically induced optical emission from a carbon nanotube FET*. Science, 2003. **300**(5620): p. 783-786.
112. Chen, J., et al., *Bright infrared emission from electrically induced excitons in carbon nanotubes*. Science, 2005. **310**(5751): p. 1171-1174.
113. Freitag, M., et al., *Photoconductivity of single carbon nanotubes*. Nano letters, 2003. **3**(8): p. 1067-1071.
114. Itkis, M.E., et al., *Bolometric infrared photoresponse of suspended single-walled carbon nanotube films*. Science, 2006. **312**(5772): p. 413-416.
115. Star, A., et al., *Nanotube optoelectronic memory devices*. Nano Letters, 2004. **4**(9): p. 1587-1591.
116. Pop, E., et al., *Thermal conductance of an individual single-wall carbon nanotube above room temperature*. Nano letters, 2006. **6**(1): p. 96-100.
117. Zhu, L., et al., *Growth and electrical characterization of high-aspect-ratio carbon nanotube arrays*. Carbon, 2006. **44**(2): p. 253-258.
118. Kam, N.W.S., et al., *Carbon nanotubes as multifunctional biological transporters and near-infrared agents for selective cancer cell destruction*. Proceedings of the National Academy of Sciences of the United States of America, 2005. **102**(33): p. 11600-11605.
119. Shi Kam, N.W., et al., *Nanotube molecular transporters: internalization of carbon nanotube–protein conjugates into mammalian cells*. Journal of the American Chemical Society, 2004. **126**(22): p. 6850-6851.
120. Kam, N.W.S., Z. Liu, and H. Dai, *Carbon nanotubes as intracellular transporters for proteins and DNA: an investigation of the uptake mechanism and pathway*. Angewandte Chemie, 2006. **118**(4): p. 591-595.
121. Liu, Z., et al., *siRNA delivery into human T cells and primary cells with carbon-nanotube transporters*. Angewandte Chemie International Edition, 2007. **46**(12): p. 2023-2027.
122. Akhavan, O. and E. Ghaderi, *Toxicity of graphene and graphene oxide nanowalls against bacteria*. ACS nano, 2010. **4**(10): p. 5731-5736.
123. Pantarotto, D., et al., *Functionalized carbon nanotubes for plasmid DNA gene delivery*. Angewandte Chemie, 2004. **116**(39): p. 5354-5358.
124. Zhu, W., et al., *Nanomechanical mechanism for lipid bilayer damage induced by carbon nanotubes confined in intracellular vesicles*. Proceedings of the National Academy of Sciences, 2016. **113**(44): p. 12374-12379.

125. Wang, L., et al., *Enhanced dispersibility and cellular transmembrane capability of single-wall carbon nanotubes by polycyclic organic compounds as chaperon*. *Nanoscale*, 2012. **4**(13): p. 3983-3989.
 126. Alshehri, R., et al., *Carbon Nanotubes in Biomedical Applications: Factors, Mechanisms, and Remedies of Toxicity: Miniperspective*. *Journal of medicinal chemistry*, 2016. **59**(18): p. 8149-8167.
 127. Ge, C., et al., *Binding of blood proteins to carbon nanotubes reduces cytotoxicity*. *Proceedings of the National Academy of Sciences*, 2011. **108**(41): p. 16968-16973.
 128. Wang, C., et al., *Immunological Responses Triggered by Photothermal Therapy with Carbon Nanotubes in Combination with Anti-CTLA-4 Therapy to Inhibit Cancer Metastasis*. *Advanced Materials*, 2014. **26**(48): p. 8154-8162.
 129. Mulvey, J.J., et al., *Self-assembly of carbon nanotubes and antibodies on tumours for targeted amplified delivery*. *Nature nanotechnology*, 2013. **8**(10): p. 763-771.
 130. Georgakilas, V., et al., *Amino acid functionalisation of water soluble carbon nanotubes*. *Chemical Communications*, 2002(24): p. 3050-3051.
 131. Thess, A., et al., *Crystalline ropes of metallic carbon nanotubes*. *Science*, 1996: p. 483-487.
 132. Hilding, J., et al., *Dispersion of carbon nanotubes in liquids*. *Journal of dispersion science and technology*, 2003. **24**(1): p. 1-41.
 133. Geim, A.K., *Graphene: status and prospects*. *science*, 2009. **324**(5934): p. 1530-1534.
 134. Boehm, H.-P., et al., *Das adsorptionsverhalten sehr dünner kohlenstoff-folien*. *Zeitschrift für anorganische und allgemeine Chemie*, 1962. **316**(3-4): p. 119-127.
 135. Boehm, H.P., R. Setton, and E. Stumpp, *Nomenclature and terminology of graphite intercalation compounds (IUPAC Recommendations 1994)*. *Pure and Applied Chemistry*, 1994. **66**(9): p. 1893-1901.
 136. Novoselov, K.S., et al., *Electric field effect in atomically thin carbon films*. *science*, 2004. **306**(5696): p. 666-669.
 137. Cao, Z. and H.G. Cao, *Unified field theory*. *American Journal of Modern Physics*, 2013. **2**(6): p. 292-298.
 138. Geim, A. and K. Novoselov, *For groundbreaking experiments regarding the two-dimensional material graphene*. *The Nobel Prize in Physics*, 2010.
-

139. Cooper, D., et al., *Experimental Review of Graphene. ISRN Condensed Matter Physics, 2012, Article ID: 501686.* 2012.
140. Carlsson, J.M., *Graphene: buckle or break.* Nature materials, 2007. **6**(11): p. 801-802.
141. Fasolino, A., J. Los, and M.I. Katsnelson, *Intrinsic ripples in graphene.* Nature materials, 2007. **6**(11): p. 858-861.
142. Bolmatov, D. and C.-Y. Mou, *Graphene-based modulation-doped superlattice structures.* Journal of Experimental and Theoretical Physics, 2011. **112**(1): p. 102-107.
143. Majidi, R. and K. Ghafoori Tabrizi, *Electronic properties of defect-free and defective bilayer graphene in an electric field.* Fullerenes, Nanotubes, and Carbon Nanostructures, 2011. **19**(6): p. 532-539.
144. Jussila, H., et al., *Surface plasmon resonance for characterization of large-area atomic-layer graphene film.* Optica, 2016. **3**(2): p. 151-158.
145. Ni, Z., et al., *Raman spectroscopy and imaging of graphene.* Nano Research, 2008. **1**(4): p. 273-291.
146. Akinwande, D., et al., *Large-Area Graphene Electrodes: Using CVD to facilitate applications in commercial touchscreens, flexible nanoelectronics, and neural interfaces.* IEEE Nanotechnology Magazine, 2015. **9**(3): p. 6-14.
147. Zhong, M., et al., *Interface coupling in graphene/fluorographene heterostructure for high-performance graphene/silicon solar cells.* Nano Energy, 2016. **28**: p. 12-18.
148. Tu, Y., et al., *Destructive extraction of phospholipids from Escherichia coli membranes by graphene nanosheets.* Nature nanotechnology, 2013. **8**(8): p. 594-601.
149. Lalwani, G., et al., *Toxicology of graphene-based nanomaterials.* Advanced drug delivery reviews, 2016. **105**: p. 109-144.
150. Talukdar, Y., et al., *The effects of graphene nanostructures on mesenchymal stem cells.* Biomaterials, 2014. **35**(18): p. 4863-4877.
151. Humers, W. and R. Offeman, *Preparation of graphitic oxide [J].* J Am Chem Soc, 1958. **80**(6): p. 1339.
152. Kim, H.W., et al., *Selective gas transport through few-layered graphene and graphene oxide membranes.* Science, 2013. **342**(6154): p. 91-95.
153. Zhu, Y., et al., *Graphene and graphene oxide: synthesis, properties, and applications.* Advanced materials, 2010. **22**(35): p. 3906-3924.

154. Brodie, B.C., *On the atomic weight of graphite*. Philosophical Transactions of the Royal Society of London, 1859. **149**: p. 249-259.
155. Kim, F., L.J. Cote, and J. Huang, *Graphene Oxide: Surface Activity and Two-Dimensional Assembly*. Advanced Materials, 2010. **22**(17): p. 1954-1958.
156. Mkhoyan, K.A., et al., *Atomic and electronic structure of graphene-oxide*. Nano letters, 2009. **9**(3): p. 1058-1063.
157. Hirata, M., et al., *Thin-film particles of graphite oxide 1:: High-yield synthesis and flexibility of the particles*. Carbon, 2004. **42**(14): p. 2929-2937.
158. Liu, Z.-B., et al., *Ultrafast dynamics and nonlinear optical responses from sp²-and sp³-hybridized domains in graphene oxide*. The Journal of Physical Chemistry Letters, 2011. **2**(16): p. 1972-1977.
159. Nakajima, T., A. Mabuchi, and R. Hagiwara, *A new structure model of graphite oxide*. Carbon, 1988. **26**(3): p. 357-361.
160. Dreyer, D.R., et al., *The chemistry of graphene oxide*. Chemical Society Reviews, 2010. **39**(1): p. 228-240.
161. Titelman, G., et al., *Characteristics and microstructure of aqueous colloidal dispersions of graphite oxide*. Carbon, 2005. **43**(3): p. 641-649.
162. Sydlik, S.A., et al., *In vivo compatibility of graphene oxide with differing oxidation states*. ACS nano, 2015. **9**(4): p. 3866-3874.
163. Schniepp, H.C., et al., *Functionalized single graphene sheets derived from splitting graphite oxide*. The Journal of Physical Chemistry B, 2006. **110**(17): p. 8535-8539.
164. Pandey, D., R. Reifengerger, and R. Piner, *Scanning probe microscopy study of exfoliated oxidized graphene sheets*. Surface Science, 2008. **602**(9): p. 1607-1613.
165. Li, H., et al., *Spontaneous protein adsorption on graphene oxide nanosheets allowing efficient intracellular vaccine protein delivery*. ACS applied materials & interfaces, 2016. **8**(2): p. 1147-1155.
166. Tkachev, S., et al., *Reduced graphene oxide*. Inorganic Materials, 2012. **48**(8): p. 796-802.
167. Compton, O.C. and S.T. Nguyen, *Graphene oxide, highly reduced graphene oxide, and graphene: versatile building blocks for carbon-based materials*. small, 2010. **6**(6): p. 711-723.

168. Boehm, H.-P., A. Clauss, and U. Hofmann, *Graphite oxide and its membrane properties*. Journal de Chimie Physique, 1961. **58**: p. 141-147.
169. Eda, G., et al., *Partially oxidized graphene as a precursor to graphene*. Journal of Materials Chemistry, 2011. **21**(30): p. 11217-11223.
170. Eigler, S., et al., *Wet chemical synthesis of graphene*. Advanced materials, 2013. **25**(26): p. 3583-3587.
171. Kumar, H.V., S.J. Woltornist, and D.H. Adamson, *Fractionation and characterization of graphene oxide by oxidation extent through emulsion stabilization*. Carbon, 2016. **98**: p. 491-495.
172. Gómez-Navarro, C., et al., *Electronic transport properties of individual chemically reduced graphene oxide sheets*. Nano letters, 2007. **7**(11): p. 3499-3503.
173. Eigler, S., et al., *Graphene oxide: efficiency of reducing agents*. Chemical Communications, 2013. **49**(67): p. 7391-7393.
174. Sun, X., et al., *Nano-graphene oxide for cellular imaging and drug delivery*. Nano research, 2008. **1**(3): p. 203-212.
175. Ogino, I., et al., *Exfoliation of graphite oxide in water without sonication: bridging length scales from nanosheets to macroscopic materials*. Chemistry of Materials, 2014. **26**(10): p. 3334-3339.
176. Ou, J., et al., *Self-assembly of octadecyltrichlorosilane on graphene oxide and the tribological performances of the resultant film*. The Journal of Physical Chemistry C, 2011. **115**(20): p. 10080-10086.
177. Wang, Y., et al., *Graphene and graphene oxide: biofunctionalization and applications in biotechnology*. Trends in biotechnology, 2011. **29**(5): p. 205-212.
178. Yoon, H.J., et al., *Sensitive capture of circulating tumour cells by functionalized graphene oxide nanosheets*. Nature nanotechnology, 2013. **8**(10): p. 735-741.
179. Hu, W., et al., *Graphene-based antibacterial paper*. ACS nano, 2010. **4**(7): p. 4317-4323.
180. Liu, S., et al., *Antibacterial activity of graphite, graphite oxide, graphene oxide, and reduced graphene oxide: membrane and oxidative stress*. ACS nano, 2011. **5**(9): p. 6971-6980.
181. Kim, H., et al., *Photothermally triggered cytosolic drug delivery via endosome disruption using a functionalized reduced graphene oxide*. ACS nano, 2013. **7**(8): p. 6735-6746.

182. Loh, K.P., et al., *Graphene oxide as a chemically tunable platform for optical applications*. Nature chemistry, 2010. **2**(12): p. 1015-1024.
183. Ma, J., et al., *Preparation, characterization and antibacterial properties of silver-modified graphene oxide*. Journal of Materials Chemistry, 2011. **21**(10): p. 3350-3352.
184. Singh, S.K., et al., *Amine-modified graphene: thrombo-protective safer alternative to graphene oxide for biomedical applications*. ACS nano, 2012. **6**(3): p. 2731-2740.
185. Watanabe, K., T. Taniguchi, and H. Kanda, *Direct-bandgap properties and evidence for ultraviolet lasing of hexagonal boron nitride single crystal*. Nature materials, 2004. **3**(6): p. 404-409.
186. Giovannetti, G., et al., *Substrate-induced band gap in graphene on hexagonal boron nitride: Ab initio density functional calculations*. Physical Review B, 2007. **76**(7): p. 073103.
187. Song, L., et al., *Large scale growth and characterization of atomic hexagonal boron nitride layers*. Nano letters, 2010. **10**(8): p. 3209-3215.
188. Cao, S., et al., *Polymeric photocatalysts based on graphitic carbon nitride*. Advanced Materials, 2015. **27**(13): p. 2150-2176.
189. Wang, Q.H., et al., *Electronics and optoelectronics of two-dimensional transition metal dichalcogenides*. Nature nanotechnology, 2012. **7**(11): p. 699-712.
190. Wilson, J. and A. Yoffe, *The transition metal dichalcogenides discussion and interpretation of the observed optical, electrical and structural properties*. Advances in Physics, 1969. **18**(73): p. 193-335.
191. Delhaes, P., *Graphite and precursors*. Vol. 1. 2000: CRC Press.
192. Lipson, H. and A. Stokes, *A new structure of carbon*. Nature, 1942. **149**(3777): p. 328-328.
193. Hershey, J.W., *The book of diamonds: their curious lore, properties, tests and synthetic manufacture*. 1940: Hearthsides Press.
194. Molčanov, K. and V. Stilinović, *Chemical Crystallography before X-ray Diffraction*. Angewandte Chemie International Edition, 2014. **53**(3): p. 638-652.
195. Carlson, R.W., *The Mantle and Core: Treatise on Geochemistry*. Vol. 2. 2005: Elsevier.
196. Wei, L., et al., *Thermal conductivity of isotopically modified single crystal diamond*. Physical Review Letters, 1993. **70**(24): p. 3764.
-

197. John, P., et al., *The oxidation of (100) textured diamond*. Diamond and related materials, 2002. **11**(3): p. 861-866.
198. Moore, M. and A. Lang, *On the internal structure of natural diamonds of cubic habit*. Philosophical Magazine, 1972. **26**(6): p. 1313-1325.
199. Kamiya, Y. and A. Lang, *On the structure of coated diamonds*. Philosophical Magazine, 1965. **11**(110): p. 347-356.
200. Daniel, M.-C. and D. Astruc, *Gold nanoparticles: assembly, supramolecular chemistry, quantum-size-related properties, and applications toward biology, catalysis, and nanotechnology*. Chemical reviews, 2004. **104**(1): p. 293-346.
201. Johnson, P.B. and R.-W. Christy, *Optical constants of the noble metals*. Physical review B, 1972. **6**(12): p. 4370.
202. Hammer, B. and J. Norskov, *Why gold is the noblest of all the metals*. Nature, 1995. **376**(6537): p. 238-240.
203. Cretu, C. and E. Van Der Lingen, *Coloured gold alloys*. Gold Bulletin, 1999. **32**(4): p. 115-126.
204. Brill, M. and K.-H. Wiedemann, *Determination of gold in gold jewellery alloys by ICP spectrometry*. Gold Bulletin, 1992. **25**(1): p. 13-26.
205. Rothbard, M.N., *Man, economy, and state*. 2009: Ludwig von Mises Institute.
206. Seltman, C.T., *Athens, its history and coinage before the Persian invasion*. 1924: CUP Archive.
207. Nagarajan, N., *Development of Artificial Gold from Copper Based Alloy*.
208. Polk, P., *The Crystal Guide: Identification, Purpose and Values*. 2016: " F+ W Media, Inc."
209. Schmidbaur, H., et al., *Understanding gold chemistry through relativity*. Chemical physics, 2005. **311**(1): p. 151-161.
210. Webster, M., *definitions-gold report a problem*.
211. Mallan, L., *Suiting up for space: the evolution of the space suit*. 1971: John Day Co.
212. Kean, W. and I. Kean, *Clinical pharmacology of gold*. Inflammopharmacology, 2008. **16**(3): p. 112-125.
213. Moir, D.M., *Outlines of the ancient history of medicine*. 1831: William Blackwood.
-

214. Mortier, T., *An experimental study on the preparation of gold nanoparticles and their properties*. 2006.
215. Richards, D.G., et al., *Gold and its relationship to neurological/glandular conditions*. International journal of neuroscience, 2002. **112**(1): p. 31-53.
216. Zeng, S., et al., *A review on functionalized gold nanoparticles for biosensing applications*. Plasmonics, 2011. **6**(3): p. 491.
217. Faulk, W.P. and G.M. Taylor, *Communication to the editors: an immunocolloid method for the electron microscope*. Immunochemistry, 1971. **8**(11): p. 1081-1083.
218. Roth, J., M. Bendayan, and L. Orci, *FITC-protein A-gold complex for light and electron microscopic immunocytochemistry*. Journal of Histochemistry & Cytochemistry, 1980. **28**(1): p. 55-57.
219. Bozzola, J.J. and L.D. Russell, *Electron microscopy: principles and techniques for biologists*. 1999: Jones & Bartlett Learning.
220. Hainfeld, J.F., et al., *Radiotherapy enhancement with gold nanoparticles*. Journal of Pharmacy and Pharmacology, 2008. **60**(8): p. 977-985.
221. Jana, N.R., L. Gearheart, and C.J. Murphy, *Wet chemical synthesis of high aspect ratio cylindrical gold nanorods*. The Journal of Physical Chemistry B, 2001. **105**(19): p. 4065-4067.
222. Dykman, L. and N. Khlebtsov, *Gold nanoparticles in biomedical applications: recent advances and perspectives*. Chemical Society Reviews, 2012. **41**(6): p. 2256-2282.
223. Faraday, M., *The Bakerian lecture: experimental relations of gold (and other metals) to light*. Philosophical Transactions of the Royal Society of London, 1857. **147**: p. 145-181.
224. Alkilany, A.M., et al., *Gold nanorods: Their potential for photothermal therapeutics and drug delivery, tempered by the complexity of their biological interactions*. Advanced Drug Delivery Reviews, 2012. **64**(2): p. 190-199.
225. Huang, X., S. Neretina, and M.A. El-Sayed, *Gold nanorods: from synthesis and properties to biological and biomedical applications*. Advanced Materials, 2009. **21**(48): p. 4880-4910.
226. Busbee, B.D., S.O. Obare, and C.J. Murphy, *An Improved Synthesis of High-Aspect-Ratio Gold Nanorods*. Advanced Materials, 2003. **15**(5): p. 414-416.
227. Gole, A. and C.J. Murphy, *Seed-mediated synthesis of gold nanorods: role of the size and nature of the seed*. Chemistry of Materials, 2004. **16**(19): p. 3633-3640.
-

228. Liu, M. and P. Guyot-Sionnest, *Mechanism of silver (I)-assisted growth of gold nanorods and bipyramids*. The Journal of Physical Chemistry B, 2005. **109**(47): p. 22192-22200.
229. Jana, N.R., L. Gearheart, and C.J. Murphy, *Seed-mediated growth approach for shape-controlled synthesis of spheroidal and rod-like gold nanoparticles using a surfactant template*. Advanced Materials, 2001. **13**(18): p. 1389.
230. Orendorff, C.J. and C.J. Murphy, *Quantitation of metal content in the silver-assisted growth of gold nanorods*. The Journal of Physical Chemistry B, 2006. **110**(9): p. 3990-3994.
231. Gou, L. and C.J. Murphy, *Fine-tuning the shape of gold nanorods*. Chemistry of materials, 2005. **17**(14): p. 3668-3672.
232. Abdelmoti, L.G. and F.P. Zamborini, *Potential-controlled electrochemical seed-mediated growth of gold nanorods directly on electrode surfaces*. Langmuir, 2010. **26**(16): p. 13511-13521.
233. Wang, Z., et al., *Crystallographic facets and shapes of gold nanorods of different aspect ratios*. Surface science, 1999. **440**(1): p. L809-L814.
234. Dreaden, E.C., et al., *The golden age: gold nanoparticles for biomedicine*. Chemical Society Reviews, 2012. **41**(7): p. 2740-2779.
235. Nikoobakht, B., J. Wang, and M.A. El-Sayed, *Surface-enhanced Raman scattering of molecules adsorbed on gold nanorods: off-surface plasmon resonance condition*. Chemical Physics Letters, 2002. **366**(1): p. 17-23.
236. Nikoobakht, B. and M.A. El-Sayed, *Preparation and growth mechanism of gold nanorods (NRs) using seed-mediated growth method*. Chem. Mater, 2003. **15**(10): p. 1957-1962.
237. Zijlstra, P., P.M. Paulo, and M. Orrit, *Optical detection of single non-absorbing molecules using the surface plasmon resonance of a gold nanorod*. Nature nanotechnology, 2012. **7**(6): p. 379-382.
238. García, M., V. Bouzas, and N. Carmona. *Synthesis of Gold Nanorods for Biomedical Applications*. in *AIP Conference Proceedings*. 2010. AIP.
239. Pérez-Juste, J., et al., *Gold nanorods: synthesis, characterization and applications*. Coordination Chemistry Reviews, 2005. **249**(17): p. 1870-1901.
240. Chen, H., et al., *Shape-and size-dependent refractive index sensitivity of gold nanoparticles*. Langmuir, 2008. **24**(10): p. 5233-5237.
-

241. Huang, X., et al., *Cancer cell imaging and photothermal therapy in the near-infrared region by using gold nanorods*. Journal of the American Chemical Society, 2006. **128**(6): p. 2115-2120.
242. Alkilany, A.M., et al., *Cellular uptake and cytotoxicity of gold nanorods: molecular origin of cytotoxicity and surface effects*. small, 2009. **5**(6): p. 701-708.
243. Hauck, T.S., A.A. Ghazani, and W.C. Chan, *Assessing the effect of surface chemistry on gold nanorod uptake, toxicity, and gene expression in mammalian cells*. Small, 2008. **4**(1): p. 153-159.
244. Takahashi, H., et al., *Surface modification of gold nanorods using layer-by-layer technique for cellular uptake*. Journal of Nanoparticle Research, 2008. **10**(1): p. 221-228.
245. Huang, X.H., et al., *Plasmonic photothermal therapy (PPTT) using gold nanoparticles*. Lasers in Medical Science, 2008. **23**(3): p. 217-228.
246. Pissuwan, D., et al., *Targeted destruction of murine macrophage cells with bioconjugated gold nanorods*. Journal of Nanoparticle Research, 2007. **9**(6): p. 1109-1124.
247. Wijaya, A., et al., *Selective release of multiple DNA oligonucleotides from gold nanorods*. ACS nano, 2008. **3**(1): p. 80-86.
248. Lee, S.E., et al., *Biologically functional cationic phospholipid– gold nanoplasmonic carriers of RNA*. Journal of the American Chemical Society, 2009. **131**(39): p. 14066-14074.
249. Shi, S., et al., *Thermo-, pH-, and light-responsive poly (N-isopropylacrylamide-co-methacrylic acid)–Au hybrid microgels prepared by the in situ reduction method based on Au-thiol chemistry*. The journal of physical chemistry B, 2014. **118**(25): p. 7177-7186.
250. Vanparijs, N., L. Nuhn, and B.G. De Geest, *Transiently thermoresponsive polymers and their applications in biomedicine*. Chem Soc Rev, 2017. **46**(4): p. 1193-1239.
251. Schmaljohann, D., *Thermo- and pH-responsive polymers in drug delivery*. Advanced Drug Delivery Reviews, 2006. **58**(15): p. 1655-1670.
252. leong, N.S., et al., *The critical importance of size on thermoresponsive nanoparticle transition temperatures: gold and micelle-based polymer nanoparticles*. Chemical Communications, 2011. **47**(42): p. 11627-11629.
253. Ward, M.A. and T.K. Georgiou, *Thermoresponsive Polymers for Biomedical Applications*. Polymers, 2011. **3**(3): p. 1215-1242.
-

254. Aseyev, V., H. Tenhu, and F.M. Winnik, *Non-ionic Thermoresponsive Polymers in Water. Self Organized Nanostructures of Amphiphilic Block Copolymers* li, 2011. **242**: p. 29-89.
255. Li, W., et al., *Antitumor drug delivery modulated by a polymeric micelle with an upper critical solution temperature*. *Angew Chem Int Ed Engl*, 2015. **54**(10): p. 3126-31.

PART II

Carbon-Derived

Multi-Dimensional Nanomaterials

Chapter 1

The Role of Tannic Acid for Intracellular Protein Delivery by Carbon Nanotubes

The Role of Tannic Acid for Intracellular Protein Delivery by Carbon Nanotubes

Hui Li,¹ Zhiyue Zhang,¹ Bruno G. De Geest*¹

¹ Department of Pharmaceutics, Ghent University, Ottergemsesteenweg 460, 9000 Ghent, Belgium. Br.DeGeest@UGent.be.

ABSTRACT

Carbon nanotubes (CNTs) are prone to aggregation. In this chapter, we report in stable CNTs suspensions obtained by either ultra-sonication or by the use of tannic acid as dispersant. We found all of these CNTs could absorb bovine serum albumin (BSA) and ovalbumin (OVA).

INTRODUCTION

As a growth area in nanotechnology, high-aspect ratio nanomaterial carbon nanotubes (CNTs),^[1-5] since their discovery in 1991,^[6] have stimulated intense interest in their unique optical, electrical, magnetic anisotropy and biological properties which make them possess broad application prospects.^[7-12] Depending on its number of graphene layers, CNT can be classified as single-wall carbon nanotubes (SW-CNTs)^[13-17] and multi-wall carbon nanotubes (MW-CNTs).^[6, 18, 19] They are only few nanometers wide, but in length can range from micrometers to millimeters. Rated by elastic modulus, CNT are almost the strongest and stiffest materials, but by Young's modulus, they are soft in radial direction.^[20-22] Both the length as well as aspect ratio play significant roles in their biological activity. Bare CNTs are hydrophobic and trend to agglomerate and deposit in aqueous medium due to high Van der Waals interaction forces along their length axis, leading to the formation of stacking bundles.^[3, 23-27] Therefore, for biomedical applications, CNTs must be stably separated and then functionalized to afford water solubility and biocompatibility.^[18] Moreover, an ideal functional CNT should possess minimal damage of the nanotube structure and contain available functional groups for further bio-conjugation.

Among the methods that have been developed to disperse CNTs, there are two major functionalization strategies: covalent reactions^[28-30] and non-covalent coating by amphiphilic molecules.^[18, 26, 31-33] For example, with the addition of dispersants^[34] such as sodium dodecyl sulfate (SDS), Triton X-100 or polyvinyl pyrrolidone (PVP), the CNTs suspension will aggregate and deposit if the excess coating molecules are removed. In addition, several dispersants have an ill-defined structures and exhibit neurotoxicity. Therefore, in this chapter we seek to explore more benign strategies for CNT stabilization and further bio-functionalization.

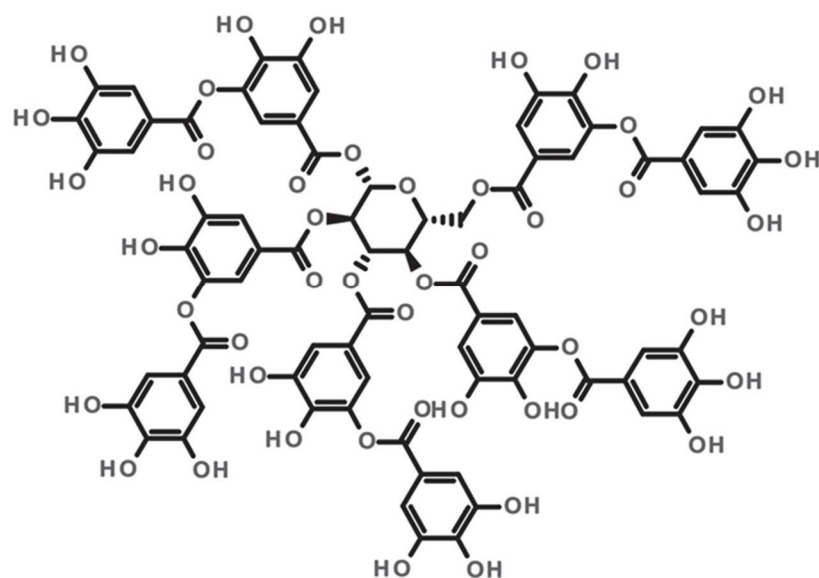


Figure 1. Chemical scheme structure of tannic acid (TA).^[35]

RESULTS AND DISCUSSION

Three different batches of carboxylic acid functionalized carbon nanotubes (CNTs-COOH) from different commercial sources were used: (1) multi-wall CNTs with a length of 1-10 μm (CNT-1), (2) single-wall CNTs with a diameter of 1.5nm and a length of 1-5 μm , (CNT-2), (3) multi-wall CNT with a diameter of 9.5 nm and a length of 1.5 μm (CNT-3). In dry state, we found by scanning electron microscopy (SEM) that all of these CNTs possess wider diameters than reported by the manufacturers (**Figure 2.**). Furthermore, attenuated total reflection fourier transform infrared spectroscopy (ATR-FTIR) in **Figure 3.A** showed that CNT-1, compared to graphite powder and the other two types of CNTs, had a distinct different spectrum, indicating the presence of carboxylic acid functional groups.^[36, 37]

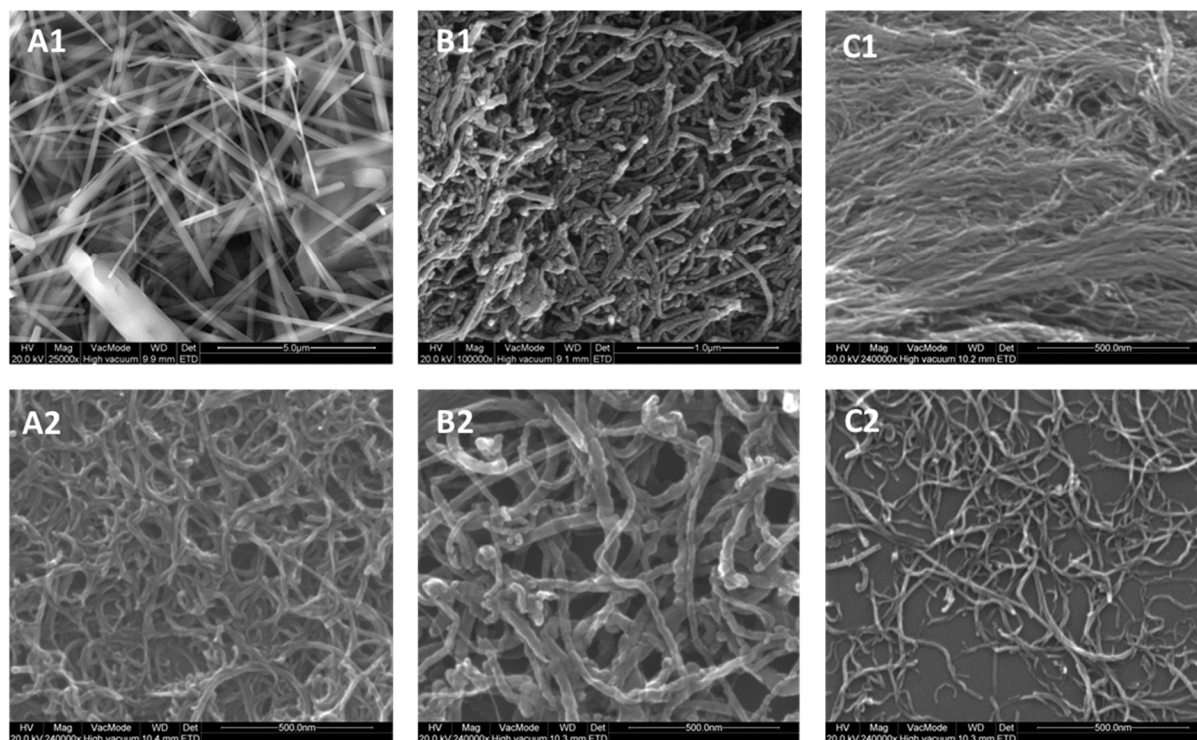


Figure 2. Scanning electron microscope (SEM) images of three different batches of carboxylic acid functionalized carbon nanotubes (A) CNT-1, (B) CNT-2, and (C) CNT-3. The numbers (1,2) in the upper left corner refer to carbon nanotubes in powder (1) and drying-state of dispersed carbon nanotubes in tannic acid (2). Scale bars are shown under each image.

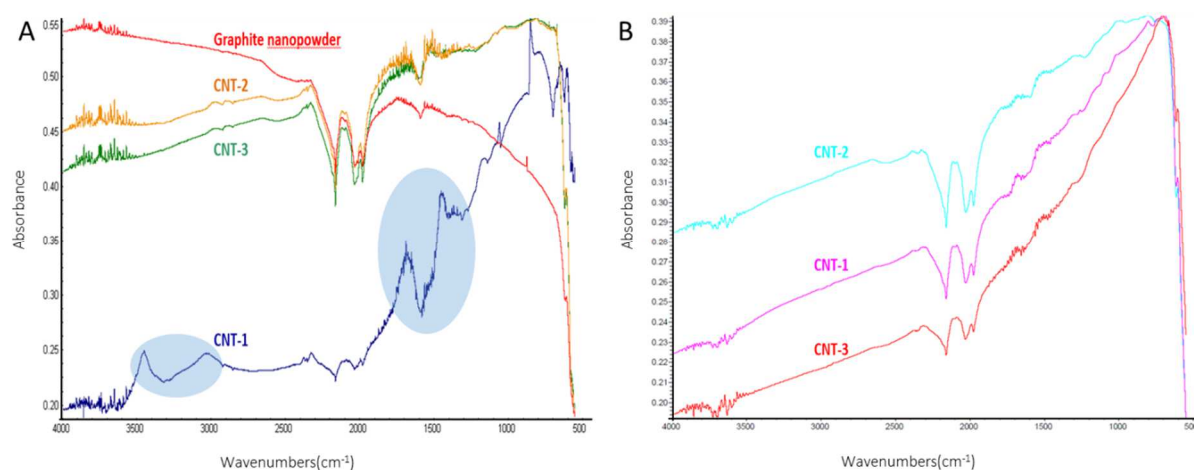


Figure 3. ATR-FTIR spectra of (A) Graphite powder and three different batches of CNTs. The marked blue areas on the spectrum are the characteristic absorption peaks of $-OH$ stretch ($3400\sim 3000\text{cm}^{-1}$) and $-C=O$ stretch ($1650\sim 1740\text{cm}^{-1}$); (B) Carbon nanotubes in tannic acid (CNT-TA);

Next, we attempted to obtain stable CNT dispersions in deionized water or phosphate buffer saline (PBS) with or without the use of ultra-sonication. The role of ultra-sonication is to promote disentangling and exfoliation of the aggregated CNT bundles.^[38-40] Without the help of ultra-sonication, CNT-1 could be well dispersed in both deionized water and PBS, whereas CNT-2 could only be well dispersed in deionized water and CNT-3 could not be dispersed in neither deionized water nor PBS (**Figure 4.**). This confirms our hypothesis that only CNT-1 contained sufficient numbers of carboxylic acid groups to be well-dispersed with the help of ultra-sonication.

As an alternative, we explored the use of a relative simple and low toxic natural surface-active compound, i.e. tannic acid (TA; **Figure 1.**), to aid in the dispersion of CNTs without the using of ultra-sonication.^[41] CNTs were mixed with TA, stirred for 2 or 3 days and dialyzed to remove the excess TA. This procedure allowed to obtain stable CNT suspensions from a batch of dry powder CNTs. SEM images (**Figure 2.**) of dried CNT-TA, showed that the CNTs were present as individual nanotubes due to the effect of tannic acid. ATR-FTIR (**Figure 3.B**) also illustrated that all of these CNT-TA batches contained TA. CNTs may be firstly coated with a monolayer of tannic acid through interaction of the aromatic rings that could adsorb onto the surface carbon rings by π - π stacking,^[18, 42] then further adsorb tannic acid by hydrogen bonds and other polar interactions.^[41, 43-45] Therefore, we hypothesize that TA provides steric and/or electrostatic repulsion between the unfolded individual CNTs, hence preventing aggregation.^[41, 46, 47]

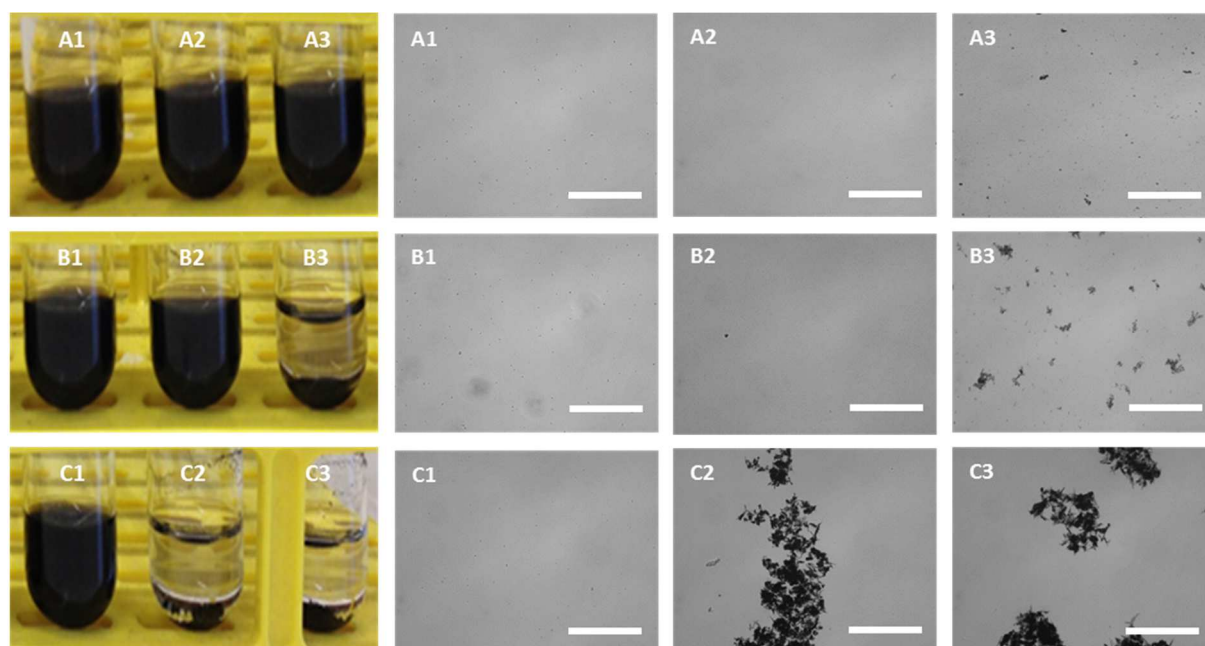


Figure 4. Photographs (left) and corresponding optical microscopy images (right) of dispersion of CNTs, (A) CNT-1, (B) CNT-2, and (C) CNT-3. The numbers (1,2 and 3) in the upper left corner refer to carbon nanotubes in tannic acid (1), in deionized water (2) and in phosphate buffer saline(PBS) (3). Scale bar represents 80 μ m. CNT-1 can be dispersed in a tannic acid (TA), deionized water and phosphate buffer saline(PBS); CNT-2 can be dispersed in a TA solution and deionized water but not in PBS buffer; CNT-3 can only be dispersed in a TA solution, and precipitates in deionized water and PBS buffer.

Once stable aqueous CNT suspensions were obtained, we subsequently aimed at investigating the interaction between these CNTs and model protein antigens (i.e. bovine serum albumin (BSA) and ovalbumin (OVA)).^[48] BSA is a 66 kDa protein with an isoelectric point of 5.0-5.6 and OVA which is isolated from chicken egg white is a 43 kDa protein with an isoelectric point of 4.3. The concentration of CNT in suspensions was measured by UV-Vis spectrophotometry at 800nm^[12, 18, 41, 49, 50] which showed good linearity in the 1 to 50 μ g/ml range and did not show interference with TA or BSA/OVA.

First, we attempted to covalently conjugate BSA to blank carbon nanotubes (CNT) and tannic acid pretreated carbon nanotubes (CNT-TA) using carbodiimide chemistry reagent in different mediums.^[13, 18, 51-55] Stable CNT suspensions were mixed with N-(3-Dimethylaminopropyl)-N'-ethylcarbodiimide hydrochloride (EDC.HCL) and sulfo-N-hydroxysulfosuccinimide sodium salt (sulfo-NHS) in 2-(N-morpholino)ethanesulfonic acid (MES) buffer (pH 5.5). The excess EDC.HCL/sulfo-NHS/MES was subsequently removed by

centrifugation. After redispersion, the CNT and CNT-TA were reacted overnight with BSA in a 1:1 weight ratio. Several washing and centrifugation cycles were performed to remove unbound proteins and concentrate the samples. Alternatively, we also mixed CNT with BSA without addition of carbodiimide coupling reagent. ATR-FTIR spectroscopy confirmed the presence (indicated by the blue area) of BSA in the respective CNT-BSA samples (**Figure 5.A** and **Figure 5.B**).

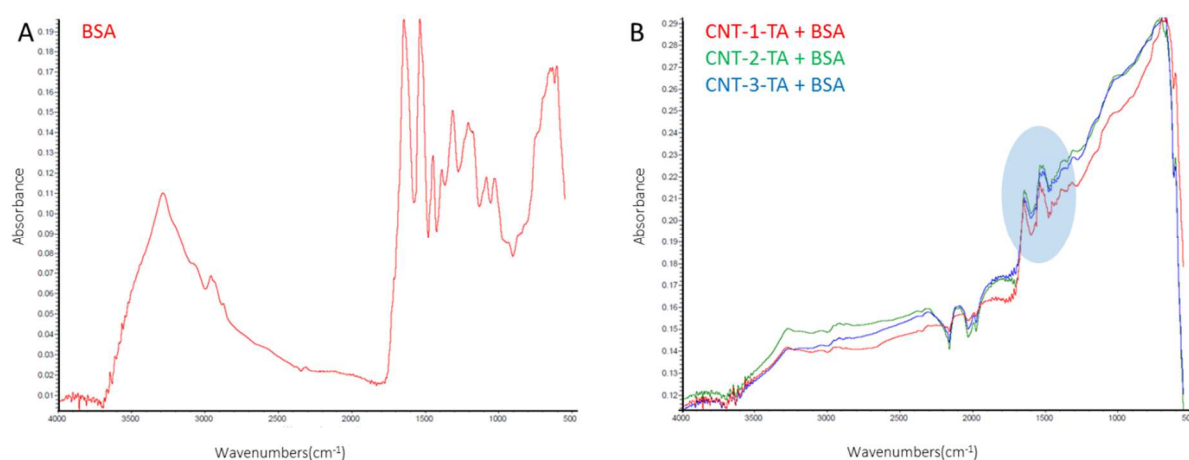


Figure 5. ATR-FTIR spectra of (A) Bovine serum albumin (BSA); (B) BSA adsorbed onto CNT-TA. The marked blue area on the spectra originates from BSA.

To allow for visualization by Fluorescence microscopy and confocal microscopy, fluorescently labeled BSA (FITC-BSA) was used. **Figure 6.** and **Figure 7.** showed a bright fluorescence emerging from the samples, whereas the bare CNTs under the same illumination and detection settings were found to be non-fluorescent. **Figure 6.** shows that FITC-BSA could spontaneously adsorb on CNT-3. The confocal microscopy images in **Figure 7.** also indicate that the FITC-BSA were capable to adsorb to these tannic acid pretreated CNTs in the absence of carbodiimide reagent. However, the use of carbodiimide reagent induces aggregation of CNTs.

To assess the protein adsorption efficiency, the unbound FITC-BSA in the supernatant of the first centrifugation cycle was loaded onto polyacrylamide (PAGE) gels and subjected to

electrophoresis. Optical integration of Coomassie-stained gels was used to quantify the unbound protein content as demonstrated in **Figure 8.A**. CNT-1 exhibited a better coupling efficiency in the presence of carbodiimide reagent, whereas CNT-2 and CNT-3 displayed almost the same coupling ability in the presence or absence of carbodiimide reagent. The same trends was also found by fluorescence spectroscopy, as shown in **Figure 8.B**. Moreover, the BSA adsorbed CNT samples which were produced using carbodiimide reagent are aggregated.

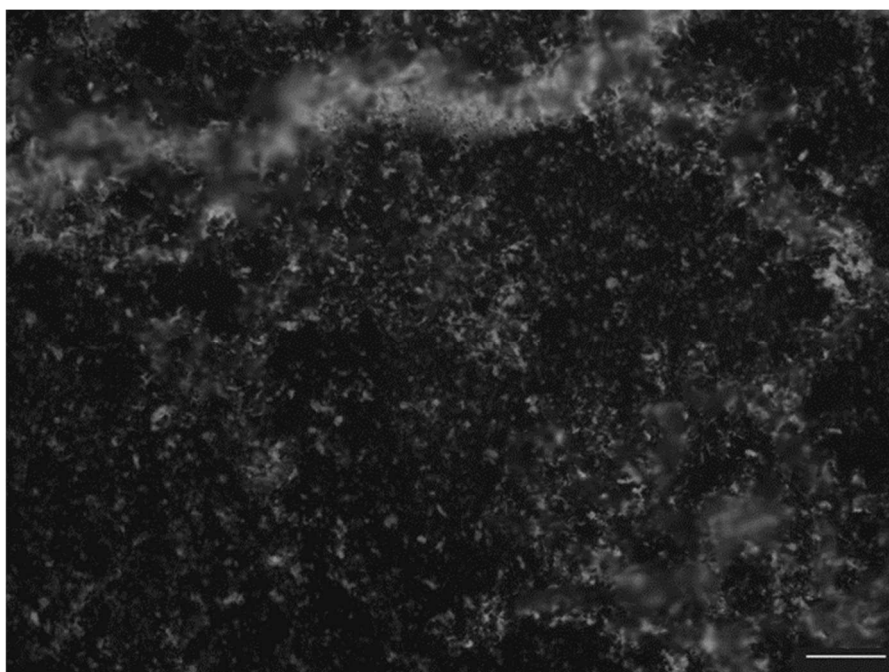


Figure 6. Fluorescence microscopy image of FITC-BSA adsorbed on CNT-3 that was pre-treated with ultra-sonication. The white appearances represent the bundled FITC-BSA. Scale bar represents 20 μ m.

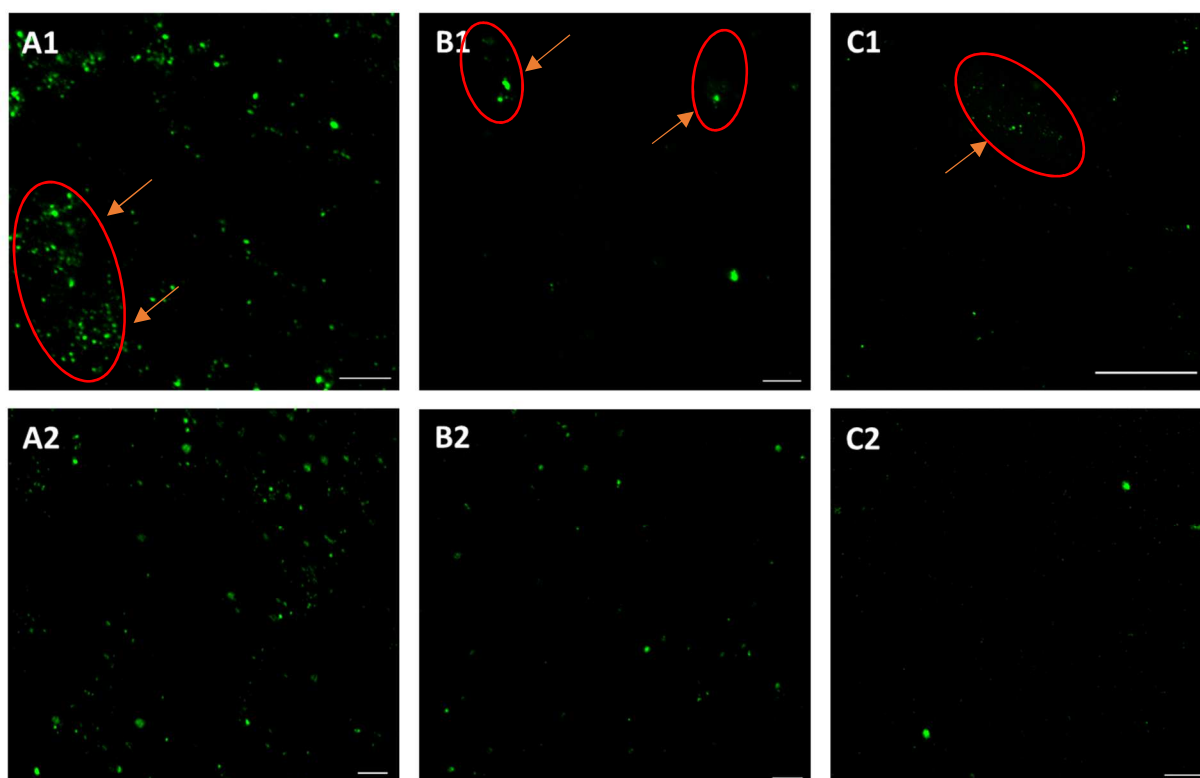


Figure 7. Confocal microscopy images of different CNT-TA suspensions, (A) CNT-1, (B) CNT-2, and (C) CNT-3 coupled to FITC-BSA in the presence (1) or absence (2) of carbodiimide reagent. The areas indicated by arrows and red circles show aggregations of CNTs by the use of carbodiimide reagent. Scale bars represent 20 μ m.

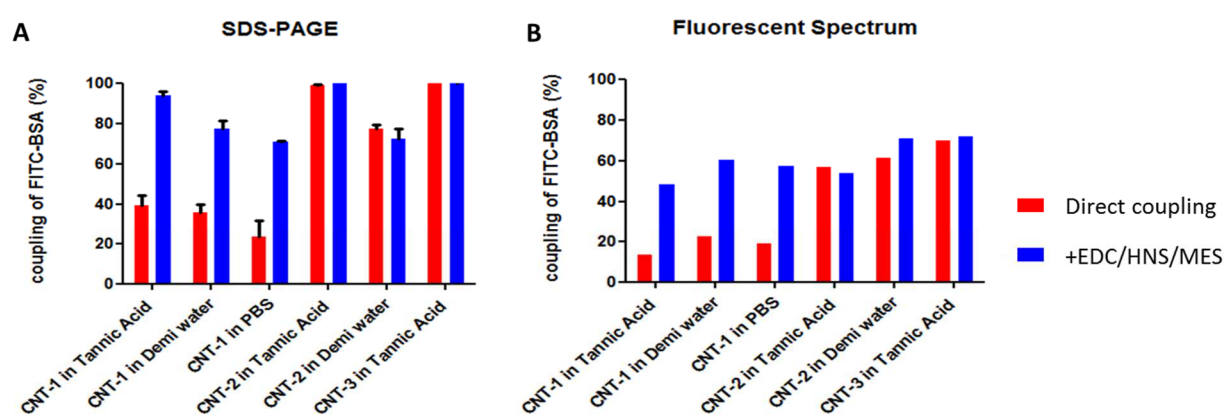


Figure 8. SDS-PAGE (A) and fluorescence spectroscopy (B) measurements of the unbound fraction of FITC-BSA.

To verify whether the high extent of protein adsorption to CNT in absence of carbodiimide reagent is unique for BSA, we also tested the adsorption of OVA. **Figure 9.** illustrated a similar tendency as observed for BSA. CNTs were previously treated with TA (CNT-TA) or ultrasonication (CNT-sonication). After reacting with AlexaFluor488 conjugated OVA (OVA-AF488) in a 1:1 weight ratio, CNT-1 in both situations (**Figure 9.B, 1+ and 2+**), CNT-2 and CNT-3 in TA (**Figure 9.B, 3+ and 5+**) were more stable than the other samples. Measuring the unbound protein fraction by SDS-PAGE and fluorescence spectroscopy (**Figure 10.**) gave further proof of the successful spontaneous adsorption of proteins on CNT-TA and CNT-sonication.

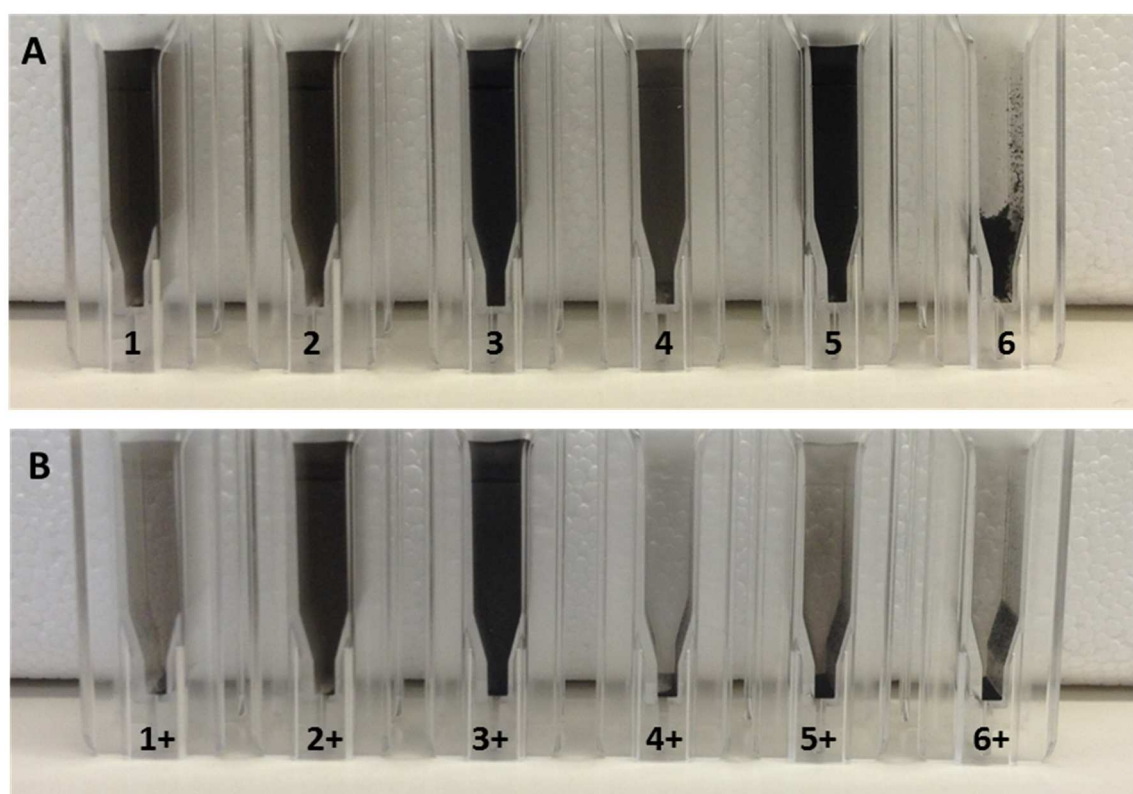


Figure 9. (A) photographs of cuvettes containing CNTs in tannic acid and deionized water: (1) CNT-1-TA; (2) CNT-1; (3) CNT-2-TA; (4) CNT-2; (5) CNT-3-TA; (6) CNT-3. Only CNT-3 in deionized water clearly deposited. (B) photographs of cuvettes containing corresponding CNTs with OVA (+): (1+) CNT-1-TA-OVA; (2+)CNT-1-sonication-OVA; (3+)CNT-2-TA-OVA; (4+)CNT-2-sonication-OVA; (5+) CNT-3-TA-OVA; (6+) CNT-3-sonication-OVA.

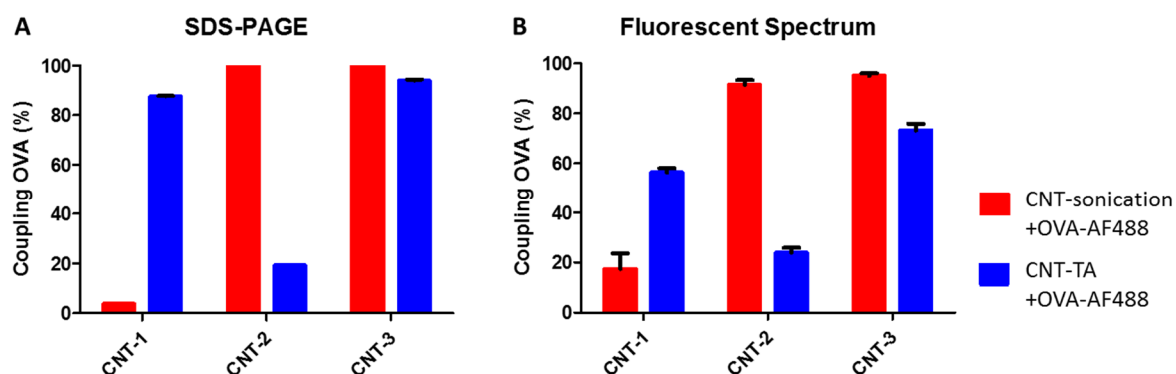


Figure 10. SDS-PAGE(A) and fluorescence spectroscopy(B) measurements of the unbound fraction of OVA.

Subsequently, we investigated the *in vitro* uptake of CNT-BSA/OVA by the immortalized mouse dendritic cell line DC2.4.^[56-58] Dendritic cells (DCs) were incubated overnight with the different CNT-BSA/OVA samples and measured by flow cytometry. **Figure 11.** & **Figure 12.** showed analogous trend to the aforementioned Fluorescence Spectrum and SDS-PAGE results. Although in presence of carbodiimide reagent, CNT and CNT-TA showed more efficient adsorption and cells uptake, the reagent disturbed the samples stability and caused aggregation. In addition, previously treated CNT with either ultra-sonication or tannic acid could spontaneous adsorb OVA. Ultra-sonication pretreatment could not only disperse CNTs, but also slice them and decrease their aspect ratio. That could be why the ultra-sonication treated CNT-OVA showed a little higher cells uptake behavior than the ones which were pretreated by tannic acid.

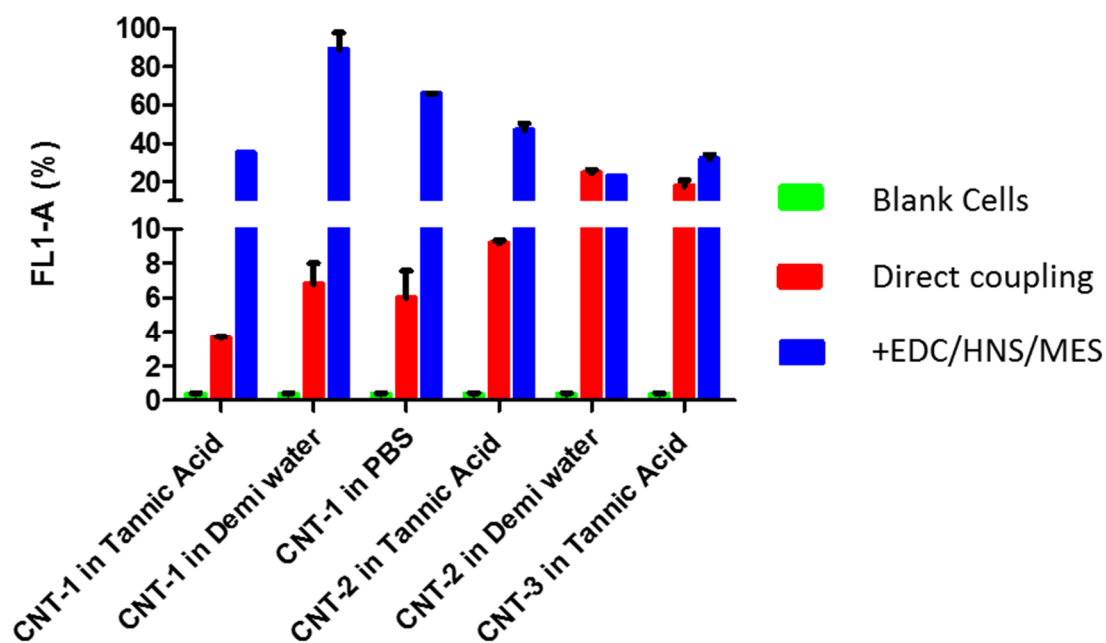


Figure 11. FACS analysis of DC2.4 cells which cultured with CNT-OVA, in the presence or absence of tannic acid.

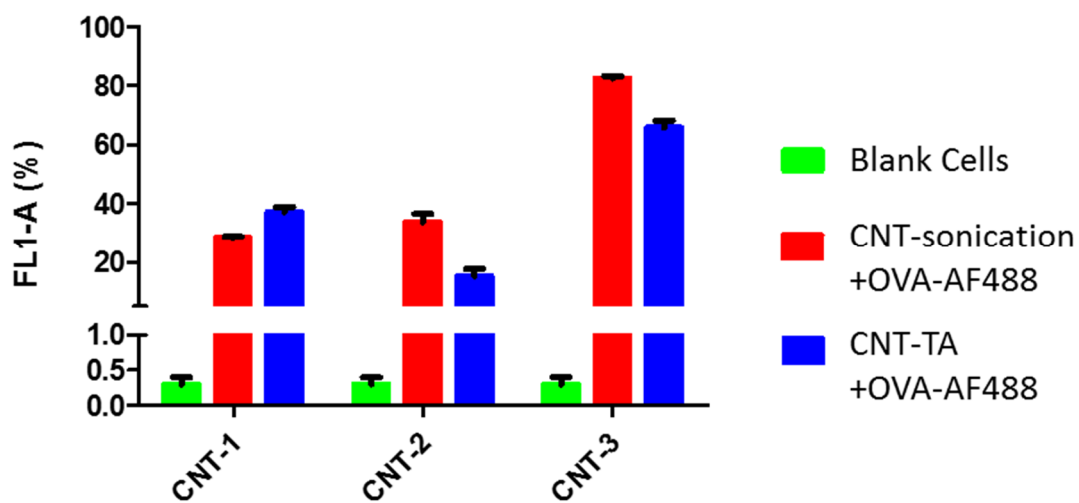


Figure 12. FACS analysis of DC2.4 cells which cultured with CNT-OVA, in the presence or absence of tannic acid.

Then, confocal microscopy was used to investigate whether these CNT-BSA/OVA were internalized by the DCs or merely bound with their surface. To be easily visualized, we used AlexaFluor555-labeled cholera toxin subunit B (CTB-AF555) to mark the cells membrane, while the cell nuclei were stained with Hoechst.^[59] From both the staining cells images and the differential interference contrast(DIC) images(from **Figure 13.** to **Figure 18.**), it is clear that CNT-BSA/OVA were located inside cells as well as stuck to the cell membrane.

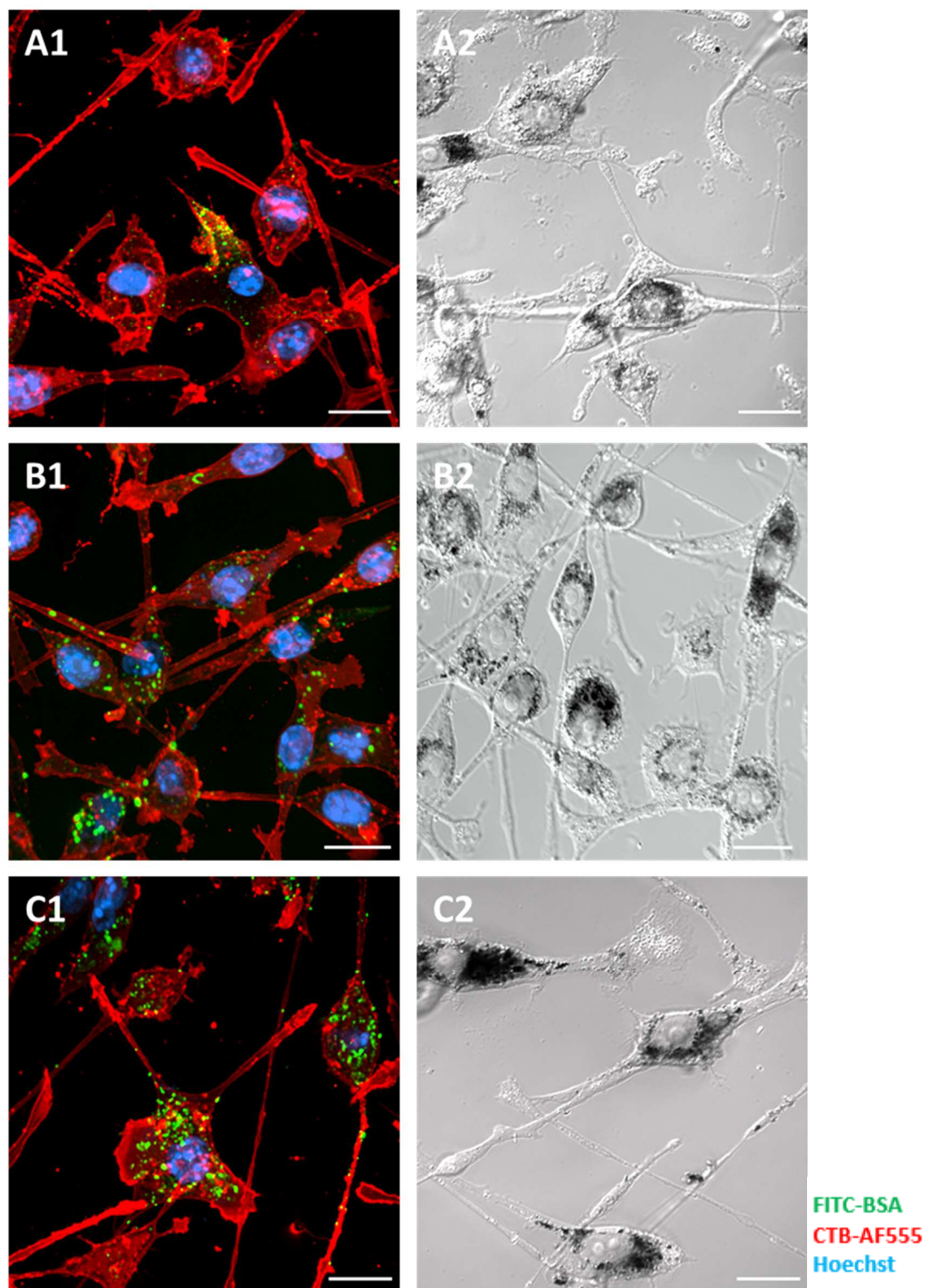


Figure 13. Confocal microscopy images of DC2.4 cells incubated with different CNT-1-FITC-BSA samples. (A) CNT-1-TA coupled with FITC-BSA, (B) CNT-1-sonication coupled with FITC-BSA, and (C) CNT-1-TA coupled with FITC-BSA in the presence of carbodiimide reagent. The numbers (1,2) in the upper left corner refer to the staining cells images (1) and differential interference contrast (DIC) cells images (2). Scale bars represent 20 μ m. (Note that, the staining cells images and DIC images are from the same samples but not from the same area or cells.)

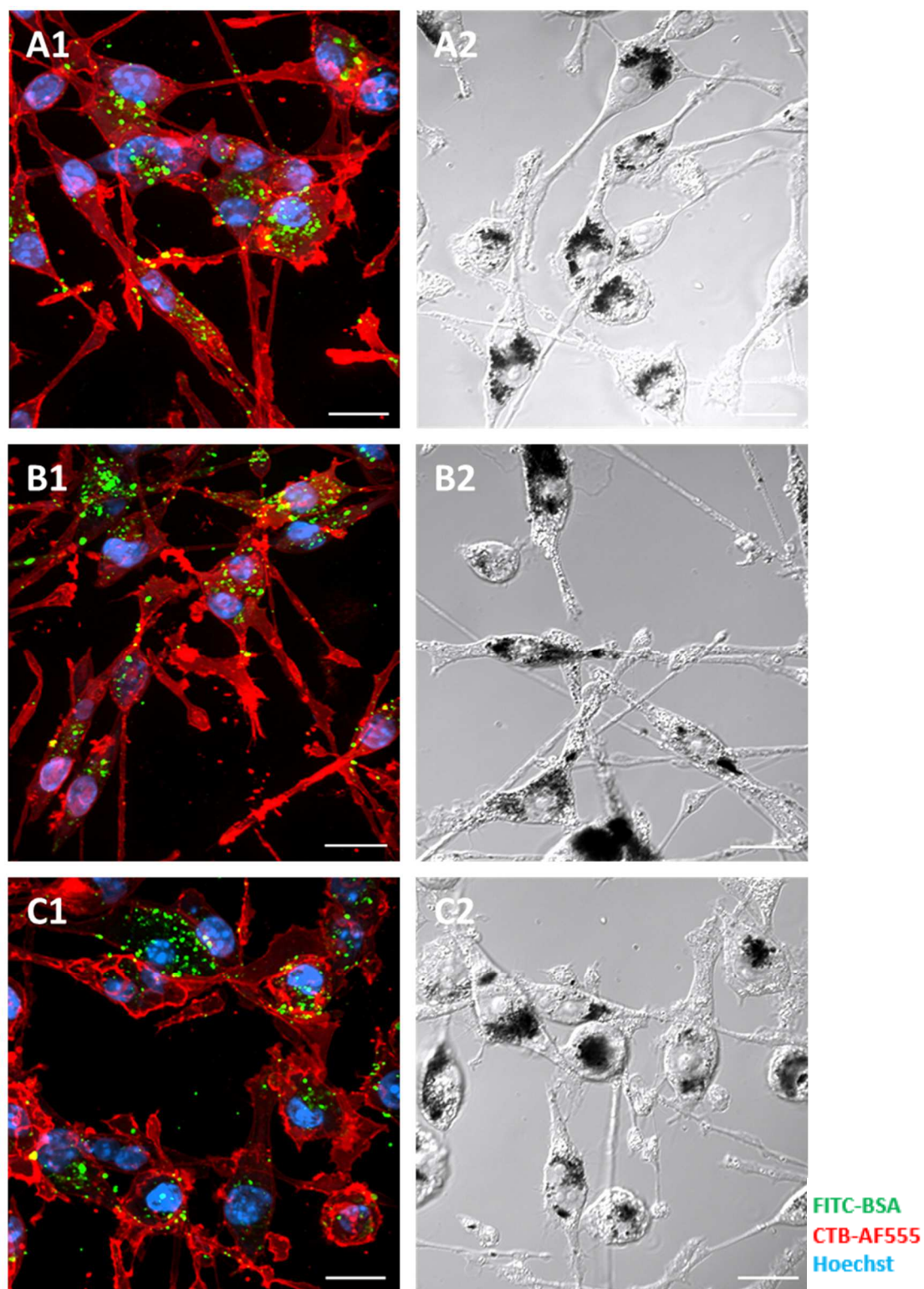


Figure 14. Confocal microscopy images of DC2.4 cells incubated with different CNT-2-FITC-BSA samples. (A) CNT-2-TA coupled with FITC-BSA, (B) CNT-2-sonication coupled with FITC-BSA, and (C) CNT-2-TA coupled with FITC-BSA in the presence of carbodiimide reagent. The numbers (1,2) in the upper left corner refer to the staining cells images (1) and differential interference contrast (DIC) cells images (2). Scale bars represent 20 μm . (Note that, the staining cells images and DIC images are from the same samples but not from the same area or cells.)

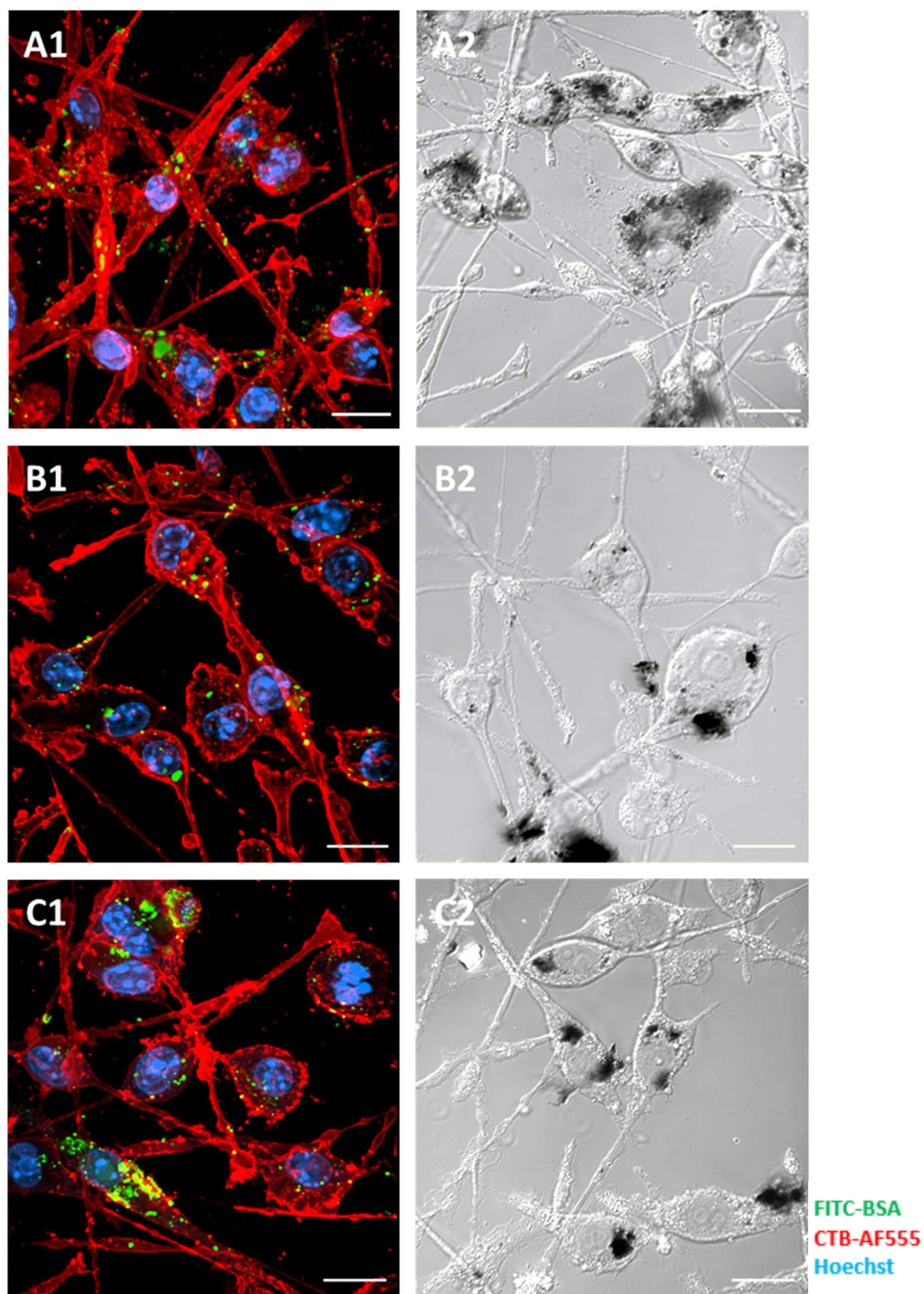


Figure 15. Confocal microscopy images of DC2.4 cells incubated with different CNT-3-FITC-BSA samples. (A) CNT-3-TA coupled with FITC-BSA, (B) CNT-3-sonication coupled with FITC-BSA, and (C) CNT-3-TA coupled with FITC-BSA in the presence of carbodiimide reagent. The numbers (1,2) in the upper left corner refer to the staining cells images (1) and differential interference contrast (DIC) cells images (2). Scale bars represent 20 μ m. (Note that, the staining cells images and DIC images are from the same samples but not from the same area or cells.)

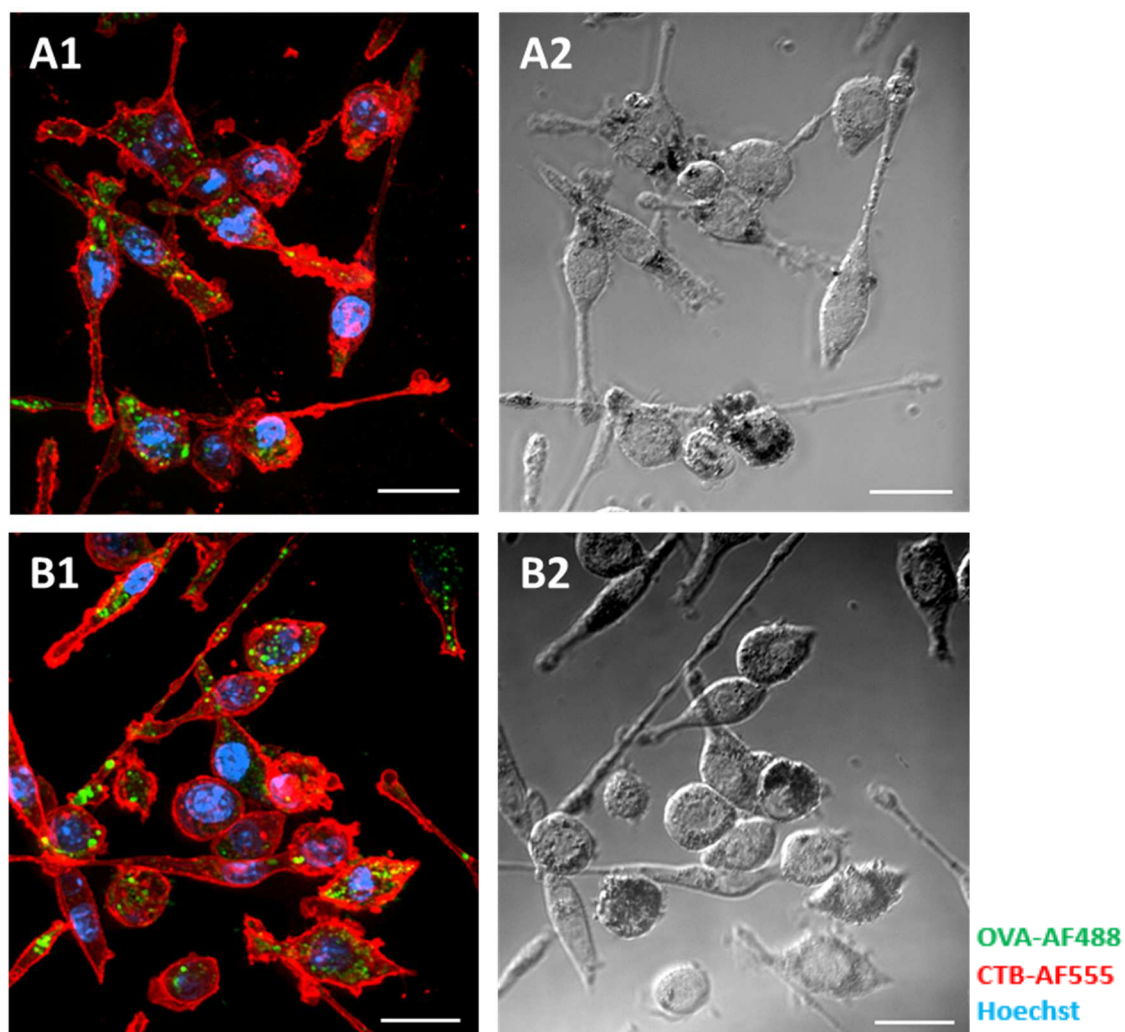


Figure 16. Confocal microscopy images of DC2.4 cells incubated with different CNT-1-OVA-AF488 samples. (A) CNT-1-TA coupled with OVA-AF488 and (B) CNT-1-sonication coupled with OVA-AF488. The numbers (1,2) in the upper left corner refer to the staining cells images (1) and differential interference contrast (DIC) cells images (2). Scale bars represent 20 μm .

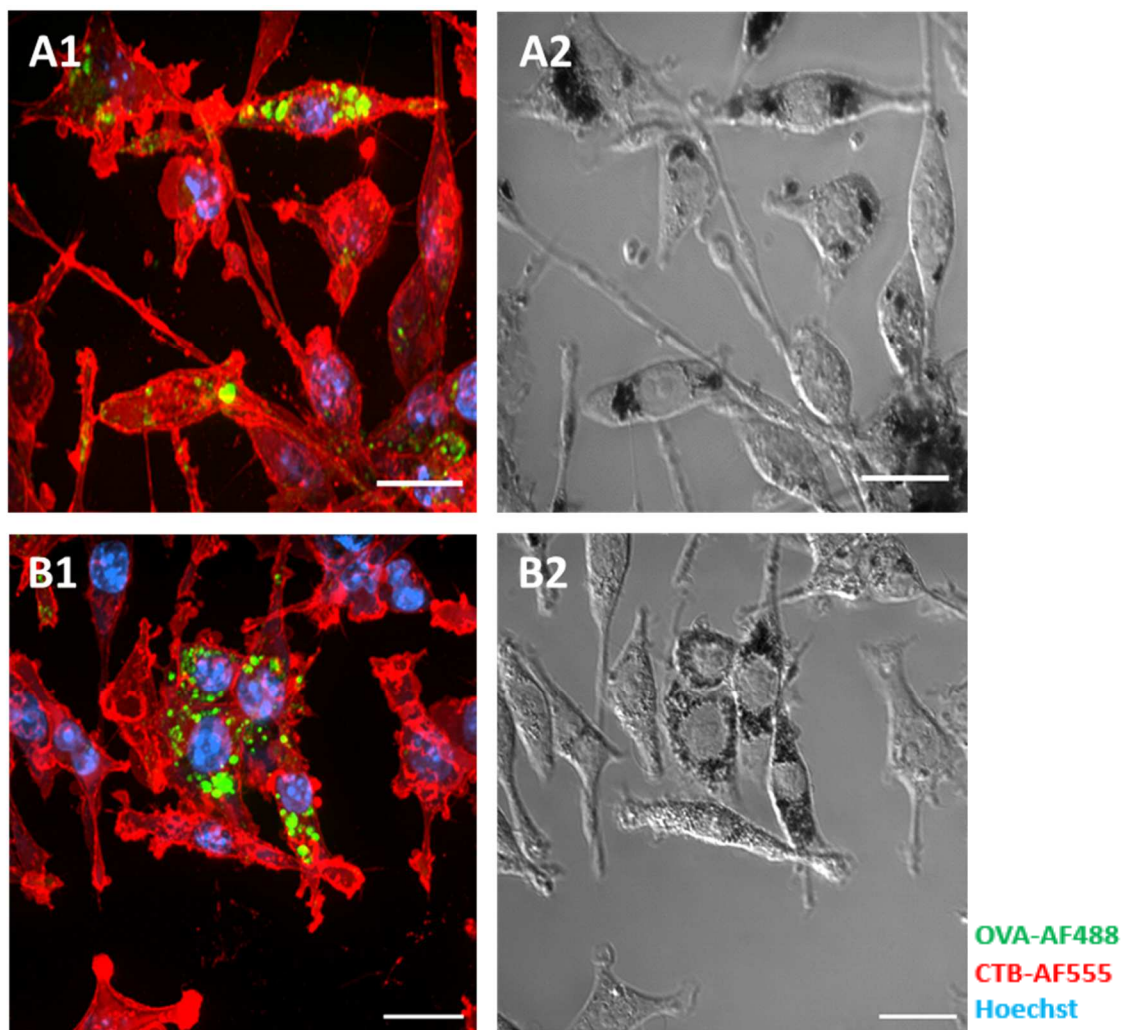


Figure 17. Confocal microscopy images of DC2.4 cells incubated with different CNT-2-OVA-AF488 samples. (A) CNT-2-TA coupled with OVA-AF488 and (B) CNT-2-sonication coupled with OVA-AF488. The numbers (1,2) in the upper left corner refer to the staining cells images (1) and differential interference contrast (DIC) cells images (2). Scale bars represent 20 μm .

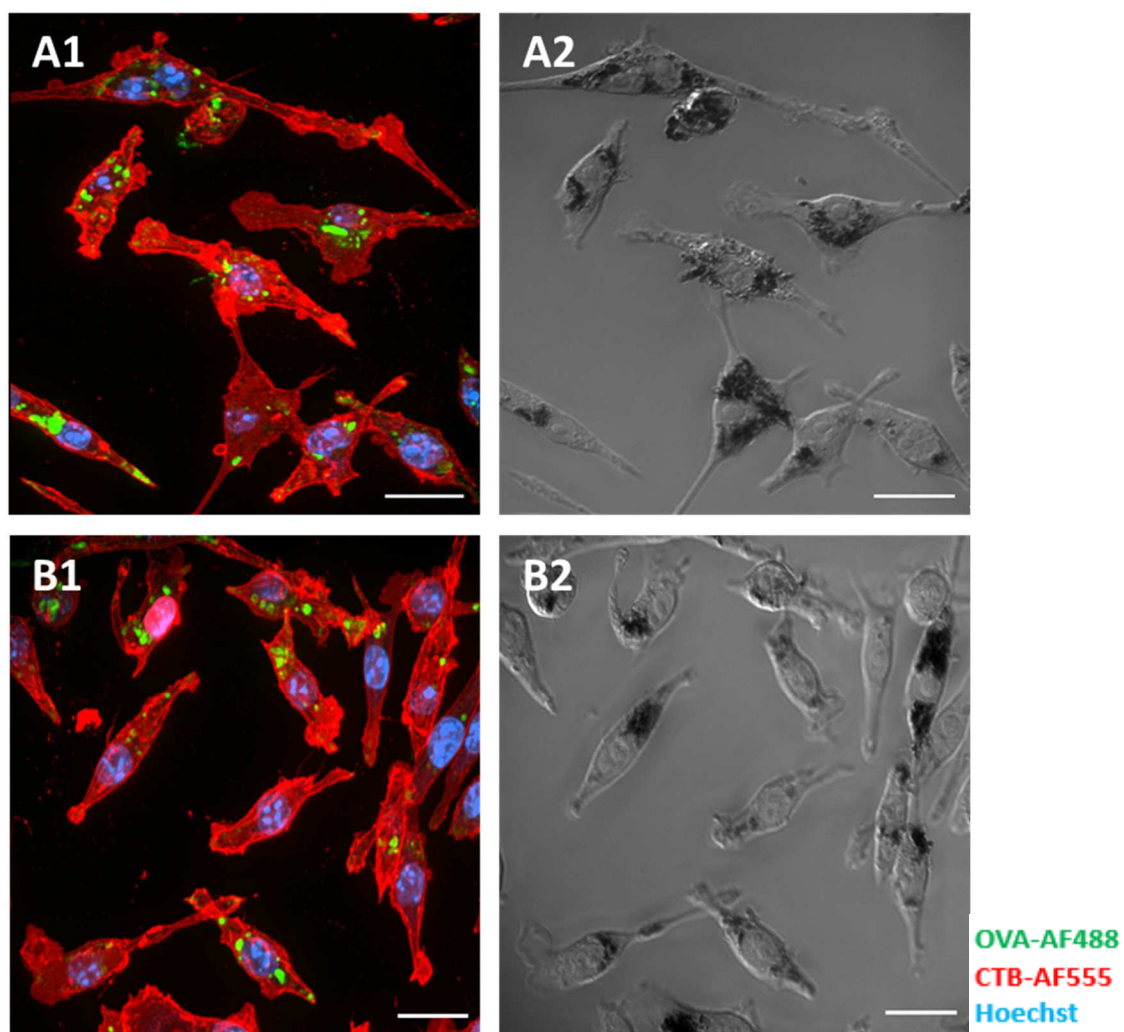


Figure 18. Confocal microscopy images of DC2.4 cells incubated with different CNT-3-OVA-AF488 samples. (A) CNT-3-TA coupled with OVA-AF488 and (B) CNT-3-sonication coupled with OVA-AF488. The numbers (1,2) in the upper left corner refer to the staining cells images (1) and differential interference contrast (DIC) cells images (2). Scale bars represent 20 μ m.

CONCLUSIONS

In summary, stable CNT suspensions could be obtained both by ultra-sonication and by treatment with TA, which provides steric and/or electrostatic repulsion between individual CNTs, thus preventing aggregation.^[46, 47] However, in order to protect the nanotubes structure and aspect ratio, tannic acid pretreatment is more reliable than ultra-sonication and the use of carbodiimide reagent. We postulate that the bio-conjugation of CNTs and proteins will open new possibilities to utilize their properties for multifunctional subcellular targeting applications.

EXPERIMENTAL SECTION

Materials

Graphite and Multi-Wall CNT (CNT-1) were purchased from PlasmaChem GmbH, with the length 1-10 μ m. Single-Wall CNT (CNT-2) was purchased from NANO LAB, with the diameter 1.5nm and length 1-5 μ m. Multi-Wall CNT (CNT-3) was purchased from Sigma-Aldrich, with the diameter 9.5nm and length 1.5 μ m. Cell culture media and additives, AlexaFluor488 labeled ovalbumin (OVA-AF488), AlexaFluor555 labeled cholera toxin subunit B (CTB-AF555), Hoechst and propidium iodide were purchased from Life Technologies. 2-Mercaptoethanol, laemli sample buffer (4x), Coomassie blue stain (G-250) were purchased from Bio-rad. All other chemicals and solvents were purchased from Sigma- Aldrich. Deionized water was used for all experiments.

Instrumentations

Scanning electron microscopy (SEM) images were recorded on a quanta FEG FEI 200 apparatus. Samples were deposited onto a silicon wafer and dried under a gentle nitrogen stream at room temperature. Prior to imaging, the samples were sputtered with a gold coating.

Attenuated Total Reflection Fourier Transform Infrared Spectroscopy (ATR-FTIR). ATR-FTIR spectra were recorded on a Thermo Scientific Nicolet iS 5 FT-IR spectrometer.

UV-VIS spectroscopy, UV-VIS spectra were acquired with a Shimadzu UV-1650PC spectrophotometer. CNTs suspension, Tannic acid solution and proteins solutions were placed in the cuvettes and spectral analysis was performed in a 200 to 1000nm range at room temperature. CNTs suspension, either Tannic acid nor protein, showed absorbance value at 800nm wavelength. UV-VIS spectra was used to evaluate the final concentration of CNTs in the CNT~protein samples. The concentration of CNTs and the absorbance value showed a good linear relationship between 1~ 50 μ g/ml.

Fluorescence microscopy

Fluorescence microscopy was performed on a Leica DM2500P microscope equipped with a 40x objective.

Confocal laser scanning microscopy.

Images were recorded on a Leica DMI6000B inverted microscope equipped with a 63x (1.4 NA) oil immersion objective and connected to an Andor DSD2 confocal scanner.

DC2.4 cells were plated a density of 5 000 per well in a small well (20 μ l * 25 000) and incubated overnight with samples. Cells were fixated with paraformaldehyde; cell nuclei were stained with Hoechst, and the cell membrane stained with CTB-AF555.

Sodium Dodecyl Sulfate-polyacrylamide Gel Electrophoresis (SDS-PAGE).

SDS-PAGE was performed with a 4-20 % polyacrylamide gradient gel using the Mini-PROTEAN Tetra Cell from Bio-Rad, at 180 V for 45 min. The unbound proteins samples which were contained in the supernatant of the first centrifugation cycle and the coupling samples were loaded onto polyacrylamide (PAGE) gels and applied an electric current. The samples were diluted with a 1:9 β -mercaptoethanol:laemli sample buffer solution (4x). After the run, visualization of the protein bands was obtained by incubated the gels into Coomassie blue stain. BIO-RAD Gel DOC™ EZ and Image Lab 5.2.1 were used to scan the gals and calculate the results.

Methods

The stability of CNTs' suspension.

Respectively dispersed our Carbon nanotubes in 0.5mg/ml original concentration of Tannic Acid solution(TA), stirred for 2 days and then dialyzed against deionized water 3 days by changing the water every half-day to remove the excess Tannic Acid. Testing by the UV-Vis, Tannic Acid (TA) could help to disperse CNTs even with a very low final concentration in CNT-TA suspension. These CNT-TA suspensions are stable at 4-7°C. And we also used ultra-sonic instrument to help these Carbon nanotubes dispersed in deionized water, the same CNTs final concentration as in CNT-TA suspension.

Coupled CNTs with proteins.

1 mg/mL of stock solution of BSA, FITC-BSA (when using fluorescence-based assays), OVA or OVA-AF488 (when using fluorescence-based assays) were prepared in phosphate buffer saline (PBS).

Efficient Two-Step Coupling Protocol

Firstly, parallel mixed different CNTs suspension with N-(3-Dimethylaminopropyl)-N'-ethylcarbodiimide hydrochloride (EDC.HCL) and N-Hydroxysulfosuccinimide sodium salt (sulfo-NHS) in 2-(N-morpholino)ethanesulfonic acid (MES) buffer (pH≈5.5) for 15min, then removed the excess EDC.HCL/sulfo-NHS/MES by high speed centrifugation (20 min at 25.000 G). Next, the re-dispersed CNTs suspensions were mixed with proteins in a 1:1 weight ratio and reacted overnight at 4-7°C. Several washing and high speed centrifugation (20 min at 25.000 G) cycles were performed to remove unbound proteins and obtain the concentrated solution of CNT~adsorbed proteins.

One-Step Coupling Protocol

The one-step coupling protocol quitted the first step above, directly mixed different CNTs suspensions with proteins in a 1:1 weight ratio by overnight stirring at 4-7°C then performed

several washing and high speed centrifugation(20 min at 25.000 G) cycles to remove unbound proteins.

In Vitro Cell Culture Experiments.

DC2.4 Cell Line.

The immortalized mouse dendritic cell line DC2.4 was a kind gift from Prof. Dr. Ken Rock (Dana-Farber Cancer Institute, Boston, MA, USA). Cell culturing was done in RPMI-glutamax, supplemented with 10% FBS, 1 mM sodium pyruvate, Glutamine, and antibiotics (50 units/ml penicillin and 50 µg/ml streptomycin). Cells were incubated at 37 °C in a controlled, sterile environment of 95% relative humidity and 5% CO₂.

Cell Uptake Studies.

DC2.4 cells were pulsed overnight with the CNT~protein samples, which containing FITC-BSA or OVA-AF488 and subsequently analyzed by FACS and Confocal Microscopy. Flow Cytometry was performed on a BD Accuri C6 flow cytometer. For Confocal Microscopy, cells were fixated with paraformaldehyde; cell nuclei were stained with Hoechst, and the cell membrane stained with CTB-AF555, both according to the supplier's instructions. Images were recorded on a Leica DMI6000B inverted microscope equipped with a 63× (1.4 NA) oil immersion objective and connected to an Andor DSD2 Confocal Scanner.

REFERENCE

1. Zhu, L., et al., *Growth and electrical characterization of high-aspect-ratio carbon nanotube arrays*. Carbon, 2006. **44**(2): p. 253-258.
2. Bauer, L.A., N.S. Birenbaum, and G.J. Meyer, *Biological applications of high aspect ratio nanoparticles*. Journal of Materials Chemistry, 2004. **14**(4): p. 517-526.
3. Jensen, K., et al., *Buckling and kinking force measurements on individual multiwalled carbon nanotubes*. Physical Review B, 2007. **76**(19): p. 195436.
4. Wang, X., et al., *Fabrication of ultralong and electrically uniform single-walled carbon nanotubes on clean substrates*. Nano letters, 2009. **9**(9): p. 3137-3141.
5. Jia, W., B. Tang, and P. Wu, *Novel Composite PEM with Long-Range Ionic Nanochannels Induced by Carbon Nanotube/Graphene Oxide Nanoribbon Composites*. ACS applied materials & interfaces, 2016. **8**(42): p. 28955-28963.
6. Iijima, S., *Helical microtubules of graphitic carbon*. nature, 1991. **354**(6348): p. 56-58.
7. Feazell, R.P., et al., *Soluble single-walled carbon nanotubes as longboat delivery systems for platinum (IV) anticancer drug design*. Journal of the American Chemical Society, 2007. **129**(27): p. 8438-8439.
8. Liu, Z., et al., *Drug delivery with carbon nanotubes for in vivo cancer treatment*. Cancer research, 2008. **68**(16): p. 6652-6660.
9. Münzer, A.M., Z.P. Michael, and A. Star, *Carbon nanotubes for the label-free detection of biomarkers*. ACS nano, 2013. **7**(9): p. 7448-7453.
10. Singh, R., et al., *Tissue biodistribution and blood clearance rates of intravenously administered carbon nanotube radiotracers*. Proceedings of the National Academy of Sciences of the United States of America, 2006. **103**(9): p. 3357-3362.
11. Xue, X., et al., *Aggregated single-walled carbon nanotubes attenuate the behavioural and neurochemical effects of methamphetamine in mice*. Nature nanotechnology, 2016. **11**(7): p. 613-620.
12. Kam, N.W.S., et al., *Carbon nanotubes as multifunctional biological transporters and near-infrared agents for selective cancer cell destruction*. Proceedings of the National Academy of Sciences of the United States of America, 2005. **102**(33): p. 11600-11605.
13. Ziegler, K.J., et al., *Controlled oxidative cutting of single-walled carbon nanotubes*. Journal of the American Chemical Society, 2005. **127**(5): p. 1541-1547.

14. Wong, E.W., P.E. Sheehan, and C.M. Lieber, *Nanobeam mechanics: elasticity, strength, and toughness of nanorods and nanotubes*. *science*, 1997. **277**(5334): p. 1971-1975.
15. Dekker, C., et al., *Individual single-wall carbon nanotubes as quantum wires*. *Nature* 386 (6624), 474-477.(1997), 1997.
16. Iijima, S. and T. Ichihashi, *Single-shell carbon nanotubes of 1-nm diameter*. *nature*, 1993. **363**(6430): p. 603-605.
17. Bethune, D., et al., *Cobalt-catalysed growth of carbon nanotubes with single-atomic-layer walls*. *Nature*, 1993. **363**(6430): p. 605-607.
18. Liu, Z., et al., *Preparation of carbon nanotube bioconjugates for biomedical applications*. *Nature protocols*, 2009. **4**(9): p. 1372-1381.
19. Ebbesen, T. and P. Ajayan, *Large-scale synthesis of carbon nanotubes*. *Nature*, 1992. **358**(6383): p. 358220a0.
20. Yakobson, B.I. and P. Avouris, *Mechanical properties of carbon nanotubes*, in *Carbon nanotubes*. 2001, Springer. p. 287-327.
21. Gupta, S., K. Dharamvir, and V. Jindal, *Elastic moduli of single-walled carbon nanotubes and their ropes*. *Physical Review B*, 2005. **72**(16): p. 165428.
22. Pampaloni, F. and E.-L. Florin, *Microtubule architecture: inspiration for novel carbon nanotube-based biomimetic materials*. *Trends in biotechnology*, 2008. **26**(6): p. 302-310.
23. Yu, M.-F., et al., *Strength and breaking mechanism of multiwalled carbon nanotubes under tensile load*. *Science*, 2000. **287**(5453): p. 637-640.
24. Peng, B., et al., *Measurements of near-ultimate strength for multiwalled carbon nanotubes and irradiation-induced crosslinking improvements*. *Nature nanotechnology*, 2008. **3**(10): p. 626-631.
25. Filleter, T., et al., *Ultrahigh strength and stiffness in cross-linked hierarchical carbon nanotube bundles*. *Advanced Materials*, 2011. **23**(25): p. 2855-2860.
26. Boyer, P.D., et al., *Delivering Single-Walled Carbon Nanotubes to the Nucleus Using Engineered Nuclear Protein Domains*. *ACS applied materials & interfaces*, 2016. **8**(5): p. 3524-3534.
27. Kaiser, J.-P., et al., *Single walled carbon nanotubes (SWCNT) affect cell physiology and cell architecture*. *Journal of Materials Science: Materials in Medicine*, 2008. **19**(4): p. 1523-1527.

28. Cheng, J., et al., *Reversible accumulation of PEGylated single-walled carbon nanotubes in the mammalian nucleus*. ACS nano, 2008. **2**(10): p. 2085-2094.
 29. Battigelli, A., et al., *Endowing carbon nanotubes with biological and biomedical properties by chemical modifications*. Advanced drug delivery reviews, 2013. **65**(15): p. 1899-1920.
 30. Pantarotto, D., et al., *Translocation of bioactive peptides across cell membranes by carbon nanotubes*. Chemical Communications, 2004(1): p. 16-17.
 31. Britz, D.A. and A.N. Khlobystov, *Noncovalent interactions of molecules with single walled carbon nanotubes*. Chemical Society Reviews, 2006. **35**(7): p. 637-659.
 32. Adeli, M., et al., *Carbon nanotubes in cancer therapy: a more precise look at the role of carbon nanotube–polymer interactions*. Chemical Society Reviews, 2013. **42**(12): p. 5231-5256.
 33. Karajanagi, S.S., et al., *Protein-assisted solubilization of single-walled carbon nanotubes*. Langmuir, 2006. **22**(4): p. 1392-1395.
 34. Hilding, J., et al., *Dispersion of carbon nanotubes in liquids*. Journal of dispersion science and technology, 2003. **24**(1): p. 1-41.
 35. Sundaramurthy, A., et al., *Hydrogen Bonded Multilayer Films Based on Poly (2-oxazoline)s and Tannic Acid*. Advanced healthcare materials, 2014. **3**(12): p. 2040-2047.
 36. Weng, X., et al., *On-chip chiral separation based on bovine serum albumin-conjugated carbon nanotubes as stationary phase in a microchannel*. Electrophoresis, 2006. **27**(15): p. 3129-3135.
 37. Chen, J., et al., *Solution properties of single-walled carbon nanotubes*. Science, 1998. **282**(5386): p. 95-98.
 38. Verneuil, L., et al., *Multi-walled carbon nanotubes, natural organic matter, and the benthic diatom *Nitzschia palea*: "A sticky story"*. Nanotoxicology, 2015. **9**(2): p. 219-229.
 39. Hollanda, L., et al., *Graphene and carbon nanotube nanocomposite for gene transfection*. Materials Science and Engineering: C, 2014. **39**: p. 288-298.
 40. Arepalli, S., et al., *Protocol for the characterization of single-wall carbon nanotube material quality*. Carbon, 2004. **42**(8): p. 1783-1791.
 41. Lin, D. and B. Xing, *Tannic acid adsorption and its role for stabilizing carbon nanotube suspensions*. Environmental science & technology, 2008. **42**(16): p. 5917-5923.
-

42. Liu, Z., et al., *Supramolecular chemistry on water-soluble carbon nanotubes for drug loading and delivery*. ACS nano, 2007. **1**(1): p. 50-56.
 43. Gotovac, S., et al., *Effect of nanoscale curvature of single-walled carbon nanotubes on adsorption of polycyclic aromatic hydrocarbons*. Nano Letters, 2007. **7**(3): p. 583-587.
 44. Woods, L., Ş. Bădescu, and T. Reinecke, *Adsorption of simple benzene derivatives on carbon nanotubes*. Physical Review B, 2007. **75**(15): p. 155415.
 45. Chen, W., L. Duan, and D. Zhu, *Adsorption of polar and nonpolar organic chemicals to carbon nanotubes*. Environmental science & technology, 2007. **41**(24): p. 8295-8300.
 46. Sano, M., J. Okamura, and S. Shinkai, *Colloidal nature of single-walled carbon nanotubes in electrolyte solution: the Schulze–Hardy rule*. Langmuir, 2001. **17**(22): p. 7172-7173.
 47. Jiang, L., L. Gao, and J. Sun, *Production of aqueous colloidal dispersions of carbon nanotubes*. Journal of colloid and interface science, 2003. **260**(1): p. 89-94.
 48. Ge, C., et al., *Binding of blood proteins to carbon nanotubes reduces cytotoxicity*. Proceedings of the National Academy of Sciences, 2011. **108**(41): p. 16968-16973.
 49. Matarredona, O., et al., *Dispersion of single-walled carbon nanotubes in aqueous solutions of the anionic surfactant NaDDBS*. The Journal of Physical Chemistry B, 2003. **107**(48): p. 13357-13367.
 50. Hyung, H., et al., *Natural organic matter stabilizes carbon nanotubes in the aqueous phase*. Environmental science & technology, 2007. **41**(1): p. 179-184.
 51. Asuri, P., et al., *Structure, function, and stability of enzymes covalently attached to single-walled carbon nanotubes*. Langmuir, 2007. **23**(24): p. 12318-12321.
 52. Grabarek, Z. and J. Gergely, *Zero-length crosslinking procedure with the use of active esters*. Analytical biochemistry, 1990. **185**(1): p. 131-135.
 53. Lomant, A.J. and G. Fairbanks, *Chemical probes of extended biological structures: synthesis and properties of the cleavable protein cross-linking reagent [35S] dithiobis (succinimidyl propionate)*. Journal of molecular biology, 1976. **104**(1): p. 243-261.
 54. Cuatrecasas, P. and I. Parikh, *Adsorbents for affinity chromatography. Use of N-hydroxysuccinimide esters of agarose*. Biochemistry, 1972. **11**(12): p. 2291-2299.
 55. Staros, J.V., R.W. Wright, and D.M. Swingle, *Enhancement by N-hydroxysulfosuccinimide of water-soluble carbodiimide-mediated coupling reactions*. Analytical biochemistry, 1986. **156**(1): p. 220-222.
-

56. Akhavan, O. and E. Ghaderi, *Toxicity of graphene and graphene oxide nanowalls against bacteria*. ACS nano, 2010. **4**(10): p. 5731-5736.
57. Pantarotto, D., et al., *Functionalized carbon nanotubes for plasmid DNA gene delivery*. Angewandte Chemie, 2004. **116**(39): p. 5354-5358.
58. Zhu, W., et al., *Nanomechanical mechanism for lipid bilayer damage induced by carbon nanotubes confined in intracellular vesicles*. Proceedings of the National Academy of Sciences, 2016. **113**(44): p. 12374-12379.
59. Li, H., et al., *Spontaneous protein adsorption on graphene oxide nanosheets allowing efficient intracellular vaccine protein delivery*. ACS applied materials & interfaces, 2016. **8**(2): p. 1147-1155.

Chapter 2

Spontaneous Protein Adsorption on Graphene Oxide Nanosheets Allows Straightforward Intracellular Vaccine Protein Delivery

Spontaneous Protein Adsorption on Graphene Oxide Nanosheets Allowing Efficient Intracellular Vaccine Protein Delivery

Hui Li,¹ Kaat Fierens,^{2, 3} Zhiyue Zhang,¹ Nane Vanparijs,¹ Martijn J. Schuijs,^{2, 3} Katleen Van Steendam,¹ Natàlia Feiner Gracia,⁴ Riet De Rycke,^{3, 5} Thomas De Beer,⁶ Ans De Beuckelaer,⁵ Stefaan De Koker,⁵ Dieter Deforce,¹ Lorenzo Albertazzi,⁴ Johan Grooten,⁵ Bart N. Lambrecht,^{2, 3} and Bruno G. De Geest^{*1}

1. Department of Pharmaceutics, Ghent University, Ottergemsesteenweg 460, 9000 Ghent, Belgium. Br.DeGeest@UGent.be.

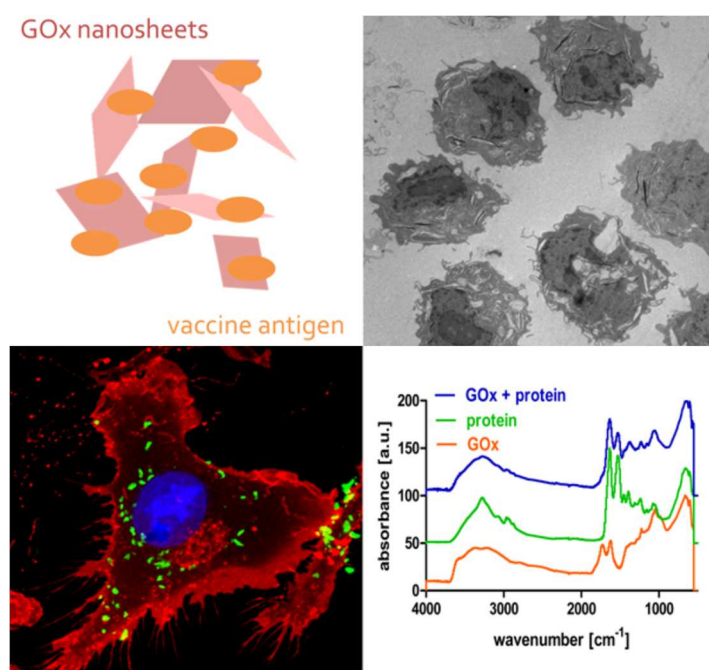
2 VIB Inflammation Research Center, Ghent University, Technologiepark 927, 9052 Zwijnaarde, Belgium

3 Department of Respiratory Medicine, University Hospital Ghent, De Pintelaan 185, 9000 Ghent, Belgium

4 Institute for Bioengineering of Catalonia, Carrer de Baldiri Reixac, 10, 08028 Barcelona, Spain

5 Department of Biomedical Molecular Biology, Ghent University, Technologiepark 927, 9052 Zwijnaarde, Belgium

6 Department of Pharmaceutical Analysis, Ghent University, Ottergemsesteenweg 460, 9000 Ghent, Belgium



ABSTRACT

Nanomaterials hold potential of altering the interaction between therapeutic molecules and target cells or tissues. High-aspect ratio nanomaterials in particular have been reported to possess unprecedented properties and are intensively investigated for their interaction with biological systems. Graphene oxide (GOx) is a water-soluble graphene derivative that combines high-aspect ratio dimension with functional groups that can be exploited for bioconjugation. Here, we demonstrate that GOx nanosheets can spontaneously adsorb proteins by a combination of interactions. This property is then explored for intracellular protein vaccine delivery, in view of the potential of GOx nanosheets to destabilize lipid membranes such as those of intracellular vesicles. Using a series of in vitro experiments, we show that GOx nanosheet adsorbed proteins are efficiently internalized by dendritic cells (DCs: the most potent class of antigen presenting cells of the immune system) and promote antigen crosspresentation to CD8 T cells. The latter is a hallmark in the induction of potent cellular antigen-specific immune responses against intracellular pathogens and cancer.

INTRODUCTION

Carbon-based nanomaterials offer a wide variety of potential applications, including those in the biomedical field. [1-4] Graphene oxide (GOx) is currently emerging as a multifunctional material, derived from graphene by oxidative treatment. [5-7] The planar structure, a water-soluble graphene derivative with a 2D atomic layer composed of crumpled sheets of sp^{2-} and sp^{3-} hybridized carbon atoms, [8-11] is enriched with oxygen-containing groups such as epoxides, hydroxyls, and carboxylic acids that render GOx its hydrophilic properties. [12-15] Graphene oxide (GOx) is known for its particularly high-aspect ratio and surface area which is almost 10-fold of other nanomaterials. [16] High-aspect ratio materials are intriguing materials with respect to their interaction with living cells as they have been reported to pierce or destabilize lipid bilayer membranes. [17] This ability has been ascribed to carbon nanotubes, [18] and recently, Tu et al. [19] reported that GOx nanosheets, which is GOx with a size of a few hundreds of nanometers in the planar direction, can destabilize the membrane of bacteria. These features could render GOx an attractive nanocarrier for intracellular delivery of therapeutic molecules. [20, 21]

In this paper, we aim at evaluating the potential of GOx nanosheets to enhance vaccine delivery efficiency. Nanomaterials hold excellent opportunities in vaccination, [22, 23] such as enhancing antigen uptake and presentation by dendritic cells (DCs) to T cells, and thereby could stimulate antigen-specific humoral and cellular immunity. [24, 25] Systems that are both of nanoparticulate nature and possess the ability to destabilize the membrane could be highly interesting. DCs are the sentinels of our immune system and continuously sample antigens that, in case these are accompanied by an appropriate “danger” signal, leads to activation of T cells and subsequently an antigen specific adaptive immune response. [26, 27] Soluble extracellular antigens, including administered vaccine antigens, are presented predominantly to CD4 T cells that play among others a role in conferring the antibody mediated humoral immune response. [28-30] However, to induce potent cellular immune responses, including the activation of cytotoxic T cells (CTLs) that can recognize and eradicate infected and malignant cells, the antigen needs to be presented to the CD8 T cells, which under normal conditions is only the case for intracellular cytoplasmic antigens. [31, 32] Thus, strategies that could delivery protein antigens into the cytoplasm of dendritic cells are of

interest for vaccination against intracellular pathogens (e.g., HIV, malaria, tuberculosis)^[33-36] and for tumor-associated antigens in view of anticancer vaccination.^[37-39] Besides this, extracellular antigens that have a particle-shape morphology can also be presented by DCs to CD8 T cells, which is called cross-presentation.^{[25], [40-42]}

In view of these considerations, we put a particular focus in this paper on investigating the interaction between GOx nanosheets and proteins and the effect on protein uptake and presentation by DCs. Contrary to several other strategies reported in the literature to bind therapeutic molecules to GOx via a linker strategy,^{[24], [43-46]} we strive in this paper to elucidate a facile method to formulate vaccine antigens with GOx without the requirement of additional reagents.

RESULTS AND DISCUSSION

GOx was prepared via a modified Hummers' method involving oxidative treatment of graphite powder.^[5-7] To produce nanosheets, the GOx suspension was extensively dialyzed until a neutral PH was reached and then ultrasonicated by a tipsonicator. To remove the fraction of nonexfoliated material, a centrifugation step at moderate force was applied and the final GOx nanosheet material was isolated in a dry state by lyophilization. This product could be readily resuspended in an aqueous medium to form a highly transparent solution, which was indicative of the presence of hydrophilic hydroxyl and carboxyl groups. Furthermore, the GOx nanosheets suspension remain colloidally stable for several days, indicating the lower micron to nanorange dimension of the material. Characterization by ATR-FTIR and AFM gave further proof of successful formation of GOx nanosheets (**Figure 1.**). The ATR-FTIR spectrum in **Figure 1.A** depicts the presence of functional groups introduced by the oxidative treatment.^[15] **Table 1.** lists the annotated peaks. AFM (**Figure 1.B**) shows the formation of sheet-like structures with planar dimensions of a few hundreds of nanometers and a thickness of a few nanometers, suggesting the presence of only a monomolecular layer.
[15], [47]

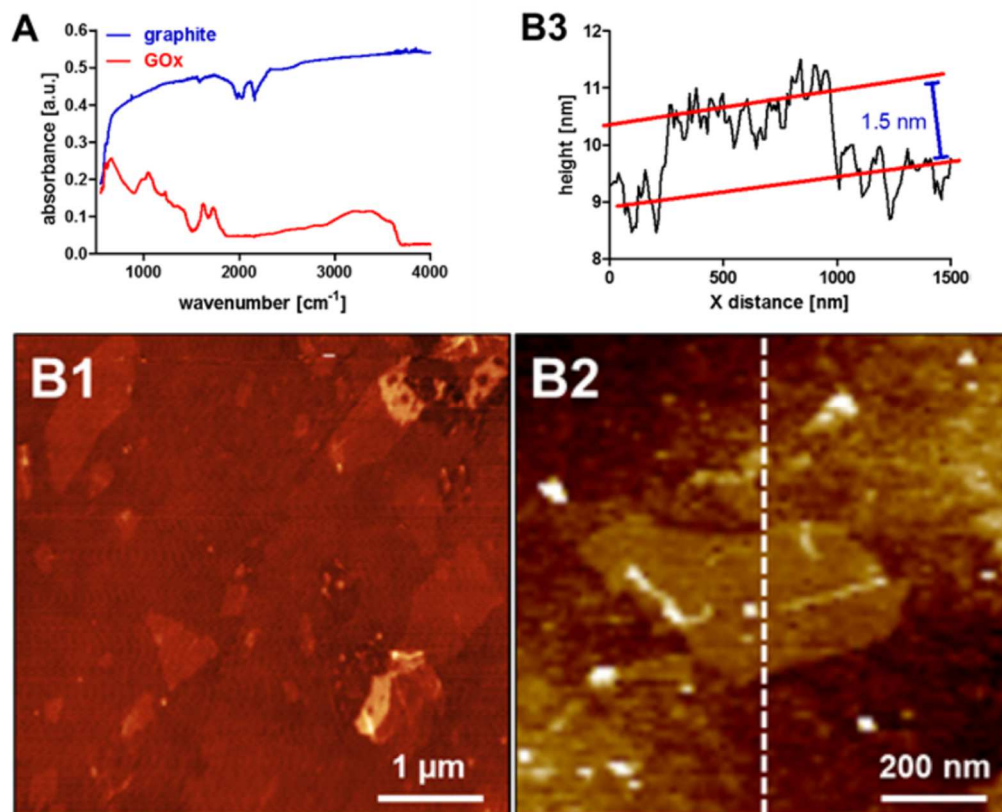


Figure 1. (A) ATR-FTIR spectrum of native graphite and GOx obtained by oxidative treatment of graphite. (B1, B2) AFM images at different magnification of GOx nanosheets and corresponding height profile (B3) along the dotted line in panel B2.

Table 1. List of functional groups in the ATR-FTIR spectrum of GOx nanosheets.

wavenumber (cm^{-1})	peak assignment
3400-2500, 1430, 950-900	-OH stretch
1740-1650	-C=O stretch
1300	-C-O
1280-1230	epoxide ring stretch
950-815	epoxide asymmetric ring deformation

Next, we aimed at investigating the interaction between the GOx nanosheets and proteins. For this purpose, we used ovalbumin (OVA) which is albumin obtained from chicken egg white. It is a 43 kDa protein with an isoelectric point of 4.3, and it is widely used as model antigen in vaccine formulation research. Its amino acid composition is listed in **Table 2.**^[48] where we have divided the amino acids into hydrophilic but neutral charged, acidic (i.e., negatively charged at neutral PH), basic (i.e., positively charged at neutrally PH), and hydrophobic. We also listed the full amino acid sequence of ovalbumin in **Table 3.** Several other groups have covalently or nonspecifically modified GOx with linker chemistry to attach proteins.^{[24], [43-46]} However, we reasoned that the presence of the remaining hydrophobic aromatic groups on the GOx surface could favor hydrophobically driven protein adsorption whereas the presence of epoxide moieties could allow covalent reaction with lysine units.

Table 2. Different Amino Acids and the number of them which contained in OVA

Hydrophilic neutral charged				Acidic negatively charged at neutral pH				Basic positively charged at neutral pH				Hydrophobic (non-polar)			
Glycine	Gly	G	19	Asparticacid	Asp	D	14	Arginine	Arg	R	15	Alanine	Ala	A	35
Serine	Ser	S	38	Glutamate	Gln	Q	15	Lysine	Lys	K	20	Valine	Val	V	31
Threonine	Thr	T	15					Histidine	His	H	7	Leucine	Leu	L	32
Cystine	Cys	C	6									Isoleucine	Ile	I	25
Tyrosine	Tyr	Y	10									Phenylalanine	Phe	F	20
Asparagine	Asn	N	17									Tryptophan	Trp	W	3
Glutamine	Glu	E	33									Methionine	Met	M	17
Proline	Pro	P	14												

Table 3. The Full Amino-Acid Sequence of Ovalbumin

1-10	11-20	21-30	31-40	41-50	51-60	61-70	71-80
MGSIGAASME	FCFDVFKELK	VHHANENIFY	CPIAIMSALA	MVYLGAKDST	RTQINKVVRV	DKLPGFGDSI	EAQCGTSVNV
81-90	91-100	101-110	111-120	121-130	131-140	141-150	151-160
HSSLRDILNQ	ITKPNDVYSF	SLASRLYAEF	RYPILPEYLQ	CVKELYRGGL	EPINFQTAAD	QARELINSWV	ESQTNGIIRN
161-170	171-180	181-190	191-200	201-210	211-220	221-230	231-240
VLQPSSVDSQ	TAMVLVNAIV	FKGLWEKAFK	DEDTQAMPFR	VTEQESKPVQ	MMYQIGLFRV	ASMASEKMKI	LELPFASGTM
241-250	251-260	261-270	271-280	281-290	291-300	301-310	311-320
SMLVLLPDEV	SGLEQLESII	NFEKLTWETS	SNVMEERKIK	VYLPRMKMEE	KYNLTSVLMA	MGITDFVSSS	ANLSGISSAE
321-330	331-340	341-350	351-360	361-370	371-380	381-386	
SLKISQAVHA	AHAEINEAGR	EVVGSAAEAGV	DAASVSEEFR	ADHPFLFCIK	HIATNAVLFF	GRCVSP	

To roughly assess this possibility, both nonultrasonicated and ultrasonicated GOx were mixed with AlexaFluor488 conjugated OVA (OVA-AF488) in a 1:1 weight ratio, centrifuged at high speed (10 min at 10,000 G), and washed with deionized water to remove unbound OVA-AF488 and imaged by confocal microscopy. The reason that we also used nonultrasonicated GOx is that its larger size affords better visualization of a full GOx flake, whereas GOx nanosheets have diffraction limited dimensions. The images in **Figure 2.** show a bright fluorescence emerging from both samples, whereas blank GOx images under the same illumination and detection settings were found to be nonfluorescent (data not shown). This provides a strong indication that OVA-AF488 is capable of spontaneously adsorbing onto GOx. Further proof of OVA adsorption on GOx nanosheets was obtained by ATR-FTIR spectroscopy. These experiments were performed using native, thus without fluorescent dye, OVA, and several washing and centrifugation steps were performed to remove unbound OVA. **Figure 3.**

depicted the ATR-FTIR spectrum of GOx~OVA in drying state after lyophilization. The characteristic bands at 1550 cm^{-1} (amide II band: C–N stretching vibration and N–H bending vibration) of OVA and 1750 cm^{-1} (–C=O stretch; left shoulder marked with green arrow in **Figure 3.A**) of GOx can be observed in the spectrum of GOx~OVA, indicating the presence of OVA on the GOx nanosheets. To investigate whether the secondary structure of OVA changes upon adsorption to GOx, we measured the circular dichroism (CD) spectrum for OVA mixed in different ratios to GOx. The reduction of the negative band at 222 nm that corresponds to α -helix formation shown **Figure 3.B** indicates that the higher the ratio of GOx to OVA, the more OVA undergoes conformation changes and possibly denaturation. Of note is that, for enhancing T cell responses, the antigen needs to be processed into peptide fragments by dendritic cells (DCs) which does not depend on the structural integrity of the concerned protein. Liquid chromatography with tandem mass spectrometry/mass spectrometry detection of trypsin-digested OVA and GOx~OVA (2:1 ratio) was used to detect differences in the peptide composition after GOx adsorption. **Figure 4.** depicts a heat map of the abundance of the peptide sequences that could be annotated by the mass spectrometer. Overall, a much lower total ion count was obtained from the GOx~OVA sample which indicates that GOx adsorption reduces to a certain extent the availability of the protein to be cleaved by trypsin (i.e., after lysine (K) and arginine (R) residues). Furthermore, significant differences in the abundance of the different peptide sequences were observed. However, it remains elusive whether this is due to covalent, hydrophobic, or other interactions between GOx and OVA.

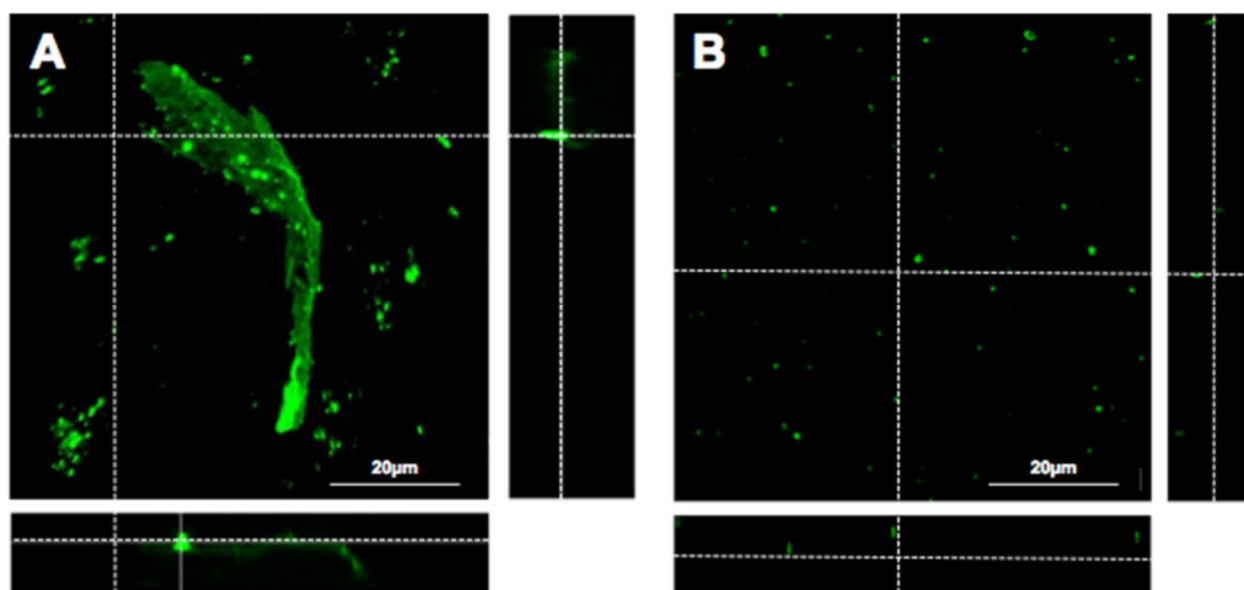


Figure 2. Confocal fluorescence microscopy images of (A) nonultrasonicated GOx and (B) ultrasonicated GOx nanosheets mixed with OVA-AF488. The main panel depicts a maximum intensity projection (MIP), with corresponding orthogonal XZ and YZ panels.

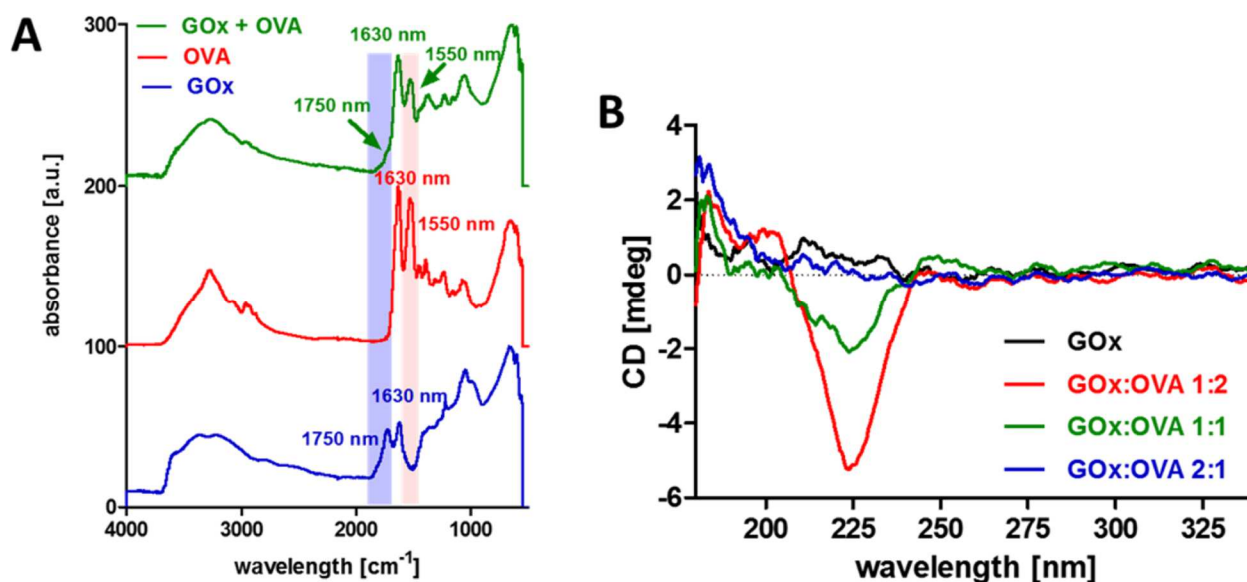


Figure 3. (A) ATR-FTIR spectra of GOx, OVA, and GOx~OVA after removal of unbound OVA. Characteristic bands of GOx and OVA are highlighted in the respective spectra. (B) CD spectrum of OVA mixed with different ratios of GOx. The OVA concentration was kept constant at 1 mg/mL.

Next, we aimed to quantify the extent of GOx~OVA adsorption and to gather insight in whether the OVA is bound with the GOx via merely electrostatic interaction or also in part by covalent interaction. GOx and OVA were mixed in different weight ratios for 24 h, and subsequently, the GOx~OVA mixture and the supernatant after centrifugation was loaded onto polyacrylamide (PAGE) gels. By applying an electric current, GOx-bound OVA is separated from unbound OVA by electrophoresis. As the samples were first mixed with sodium dodecyl sulfate (SDS), we hypothesize that, in the case of the GOx~OVA mixture, most of the electrostatic and hydrophobic bonds will be broken and the fraction that will remain bound to the GOx will be predominantly covalently bound. Optical integration of Coomassie stained gels was used to quantify the free protein content, as illustrated in **Figure 4**. As shown in **Figure 5A.**, maximal GOx~OVA adsorption is reached at a 1:1 GOx:OVA ratio, as for this ratio onward no free OVA was detected in the supernatant anymore. However, at this and even higher GOx:OVA ratio, free OVA does become detected when the GOx~OVA mixture is loaded onto the SDS-PAGE. We attribute this to a fraction of weakly bound OVA that is released from the GOx nanosheets by the SDS and/or the electric current. We also assessed the effect of incubation time on protein adsorption and found (**Figure 5.B**) that incubation times shorter than 24 h led to a decrease in protein adsorption, although saturation emerged from 4 h onward.

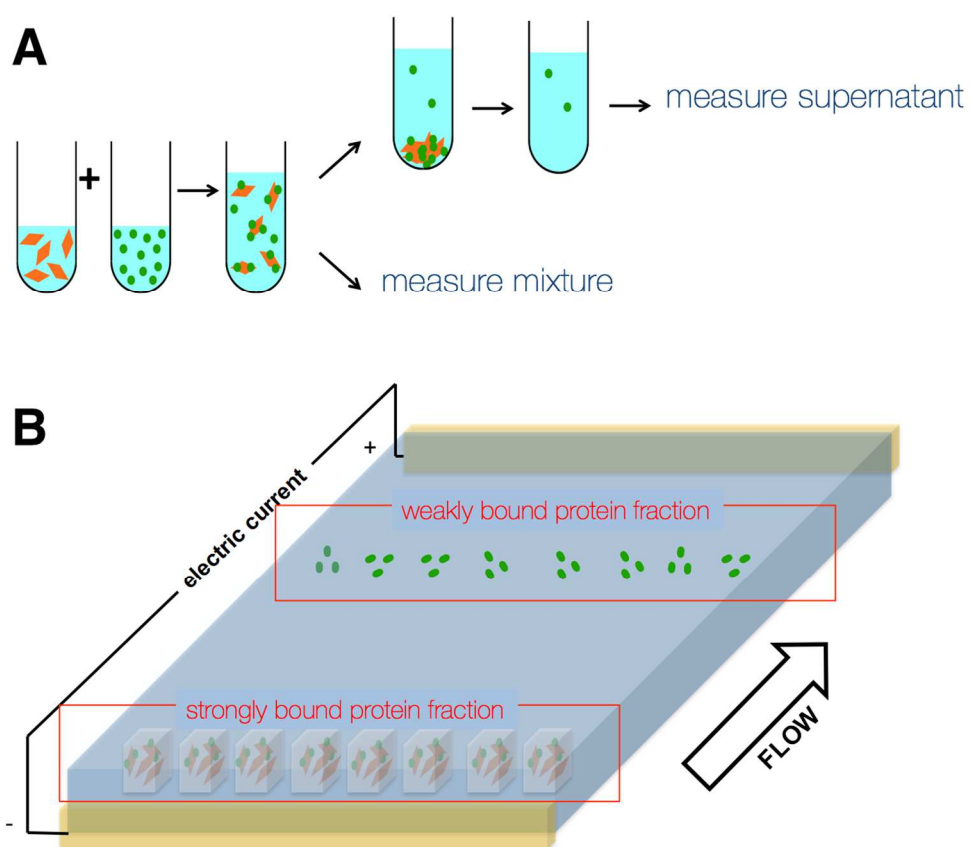


Figure 4. Schematic illustration of the procedure to measure OVA binding to GOx. (A) Sample preparation by mixing stock solution of GOx (orange sheets) and OVA (green dots), followed by sampling respectively the GOx~OVA mixture and the supernatant after centrifugation. (B) Sample analysis by SDS-PAGE. Strongly - presumably covalently - bound OVA will be retained in the wells, whereas the weakly - presumably non-covalently - bound OVA will be able to migrate in the gel due to the applied electric current.

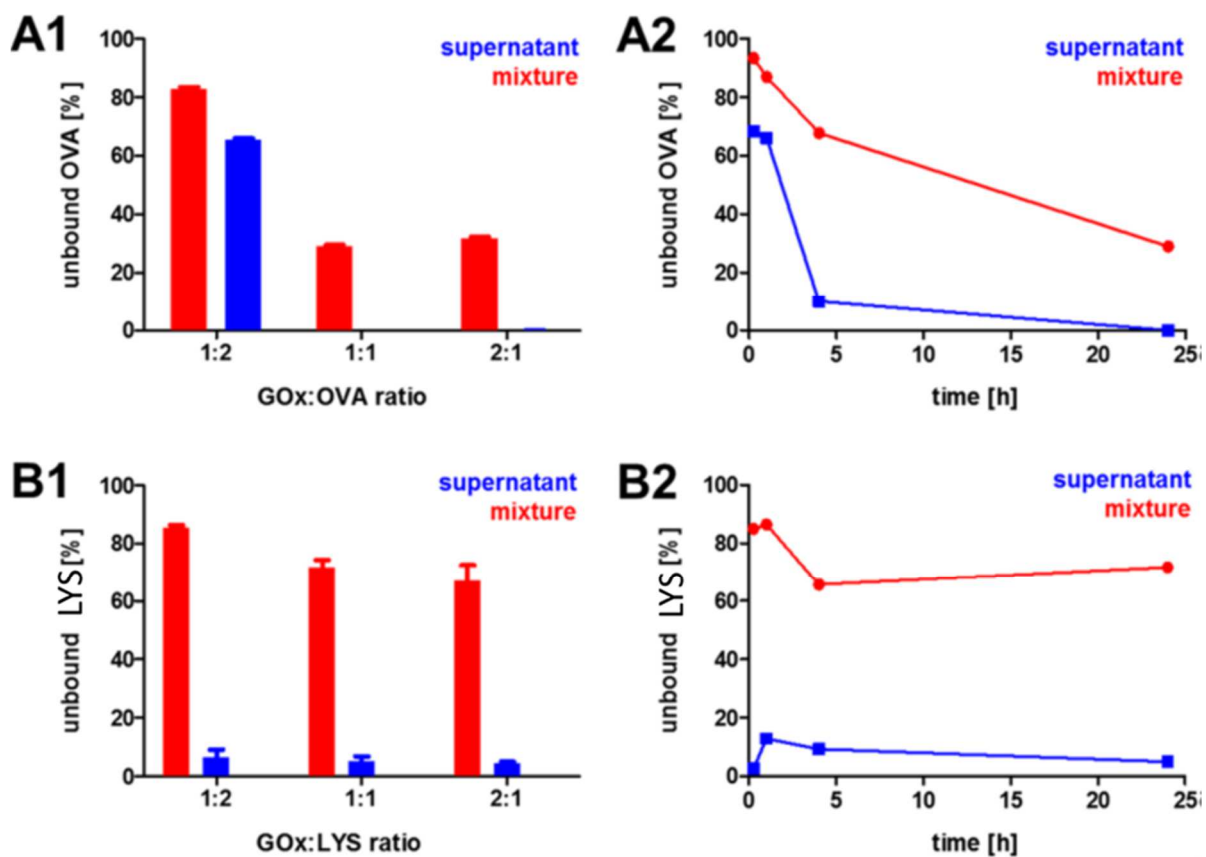


Figure 5. Adsorption efficiency of (A) OVA and (B) lysozyme to GOx nanosheets as a function of (A1, B1) the GOx:proteins weight ratio and (A2, B2) mixing time.

To verify whether the high extent of protein adsorption to GOx nanosheets is unique for OVA but also valid for other proteins, we investigated the GOx adsorption behavior of lysozyme (LYS). LYS is a 14 kDa protein with an isoelectric point of 11.35. Taking into account the negative zeta-potential of -37 ± 1 mV of GOx, LYS is expected to strongly interact with GOx through electrostatic interaction. This is confirmed by the experimental data in **Figure 5.B**, which show that, contrary to OVA, LYS is almost fully (B1) and rapidly (B2) bound to GOx at a GOx:protein ratio of 1:2. Interestingly, when analyzing the GOx~LYS mixture by SDS-PAGE, a large fraction of the LYS appears to be released from the GOx nanosheets. This suggests that the presence of the SDS can efficiently break the electrostatic interactions between LYS and GOx. Such influence of SDS on electrostatically bound macromolecules is well-known and not unexpected. However, the resilience of the GOx~OVA complexes against high surfactant concentrations is attributed to the strong nature of the interaction between both components. The nature of these interactions, however, remains elusive. On the one hand, the 20 lysine residues in OVA give more likeliness for covalent interaction with epoxy groups on the GOx surface than the 6 (of which 3 are hidden within the 3D structure) lysines residues of LYS. On the other hand, the fact that 163 out of 386 amino acid residues of OVA are hydrophobic, whereas only 44 out of 129 for LYS, might also contribute to the likeliness of hydrophobic interactions to be the driving force for GOx~OVA complexation.

In a subsequent series of experiments, we investigated the in vitro interaction between OVA-AF488 loaded GOx nanosheets and dendritic cells (DCs). For this purpose, we used the immortalized mouse dendritic cell line DC2.4. DCs were incubated overnight with GOx~(OVA-AF488) nanosheets and subsequently measured by flow cytometry. A dose-dependent cellular-association of OVA-AF488 is observed with a 1:1 ratio yielding the highest extent of cell association (**Figure 6.**). Confocal microscopy was used to investigate whether the GOx~(OVA-AF488) nanosheets were internalized by the DC or merely bound with their surface. To mark the cell membrane, we used AlexaFluor555-labeled cholera toxin subunit B (CTB-AF555) while cell nuclei were stained with Hoechst. The images in **Figure 7.** consist of a confocal section in combination with the orthogonal XZ and YZ planes and a maximum intensity projection (MIP), to provide a maximum of information. From the orthogonal planes, it is clear that the GOx~(OVA-AF488) nanosheets are located inside cells as well as stuck to

the cell membrane. Control experiments with soluble OVA yielded a punctuated pattern of green fluorescence inside the cells with no OVA being located on the cell membrane.

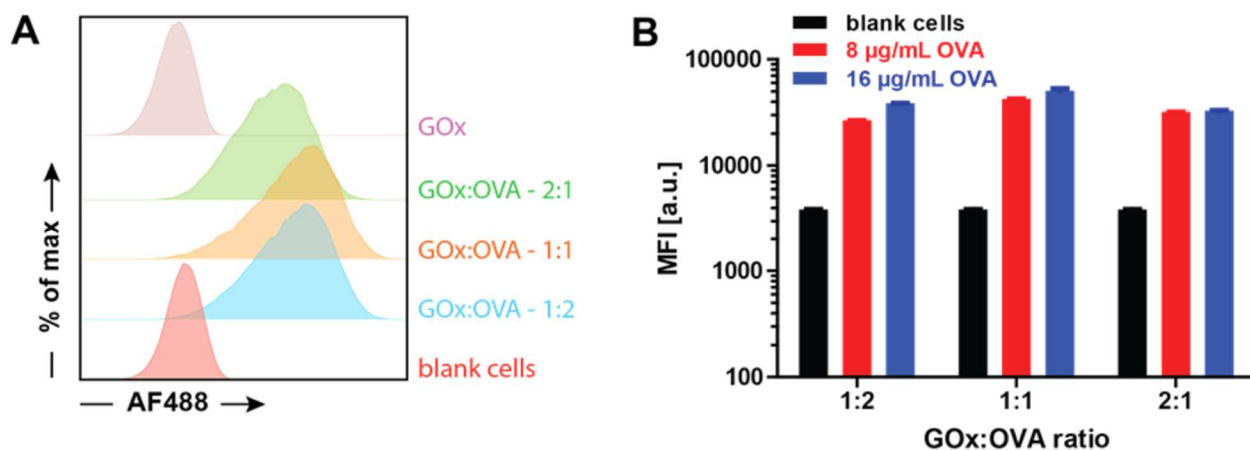


Figure 6. Flow cytometry analysis (A) histograms exemplified for 0.08 µg/mL ova and (B) mean cell fluorescence of cellular association of GOx~(OVA-AF488) after overnight incubation with different doses and ratios of GOx:OVA. Note that, for the different GOx:OVA ratios, the concentration of OVA was kept constant in the respective experiments.

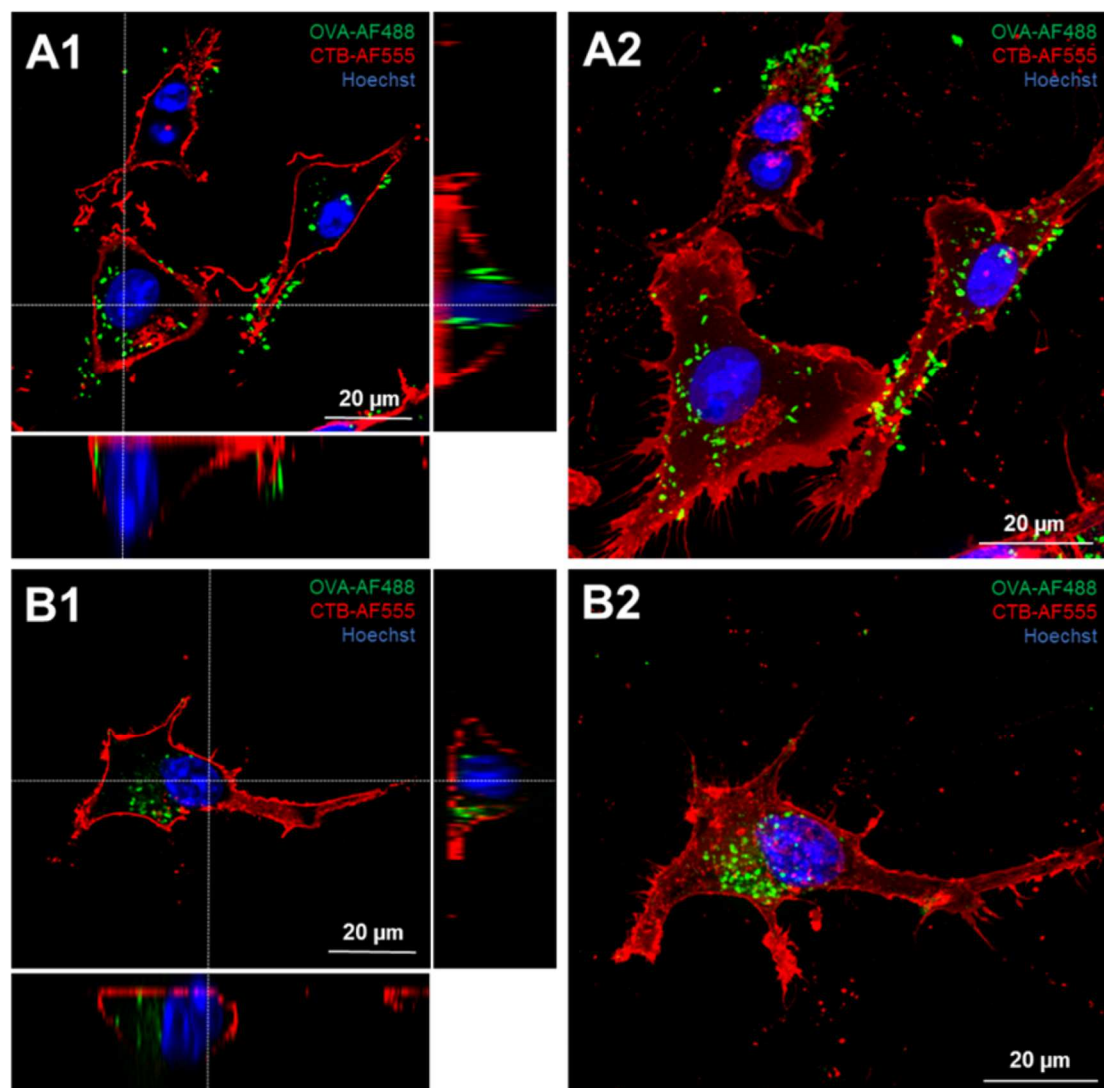


Figure 7. Confocal microscopy images of DC incubated with (A) GOx~(OVA-AF488) nanosheets and (B) soluble OVA-AF488. Cell membrane was stained red fluorescent with cholera toxin subunit B, and cell nuclei were stained with Hoechst. The left panels represent a confocal section and the corresponding orthogonal planes; the right panels represent a maximum intensity projection (MIP).

Due to the diffraction limit of light, optical microscopy does not offer sufficient resolution to investigate in detail the intracellular behavior of the GOx~OVA nanosheets; transmission electron microscopy (TEM) was performed after osmium staining and embedding of the cells in epoxy resin followed by ultramicrotomy. The resulting TEM images are shown in **Figure 8.** for DCs pulsed with GOx~OVA, whereas **Figure 9.** also depicts TEM images of blank DCs, DCs pulsed with OVA, and DCs pulsed with GOx without OVA. The panels at higher magnification in Figure 8B–D highlight the different intracellular behavior of the nanosheets that is observed for both GOx and GOx~OVA. Nanosheets are found both inside and outside vesicles; the latter ones can be endosomes or phagosomes and are also found to be piercing through vesicle membranes. This gives proof that GOx is to a certain extent capable of destabilizing endo/lysosomal membranes and thus holds the potential to promote release of a GOx-associated payload into the cytoplasm of the cell. It is also of note that even though the DCs contain fairly large amounts of nanosheets this does not have a severe effect on their morphology.

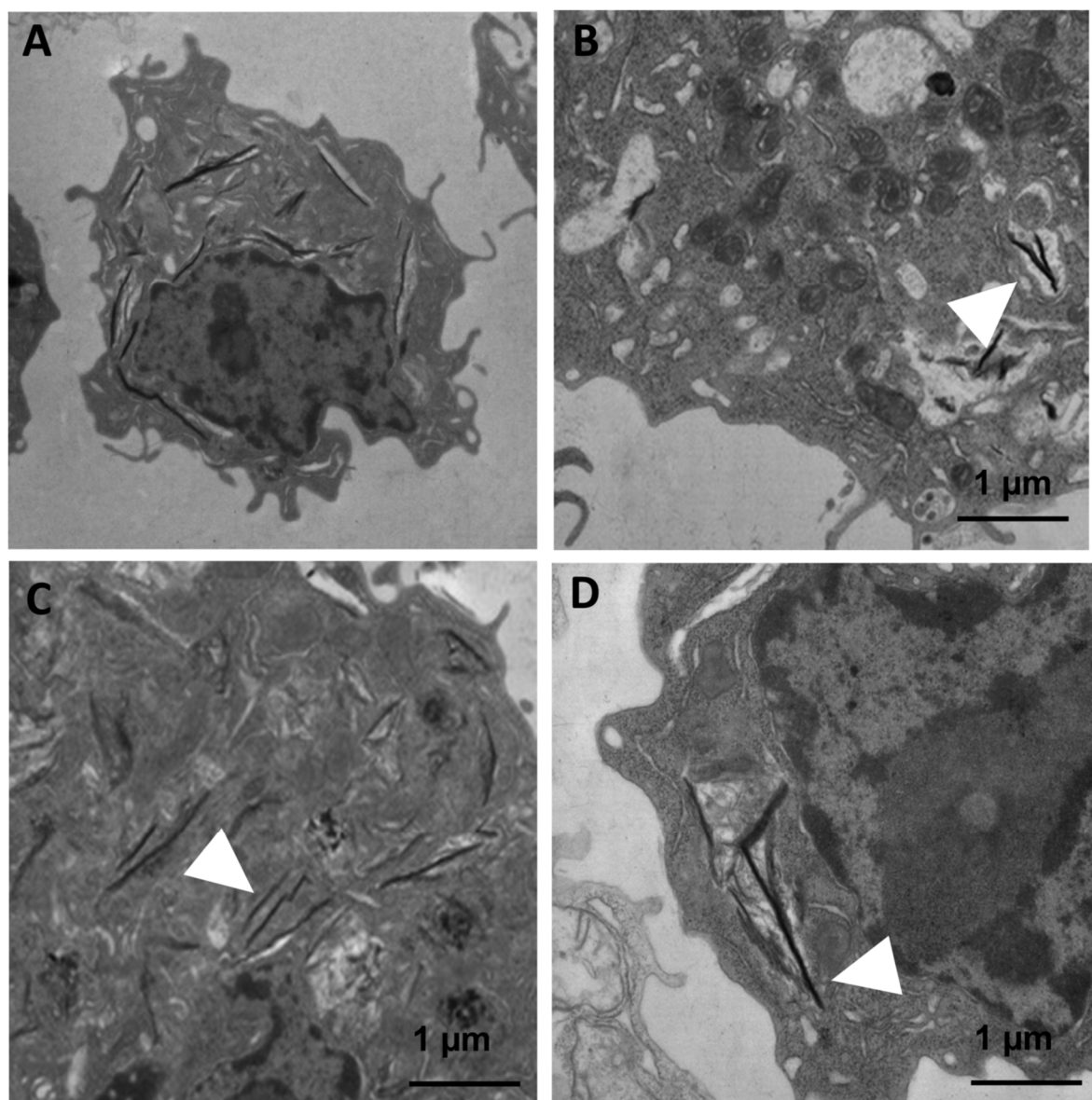


Figure 8. Transmission electron microscopy (TEM) images of DCs pulsed with incubated with GOx~OVA. (A) Overview, (B) zoomed image depicting nanosheets inside a vesicle, (C) zoomed image depicting nanosheets outside vesicles, and (D) zoomed image depicting nanosheets piercing through the membrane of a vesicle. White arrows indicate the events of interest.

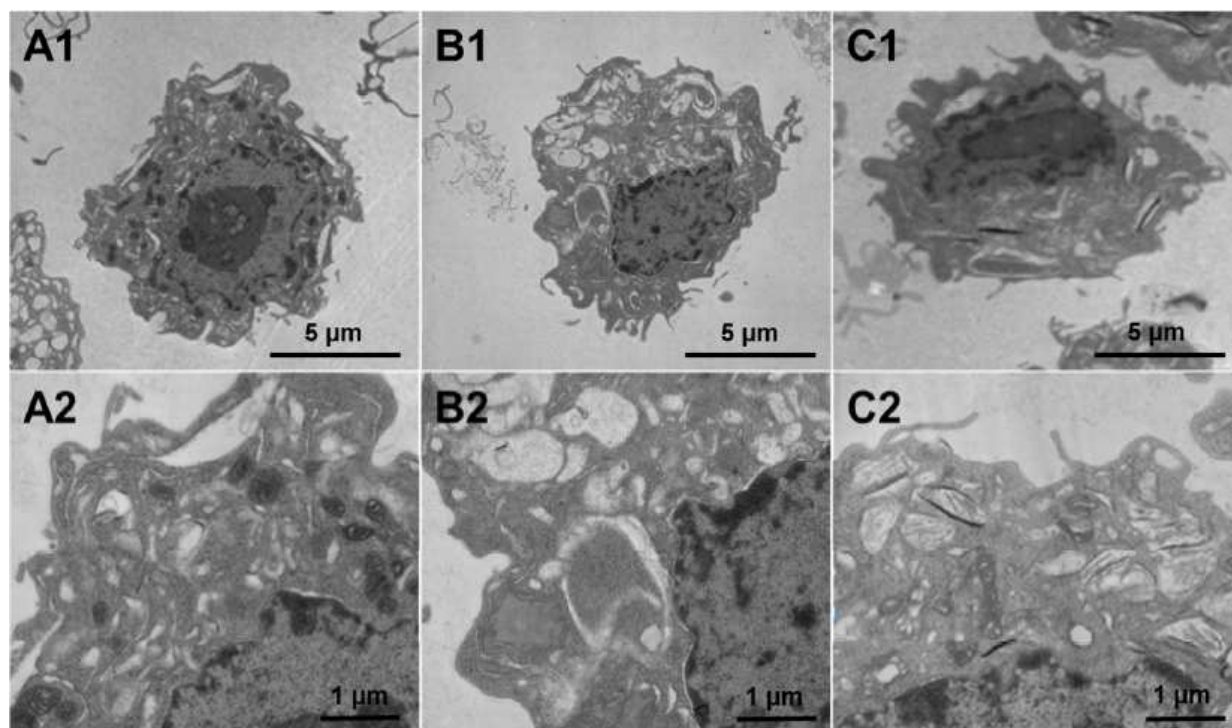


Figure 9. TEM images of blank DCs (A) and DCs pulsed with (B) OVA and (C) GOx.

Finally, we aimed to investigate the immunobiological behavior of GOx in terms of enhancing antigen presentation by DCs to CD8 T cells. First, we investigated to which extent GOx induces toxicity and maturation of DCs. For this purpose, mouse bone marrow DCs were pulsed in vitro with different concentrations of GOx, followed by flow cytometry analysis of the cell viability (**Figure 10.A**) and upregulation (**Figure 10.B**) of the surface maturation markers MHCII and CD86. GOx by itself does not lead to significant DCs activation even up to toxic concentrations, which is in line with several other studies on nanoparticulate materials that without addition of specific immune-modulating compounds (such as, e.g., Toll-like receptor ligands) do not spontaneously activate DCs.^[17] To investigate the effect of GOx on antigen presentation, mouse bone marrow derived DCs were pulsed with different concentrations of soluble OVA or GOx~OVA at different GOx:OVA ratios. Note that when preparing these samples, the OVA concentration was kept constant and the amount of GOx was varied. Subsequently, the DCs were cocultured with CFSE-labeled (CFSE: carboxyfluorescein succinimidyl ester) OT-I cells. The latter are CD8 T cells from transgenic

mice that carry the transgenic CD8 T cell receptor for the complex of MHC I with the OVA CD8 peptide epitope SIINFEKL. Upon proliferation, the CD8 T cells divide their fluorescence over their daughter cells which allows measuring cell proliferation by flow cytometry analysis. Two ratios (i.e., 1:5 and 1:20) of DCs response, on both the T cells and cytokine level. Relative to soluble OVA, T cell proliferation is increased in the case of the GOx:OVA 1:1 and GOx:OVA 2:1 formulations to a moderate extent whereas the GOx:OVA 1:2 formulation does not enhance T cell proliferation. This could suggest that the presence of an excess of GOx is favorable for enhancing antigen presentation rather than the presence of an excess of OVA. At the cytokine level (**Figure 10.C**) in the supernatant of the DC-T cell cocultures, very apparent trends can be observed, showing all three of the GOx~OVA formulations strongly promote DCs to secrete effector cytokines. These effects are not supported by large differences in proliferated T cells but are due to an enhanced capacity of the proliferating T cells to differentiate into effector T cells. The latter is an important aspect for future in vivo application of GOx-based vaccine formulations aiming for the induction of cytotoxic T cells, as has been observed in our previous work.^[23]

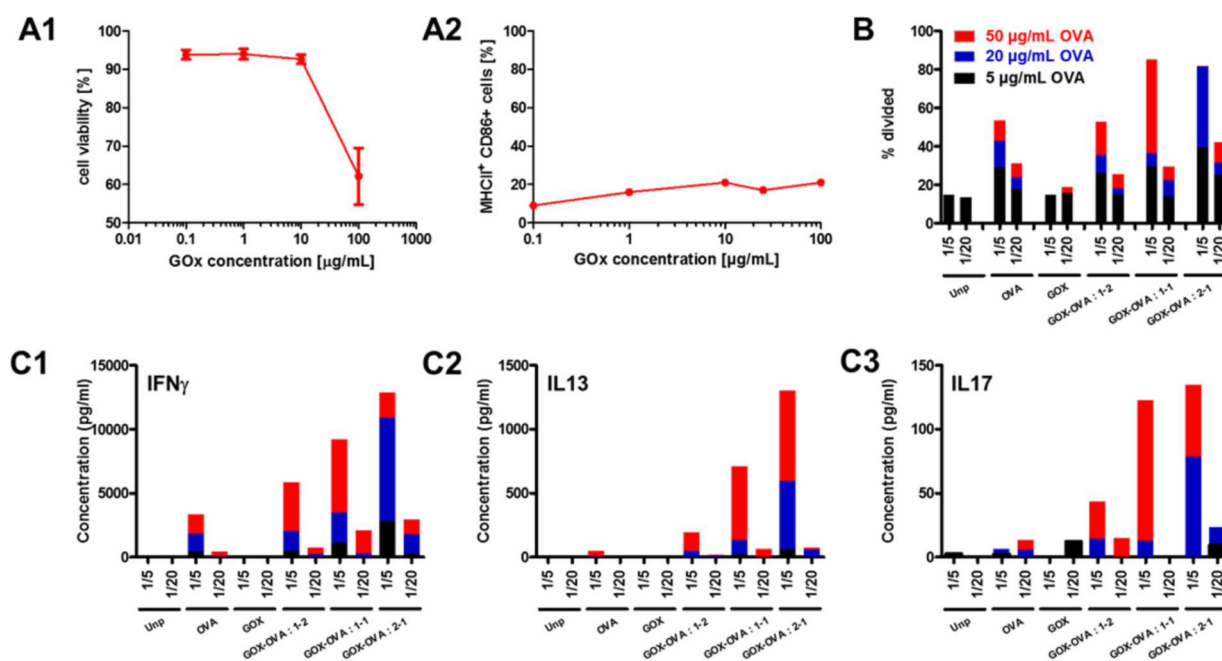


Figure 10. (A1) In vitro cell toxicity of GOx measured by flow cytometry. (A2) Dendritic cell maturation, measured by flow cytometry. (B) OVA specific CD8 T cell proliferation. (C) Cytokine (C1: IFN γ ; C2: IL13; C3: IL17) IFN γ secretion in cell culture medium measured by ELISA. The colored bars in B–C represent the level of T cell division, and respectively cytokine secretion, at that specific OVA dose.

CONCLUSIONS

In conclusion, we have shown in this paper that GOx nanosheets can be used for adsorption of proteins, without the requirement of any additional linker strategy. When bound with GOx, ovalbumin, which was used as model protein antigen in this study, could still be internalized by dendritic cells. Importantly, we demonstrated in vivo in mice that GOx adsorption strongly enhances the antigen presentation in vitro. In view of these findings, GOx nanosheets could be attractive nanocarriers for vaccine formulation. GOx adsorption could, e.g., facilitate the formulation of vaccine antigens containing hydrophobic domains that would otherwise lead to macroscopic precipitation in pure aqueous medium. In addition, GOx could also be used for coformulation of molecular adjuvants^[24] (e.g., the hydrophobic lipid derivatives MPLA and Pam-3-Cys) that can stimulate Toll-like receptors that are present on DCs and are potent stimulators of cellular immunity. These opportunities are currently being investigated in our laboratories.

Besides that, it is important to highlight the current challenges regarding the use of GOx for biomedical applications. In addition to the uncertainty on the long-term fate of GOx and possible nanotoxicity issues, important work needs to be done in standardizing GOx production, especially in obtaining GOx with reproducible dimensions. However, owing to the unique features of GOx, in particular its planar ultrathin morphology and protein-adsorbing capacity, we do believe GOx merits the effort of being further investigated for intracellular delivery applications.

EXPERIMENTAL SECTION

Materials

Graphite was purchased from PlasmaChem GmbH. Cell culture media and additives, AlexaFluor488 labeled ovalbumin (OVA-AF488), AlexaFluor555 labeled cholera toxin subunit B (CTB-AF555), Hoechst and propidium iodide were purchased from Life Technologies. 2-Mercaptoethanol, laemli sample buffer (4x), Coomassie blue stain (G-250) were purchased from Bio-rad. All other chemicals and solvents were purchased from Sigma- Aldrich. Purified Milli-Q grade water was used for all experiments.

Instrumentations and Characterizations

Attenuated Total Reflection Fourier Transform Infrared Spectroscopy (ATR-FTIR). ATR-FTIR spectra were recorded on a Thermo Scientific Nicolet IS 5 FT-IR spectrometer.

Atomic Force Microscopy (AFM).

AFM images were recorded on a Bruker Innova in dry state. The morphology of the graphene oxide nanosheets was investigated by tapping mode AFM. Air-dried films were deposited onto silicon wafers. Bruker Innova (a 100 μm scanner, a nominal spring constant of 3 N/m, and a frequency of 75 kHz) was used to obtain the samples' images in tapping mode under ambient conditions in air.

Transmission Electron Microscopy (TEM)

Carbon-coated Cu grids (200-mesh) were used in all experiments. For TEM, a drop of GOx solution or GOx~OVA solution (at different GOx:OVA ratios) were allowed to air-dry onto a grid, and visualized using 80 keV TEM (Jeol 1010, Japan).

CD Spectrometry.

CD spectra were recorded on a Jasco J-1100 CD spectrometer at a constant OVA concentration of 1 mg/mL (**Figure 11.**).

Liquid Chromatography–Mass Spectrometry/Mass Spectrometry (LC-MS/MS).

Extraction and digestion of OVA and GOx~OVA was performed as previously described.^[49] Dried peptides were dissolved in 0.1% formic acid (FA) in water (buffer A), and half of the sample was injected on a reversed phase nanoHPLC column (Pepmap C18 column 15 cm, particle size 3 μm , 0.3 mm internal diameter by 150 mm; Dionex, Sunnyvale, CA, USA) using a linear gradient of 97:3 buffer A/buffer B to 20:80 buffer A/buffer B at 300 nL min⁻¹ over 70 min (buffer B: 80% ACN/0.1% FA). The different peptides were analyzed on a TripleTOF 5600 (ABSciex, Framingham, MA, USA) in a data dependent mode. Data analysis was performed with Mascot Daemon (Matrix Science, London, UK) (peptide mass tolerance: 15 ppm; fragment mass tolerance: 0.3 Da; fixed modification: carbamidomethyl (C); variable modifications: carbamidomethyl (N-term), oxidation (M), deamidation (NQ)).

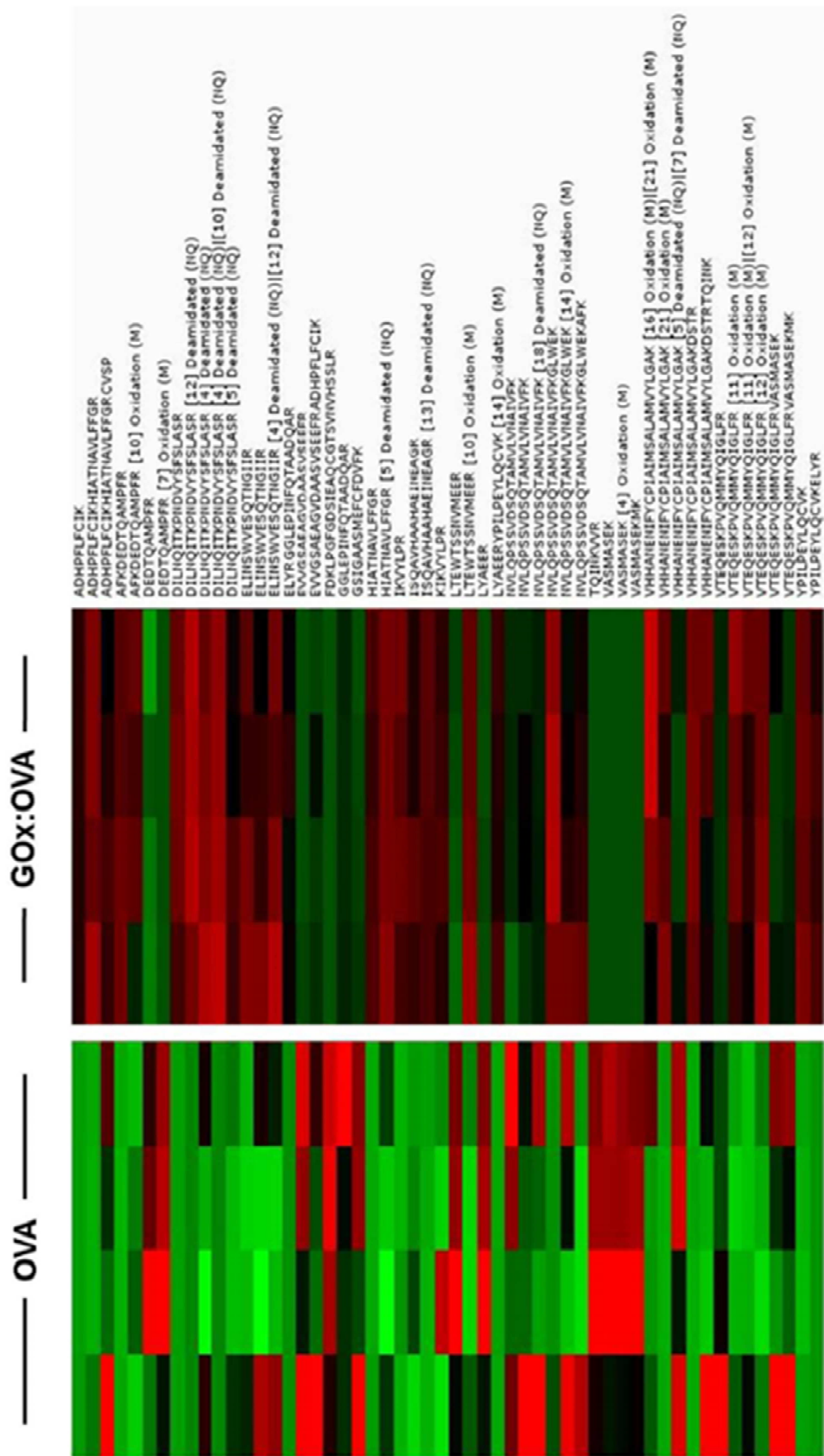


Figure 11. Heat map depicting the abundance of the respective peptide sequences detected by LCMS/MS of OVA and GOx:OVA (2:1 ratio).

Methods

Synthesis of GOx Nanosheets.

GOx was prepared by a modified Hummers' method by reacting graphite powder with the strong oxidizing agent potassium permanganate (KMnO_4) in concentrated sulfuric acid.^{[5], [50-53]} A typical procedure was as follows: 110 mg of graphite powder and 55 mg of sodium nitrate were added to 6 mL of concentrated sulfuric acid in a 50 mL round-bottomed flask which was chilled in an ice-bath to maintain the reaction temperature below 10 °C. The reaction mixture was stirred overnight. The next day, 300 mg of KMnO_4 was slowly added and the reaction mixture again was stirred overnight. During this period, the solution changed in color from black to dark green. Then, a second 300 mg portion of KMnO_4 was also slowly added and again stirred overnight. Note that all these reaction steps were performed on an ice-bath.

After that, the ice-bath was removed; the mixture was stirred for 2 h, allowed to reach room temperature, then placed in an oil-bath at 40 °C, and stirred overnight. During this period, the reaction mixture thickened and changed to a brownish-gray color. Next, 7 mL of deionized water was added dropwise under vigorous stirring and heated to 98 °C. Then, 7 mL of a 30% aqueous hydrogen peroxide solution was added, and the mixture turned to bright yellow. The oilbath was removed, and the reaction mixture was allowed to reach room temperature.

After removal of the heating source and cooling to room temperature, the mixture was centrifuged at 15 000g for 30 min. The supernatant was decanted, and the pelletized material was washed 3 times with 50 mL of 10% HCL followed by repeated washing with deionized water until the PH reached a value of 3~4. After that, the mixture was put into dialysis bags and dialyzed against deionized water for several days with repeated refreshing of the water. To obtain GOx nanosheets, the GOx was dissolved in deionized water at a 1 mg/mL concentration and tip-sonicated 4 times during 30 s at a power output of 40%. The small remaining fraction of large nonexfoliated GOx was then removed by centrifugation for 10 min at 1000g. Finally, GOx was isolated in dry form by lyophilization (**Figure 12.**).



Figure 12. Photographs of GOx nanosheets before (left) and after (right) lyophilization.

Protein Adsorption to GOx Nanosheets.

A stock solution of OVA (and OVA-AF488 in a 50:1 ratio, when using fluorescence-based assays) or LYS was prepared at a total concentration of 2 mg/mL in phosphate buffer saline (PBS). A stock solution of GOx nanosheets in deionized water was also prepared at 2 mg/mL. Different OVA~GOx formulations were prepared by mixing GOx and OVA in different ratios as listed in **Table 4.**, followed by overnight stirring.

Protein adsorption to the GOx nanosheets was assessed by polyacrylamide gel electrophoresis (SDS-PAGE). Samples were stained by a MIX (4×) buffer (β -mercaptoethanol/laemli sample buffer solution (4×) = 1:9), incubated for 5 min at 95 °C, and loaded on 10–15% precast polyacrylamide gels. Gels were run for 35 min at 180 V and then stained with Coomassie Blue (Bio-Safe Coomassie Stain, Bio-Rad). Optical integration was performed using the ImageJ software package.

Table 4. Composition of the Respective GOx~OVA Formulations

GOx:OVA	GOx stock solution (2 mg/mL), mL	OVA stock solution (2 mg/mL), mL	deionized water, mL	total volume, mL	OVA conc, mg/mL
1:2	0.5	1.0	3.5	5	0.4
1:1	1.0	1.0	3.0	5	0.4
2:1	2.0	1.0	2.0	5	0.4

In Vitro Cell Culture Experiments.

DC2.4 Cell Line. The immortalized mouse dendritic cell line DC2.4 was a kind gift from Prof. Dr. Ken Rock (Dana-Farber Cancer Institute, Boston, MA, USA). Cell culturing was done in RPMI-glutamax, supplemented with 10% FBS, 1 mM sodium pyruvate, 10 mM HEPES buffer, 0.05 mM 2-mercaptoethanol, MEM NEAM, and antibiotics (50 units/mL penicillin and 50 µg/mL streptomycin). Cells were incubated at 37 °C in a controlled, sterile environment of 95% relative humidity and 5% CO₂.

Cell Uptake Studies.

DC2.4 cells were pulsed overnight with GOx~OVA nanosheets containing OVA-AF488 and subsequently analyzed by flow cytometry and confocal microscopy. Flow cytometry was performed on a BD Accuri C6 flow cytometer, and data were processed using the FlowJo software package. For confocal microscopy, cells were fixated with paraformaldehyde; cell nuclei were stained with Hoechst, and the cell membrane stained with CTB-AF555, both

according to the supplier's instructions. Images were recorded on a Leica DMI6000B inverted microscope equipped with a 63× (1.4 NA) oil immersion objective and connected to an Andor DSD2 confocal scanner.^[49] For transmission electron microscopy (TEM), cells were fixated in paraformaldehyde and glutaraldehyde and stained with osmium tetrachloride. Subsequently, the samples were embedded in epoxy matrix and ultramicrotomed. Images were recorded on a Jeol JEM 1010.

CD8 T Cell Presentation Assay.

Mouse bone marrow derived DCs were pulsed with different concentrations of soluble OVA and GOx~OVA formulations and subsequently cocultured with OVA specific transgenic CD8 T cells, according to previous protocols.^[49]

REFERENCES

1. Cha, C.Y., et al., *Carbon-Based Nanomaterials: Multifunctional Materials for Biomedical Engineering*. ACS Nano, 2013. **7**(4): p. 2891-2897.
2. Bianco, A., K. Kostarelos, and M. Prato, *Opportunities and challenges of carbon-based nanomaterials for cancer therapy*. Expert Opinion on Drug Delivery, 2008. **5**(3): p. 331-342.
3. Chung, C., et al., *Biomedical Applications of Graphene and Graphene Oxide*. Acc Chem Res, 2013. **46**(10): p. 2211-2224.
4. Jiang, T.Y., et al., *Furin-Mediated Sequential Delivery of Anticancer Cytokine and Small-Molecule Drug Shuttled by Graphene*. Advanced Materials, 2015. **27**(6): p. 1021-1028.
5. Hummers, W.S. and R.E. Offeman, *Preparation of Graphitic Oxide*. J Am Chem Soc, 1958. **80**(6): p. 1339-1339.
6. Kim, H.W., et al., *Selective Gas Transport Through Few-Layered Graphene and Graphene Oxide Membranes*. Science, 2013. **342**(6154): p. 91-95.
7. Zhu, Y.W., et al., *Graphene and Graphene Oxide: Synthesis, Properties, and Applications*. Advanced Materials, 2010. **22**(46): p. 5226-5226.
8. Kim, F., L.J. Cote, and J.X. Huang, *Graphene Oxide: Surface Activity and Two-Dimensional Assembly*. Advanced Materials, 2010. **22**(17): p. 1954-1958.
9. Mkhoyan, K.A., et al., *Atomic and Electronic Structure of Graphene-Oxide*. Nano Lett, 2009. **9**(3): p. 1058-1063.
10. Hirata, M., et al., *Thin-film particles of graphite oxide 1: High-yield synthesis and flexibility of the particles*. Carbon, 2004. **42**(14): p. 2929-2937.
11. Liu, Z.B., et al., *Ultrafast Dynamics and Nonlinear Optical Responses from $sp(2)$ - and $sp(3)$ -Hybridized Domains in Graphene Oxide*. Journal of Physical Chemistry Letters, 2011. **2**(16): p. 1972-1977.
12. Nakajima, T., A. Mabuchi, and R. Hagiwara, *A new structure model of graphite oxide*. Carbon, 1988. **26**(3): p. 357-361.
13. Dreyer, D.R., et al., *The chemistry of graphene oxide*. Chemical Society Reviews, 2010. **39**(1): p. 228-240.
14. Titelman, G., et al., *Characteristics and microstructure of aqueous colloidal dispersions of graphite oxide*. Carbon, 2005. **43**(3): p. 641-649.

15. Sydlik, S.A., et al., *In vivo compatibility of graphene oxide with differing oxidation states*. ACS nano, 2015. **9**(4): p. 3866-3874.
16. Sanchez, V.C., et al., *Biological interactions of graphene-family nanomaterials: an interdisciplinary review*. Chemical research in toxicology, 2011. **25**(1): p. 15-34.
17. Akhavan, O. and E. Ghaderi, *Toxicity of graphene and graphene oxide nanowalls against bacteria*. ACS nano, 2010. **4**(10): p. 5731-5736.
18. Pantarotto, D., et al., *Functionalized carbon nanotubes for plasmid DNA gene delivery*. Angewandte Chemie, 2004. **116**(39): p. 5354-5358.
19. Tu, Y., et al., *Destructive extraction of phospholipids from Escherichia coli membranes by graphene nanosheets*. Nature nanotechnology, 2013. **8**(8): p. 594-601.
20. Hu, W., et al., *Graphene-based antibacterial paper*. ACS nano, 2010. **4**(7): p. 4317-4323.
21. Liu, S., et al., *Antibacterial activity of graphite, graphite oxide, graphene oxide, and reduced graphene oxide: membrane and oxidative stress*. ACS nano, 2011. **5**(9): p. 6971-6980.
22. Zaman, M., M.F. Good, and I. Toth, *Nanovaccines and their mode of action*. Methods, 2013. **60**(3): p. 226-231.
23. Gill, P., *Nanocarriers, nanovaccines, and nanobacteria as nanobiotechnological concerns in modern vaccines*. Scientia Iranica, 2013. **20**(3): p. 1003-1013.
24. Cao, Y., et al., *Ultrasmall graphene oxide supported gold nanoparticles as adjuvants improve humoral and cellular immunity in mice*. Advanced Functional Materials, 2014. **24**(44): p. 6963-6971.
25. Li, H., et al., *Alpha-alumina nanoparticles induce efficient autophagy-dependent cross-presentation and potent antitumour response*. Nature nanotechnology, 2011. **6**(10): p. 645-650.
26. Banchereau, J. and R.M. Steinman, *Dendritic cells and the control of immunity*. Nature, 1998. **392**(6673): p. 245-252.
27. Palucka, K. and J. Banchereau, *Cancer immunotherapy via dendritic cells*. Nature Reviews Cancer, 2012. **12**(4): p. 265-277.
28. Dierendonck, M., et al., *Facile Two-Step Synthesis of Porous Antigen-Loaded Degradable Polyelectrolyte Microspheres*. Angewandte Chemie International Edition, 2010. **49**(46): p. 8620-8624.

-
29. Novak, E.J., et al., *MHC class II tetramers identify peptide-specific human CD4+ T cells proliferating in response to influenza A antigen*. Journal of Clinical Investigation, 1999. **104**(12): p. R63.
 30. Burgdorf, S., et al., *Distinct pathways of antigen uptake and intracellular routing in CD4 and CD8 T cell activation*. science, 2007. **316**(5824): p. 612-616.
 31. Cavanagh, L.L. and U.H. Von Andrian, *Travellers in many guises: the origins and destinations of dendritic cells*. Immunology and cell biology, 2002. **80**(5): p. 448-462.
 32. Bennett, S.R., et al., *Help for cytotoxic-T-cell responses is mediated by CD40 signalling*. Nature, 1998. **393**(6684): p. 478-480.
 33. Riddell, S.R., et al., *T-cell mediated rejection of gene-modified HIV-specific cytotoxic T lymphocytes in HIV-infected patients*. Nature medicine, 1996. **2**(2): p. 216-223.
 34. Schneider, J., et al., *Enhanced immunogenicity for CD8+ T cell induction and complete protective efficacy of malaria DNA vaccination by boosting with modified vaccinia virus Ankara*. Nature medicine, 1998. **4**(4): p. 397-402.
 35. Flynn, J.L., et al., *Major histocompatibility complex class I-restricted T cells are required for resistance to Mycobacterium tuberculosis infection*. Proceedings of the National Academy of Sciences, 1992. **89**(24): p. 12013-12017.
 36. Lalvani, A., et al., *Human cytolytic and interferon γ -secreting CD8+ T lymphocytes specific for Mycobacterium tuberculosis*. Proceedings of the National Academy of Sciences, 1998. **95**(1): p. 270-275.
 37. Luo, Y., et al., *Targeting tumor-associated macrophages as a novel strategy against breast cancer*. The Journal of clinical investigation, 2006. **116**(8): p. 2132.
 38. Akondy, R.S., et al., *Initial viral load determines the magnitude of the human CD8 T cell response to yellow fever vaccination*. Proceedings of the National Academy of Sciences, 2015. **112**(10): p. 3050-3055.
 39. Yoon, H.J., et al., *Sensitive capture of circulating tumour cells by functionalized graphene oxide nanosheets*. Nature nanotechnology, 2013. **8**(10): p. 735-741.
 40. De Koker, S., R. Hoogenboom, and B.G. De Geest, *Polymeric multilayer capsules for drug delivery*. Chemical Society Reviews, 2012. **41**(7): p. 2867-2884.
 41. Jensen, P.E., *Recent advances in antigen processing and presentation*. Nature immunology, 2007. **8**(10): p. 1041-1048.
 42. Heath, W.R. and F.R. Carbone, *Cross-presentation, dendritic cells, tolerance and immunity*. Annual review of immunology, 2001. **19**(1): p. 47-64.
-

43. Liu, J., et al., *Toward a universal "adhesive nanosheet" for the assembly of multiple nanoparticles based on a protein-induced reduction/decoration of graphene oxide*. Journal of the American Chemical Society, 2010. **132**(21): p. 7279-7281.
44. Hung, A.H., et al., *Graphene oxide enhances cellular delivery of hydrophilic small molecules by co-incubation*. ACS nano, 2014. **8**(10): p. 10168-10177.
45. Lin, D. and B. Xing, *Tannic acid adsorption and its role for stabilizing carbon nanotube suspensions*. Environmental science & technology, 2008. **42**(16): p. 5917-5923.
46. Wang, H., et al., *Graphene oxide-peptide conjugate as an intracellular protease sensor for caspase-3 activation imaging in live cells*. Angewandte Chemie International Edition, 2011. **50**(31): p. 7065-7069.
47. McGrail, B.T., B.J. Rodier, and E. Pentzer, *Rapid functionalization of graphene oxide in water*. Chemistry of Materials, 2014. **26**(19): p. 5806-5811.
48. Nisbet, A.D., et al., *The complete amino-acid sequence of hen ovalbumin*. The FEBS Journal, 1981. **115**(2): p. 335-345.
49. Dierendonck, M., et al., *Nanoporous hydrogen bonded polymeric microparticles: facile and economic production of cross presentation promoting vaccine carriers*. Advanced Functional Materials, 2014. **24**(29): p. 4634-4644.
50. Dikin, D.A., et al., *Preparation and characterization of graphene oxide paper*. Nature, 2007. **448**(7152): p. 457-460.
51. Xu, Y., et al., *Flexible graphene films via the filtration of water-soluble noncovalent functionalized graphene sheets*. Journal of the American Chemical Society, 2008. **130**(18): p. 5856-5857.
52. Mohanty, N. and V. Berry, *Graphene-based single-bacterium resolution biodevice and DNA transistor: interfacing graphene derivatives with nanoscale and microscale biocomponents*. Nano letters, 2008. **8**(12): p. 4469-4476.
53. Marcano, D.C., et al., *Improved synthesis of graphene oxide*. 2010.

PART III

Polymer-Modified Inorganic Nanomaterials

--- The Gold NR/PolyHPMA -Glycolamide

Chapter 3

A Synthetic Transiently Thermoresponsive Homopolymer with UCST Behavior within A Physiologically Relevant Window

A Synthetic Transiently Thermoresponsive Homopolymer with UCST Behavior within a Physiologically Relevant Window

Zhiyue Zhang,¹ Hui Li,¹ Sabah Kasmi,¹ Simon Van Herck,¹ Lutz Nuhn,¹ Riet De Rycke,² Richard Hoogenboom,³ Bruno G. De Geest^{*1}

1 Department of Pharmaceutics, Ghent University, Ottergemsesteenweg 460, 9000 Ghent, Belgium. Br.DeGeest@UGent.be.

2 IRC-UGent/VIB. Technologiepark 927, 9052 Gent, Belgium.

3 Supramolecular Chemistry Group, Department of Organic and Macromolecular Chemistry, Ghent University, Krijgslaan 281-S4, 9000 Ghent, Belgium.

ABSTRACT

Transiently thermoresponsive polymers that exhibit a soluble-insoluble switch in response to temperature, but gradually lose this property in response to a hydrolysis reaction have been widely reported for polymers with LCST behavior. However, transiently responsive polymers with UCST behavior in a relevant context are fairly unexplored. Here, we design such polymers by modification of poly(N-hydroxypropylmethacrylamide) with primary amide moieties that are capable to form strong hydrogen bonds, through a hydrolysable carbonate ester linkage. The resulting polymer reveals UCST behavior with a clearance temperature of 42° C in aqueous medium. Hydrolysis of the carbonate esters in the polymer side chains, over time at physiological conditions or accelerated by an external trigger such as NIR light in presence of gold nanorods, alleviates the UCST transition temperature, yielding fully soluble polymers at physiological conditions.

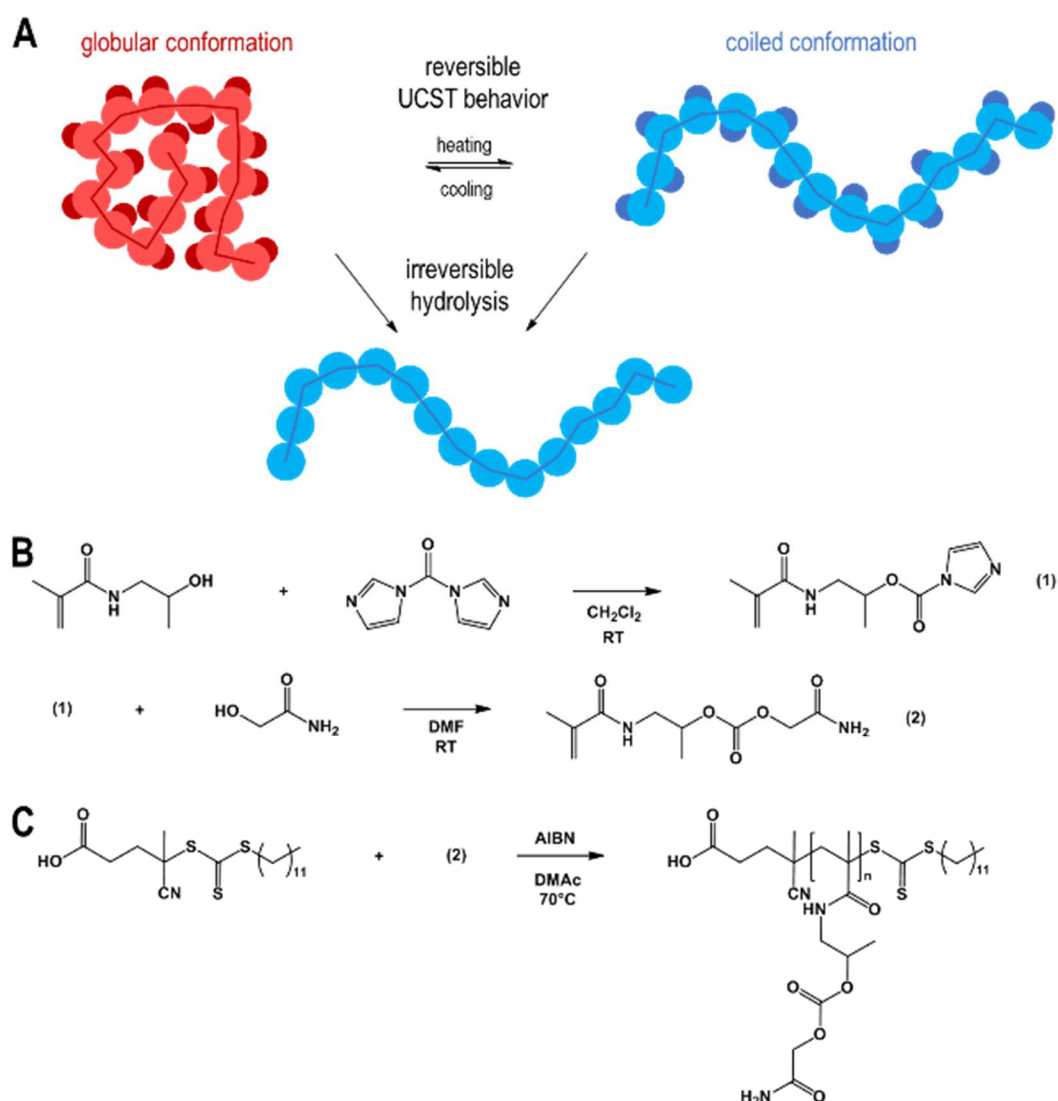
CONTENT

Stimuli-responsive polymers, also called ‘smart polymers’, respond to chemical or physical changes by a change in solution behavior.^[1-3] This unique property has fuelled the interest in these materials for a number of applications, including drug delivery, tissue engineering, separation, catalysis, sensors, etc...^[4-9] Amongst the most intensively studied stimuli-responsive polymers are those that exhibit lower critical solution temperature (LCST) behavior.^[10, 11] Such polymers are soluble at low temperature due to extensive hydrogen bonding with the surrounding water molecules and subsequent hindered polymer-polymer interactions, but become insoluble above the LCST at which these hydrogen bonds are disrupted due to entropic reasons and polymer-polymer interactions are favored leading to phase separation.^[12-15]

Compared to LCST behavior, upper critical solution temperature (UCST) behavior involves polymers being water-insoluble below the UCST and soluble above the UCST.^[16] Unlike their LCST counterparts, polymers that exhibit UCST behavior in fully aqueous environment – i.e. without the requirement of co-solvents – and which exhibit a globule-to-coil transformation close to the physiological temperature of 37 °C – could be attractive for biomedical applications, but are much less reported.^[17] Generally, UCST polymers exhibit thermoresponsiveness on the basis of cohesive enthalpic interactions between polymer chains, such as hydrogen bonds and electrostatic interactions.^[18, 19]

The latter are commonly based on polybetaines or zwitterionic polymers that lose their UCST behavior in physiological media due to screening of the electrostatic charges. Therefore, most examples of UCST polymers operating within a physiologically relevant context are based on hydrogen bond formation between amide- or urea-based repeating units in the polymer backbone.^[20, 21] Furthermore, a certain degree of hydrophobicity should be present along the polymer chain, too. In this regard, polymers containing acrylamide, acrylonitrile moieties and in particular poly(N-acryloyl glycinamide) have mostly been studied.^[22-24] However, biomedical applications require polymeric materials to be degraded into water-soluble products that can be cleared from the body. Whereas gelatin is a good example of a degradable natural macromolecular UCST system,^[25] degradable synthetic UCST systems that operate within a

physiological window are extremely rare and only a few examples have been reported. Very recent work by Wurm et al. introduced an interesting class of phosphonate based copolymers that show UCST behavior in acid condition and degradability in alkaline condition.^[26] However, due to the presence of ionizable groups these polymers cannot exhibit UCST behavior at physiological PH.



Scheme 1. Transiently responsive UCST polymers. (A) Schematic representation of polymers that undergo a reversible temperature-induced coil to globule transition by UCST behavior and can irreversibly hydrolyze into fully water-soluble polymers. (B) Synthesis of HPMA-GA via CDI activation of HPMA. (C) Synthesis of poly(HPMA-GA) by RAFT polymerization.

In this study we choose poly(*N*-(2-hydroxypropyl) methacrylamide) (poly(HPMA)) as a polymeric scaffold owing to its biocompatible and non-immunogenic nature,^[27, 28] and modified the hydroxyl-position with glycolamide through a degradable carbonate ester linkage. We reasoned that the resulting carbonate ester bond would contribute to both increased hydrophobicity and hydrogen bond formation, whereas the pending primary amide bond would be available for hydrogen bonding. Importantly, hydrolysis of the carbonate ester linkage should result in unmodified poly(HPMA) and loss of responsive behavior, i.e. water solubility (**Scheme 1A.**). The monomer synthesis is depicted in Scheme 1B, and is based on an utilization of our recently reported strategy for hydrophobic modification of HPMA.^[29] In a first step, HPMA is activated with 1,1'-carbonyldiimidazole and, after purification, reacted with glycolamide. To avoid the formation of unwanted side-products by Michael-type addition between the methacrylamide moiety and the nucleophilic amine of the imidazole by-product, only twice excess of glycolamide was used. After careful purification by silica gel column chromatography, successful synthesis of HPMA-GA (note that GA refers to glycolamide) was evidenced by ¹H, ¹³C, COSY, HSQC NMR and ESI mass spectroscopy (**Figure 1.-5.**).

Next, we performed the polymerization of monomer 2 by reversible addition-fragmentation chain transfer (RAFT) polymerization targeting a degree of polymerization (DP) of 50 using 4-cyano-4-[(dodecylsulfanylthiocarbonyl)sulfanyl]pentanoic acid as chain transfer agent (CTA) and azobisisobutyronitrile (AIBN) as radical source (Scheme 1C). Triple precipitation of the resulting polymer into cold acetone, in which both CTAs as well as unreacted monomer of HPMA-GA are soluble but poly(HPMA-GA) is not, afforded the isolation of the pure polymer, as shown by ¹H-NMR spectroscopy (**Figure 6.**) and size exclusion chromatography (SEC) (**Figure 7.**). SEC also revealed a narrow molar mass distribution of 1.21 indicating good control over the polymerization reaction. **Table 1.** summarizes the properties of the obtained polymer.

Table 1. Synthesis and structural details of poly(HPMA-GA).

sample	[M]:[CTA]:[AIBN]	Temperature [°C]	Reaction time [h]	Conversion [%]	Mn [kg/mol]	\bar{D}
poly(HPMA-GA)	50:1:0.2	70	70	75	8.0	1.21

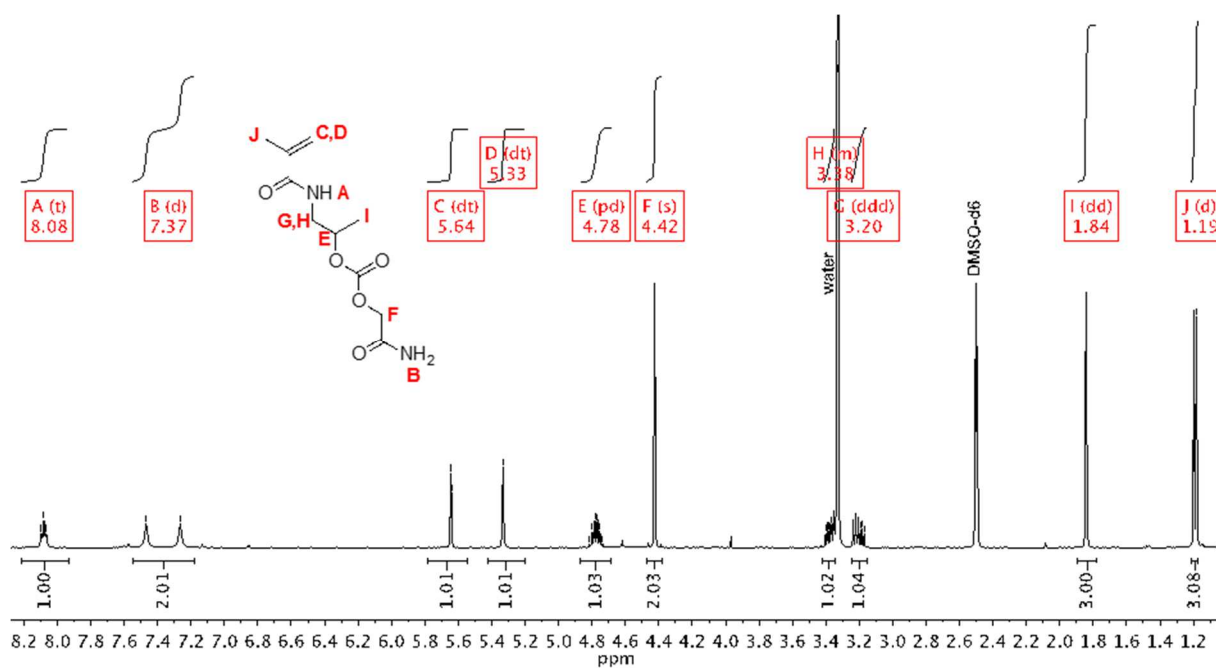


Figure 1. ¹H-NMR (400 MHz, DMSO-d₆) of HPMA-GA.

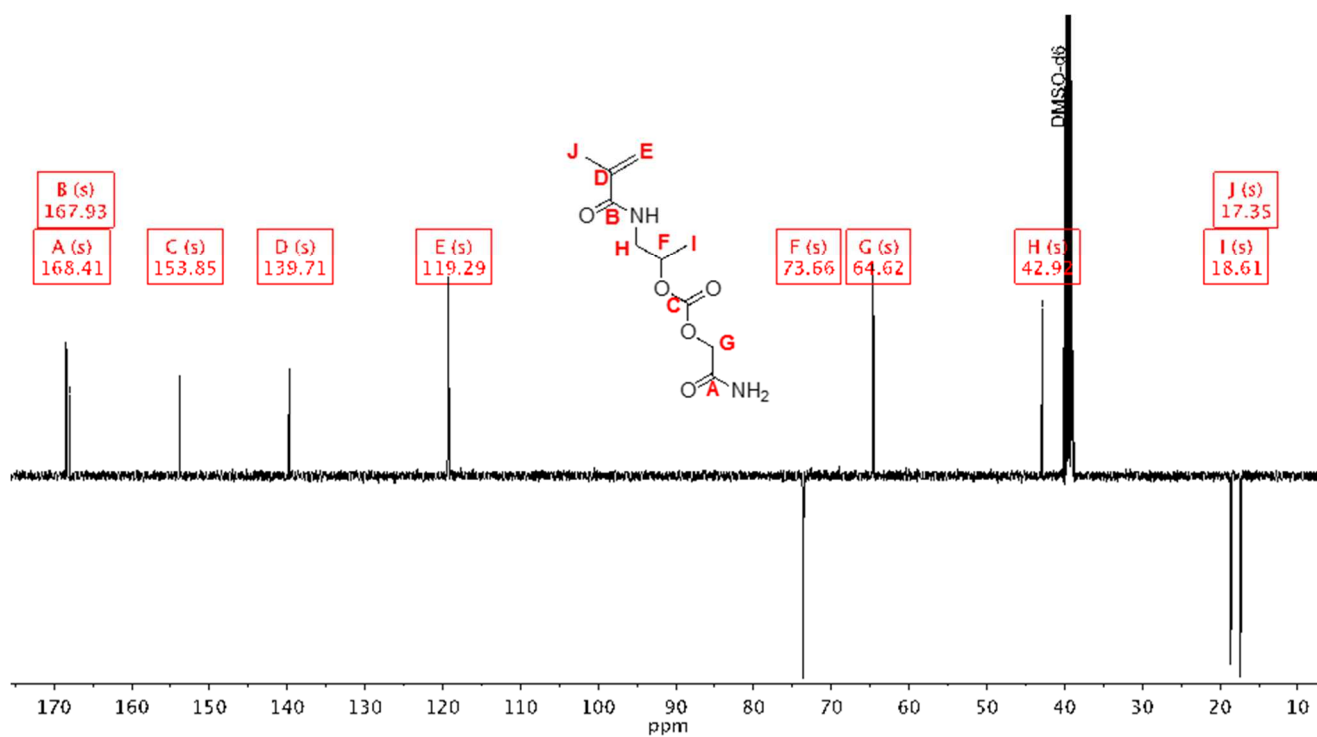


Figure 2. ¹³C-APT-NMR (100 MHz, DMSO-d₆) of HPMA-GA.

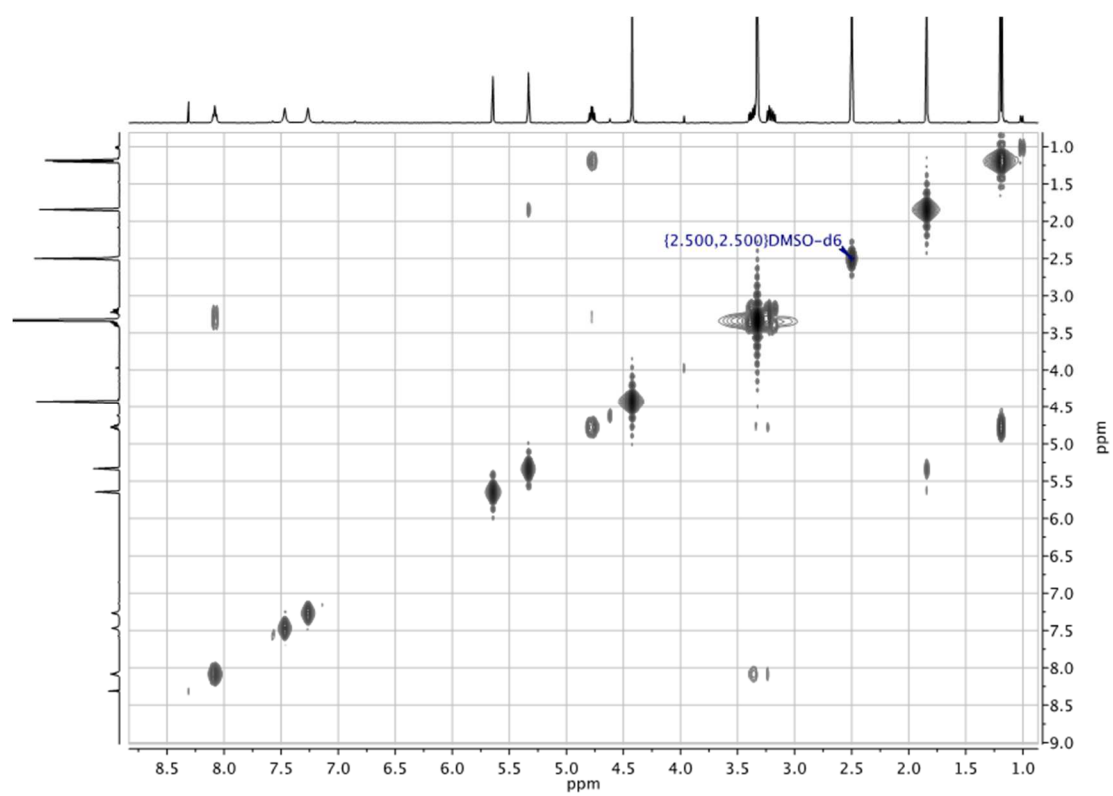


Figure 3. $^1\text{H},^1\text{H}$ -COSY-NMR (DMSO- d_6) of HPMA-GA.

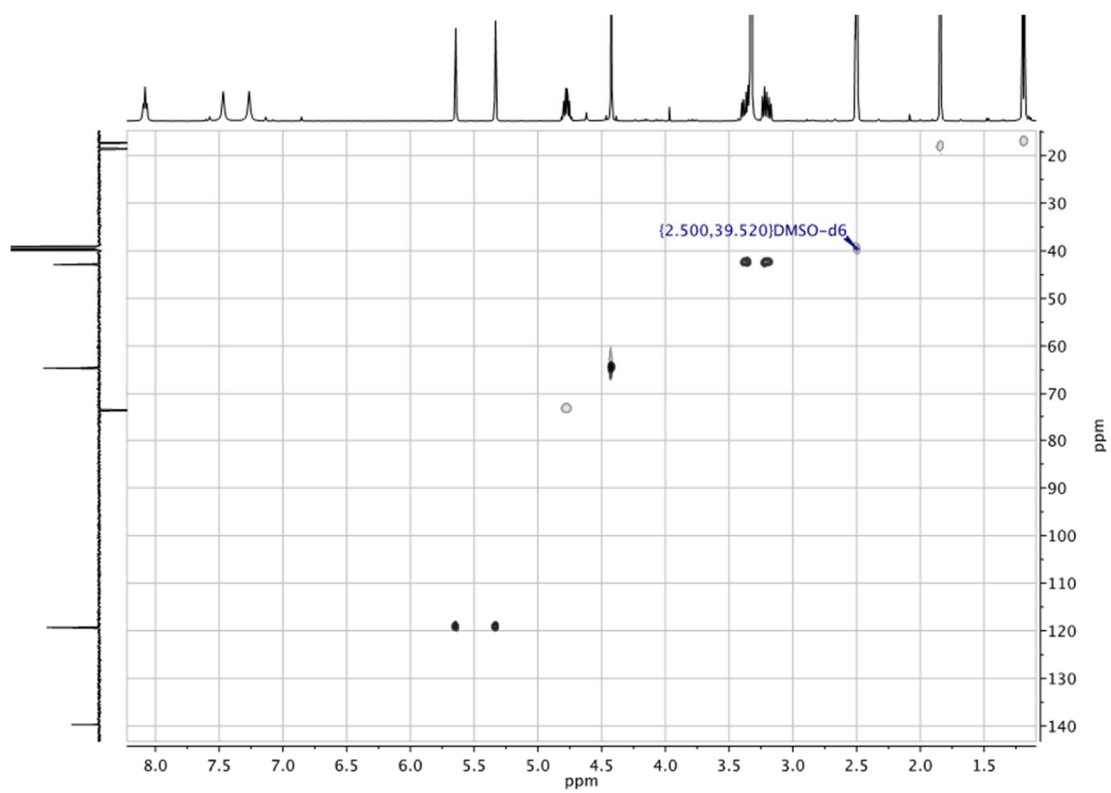


Figure 4. ¹H,¹³C-HSQC-NMR (DMSO-d₆) of HPMA-GA.

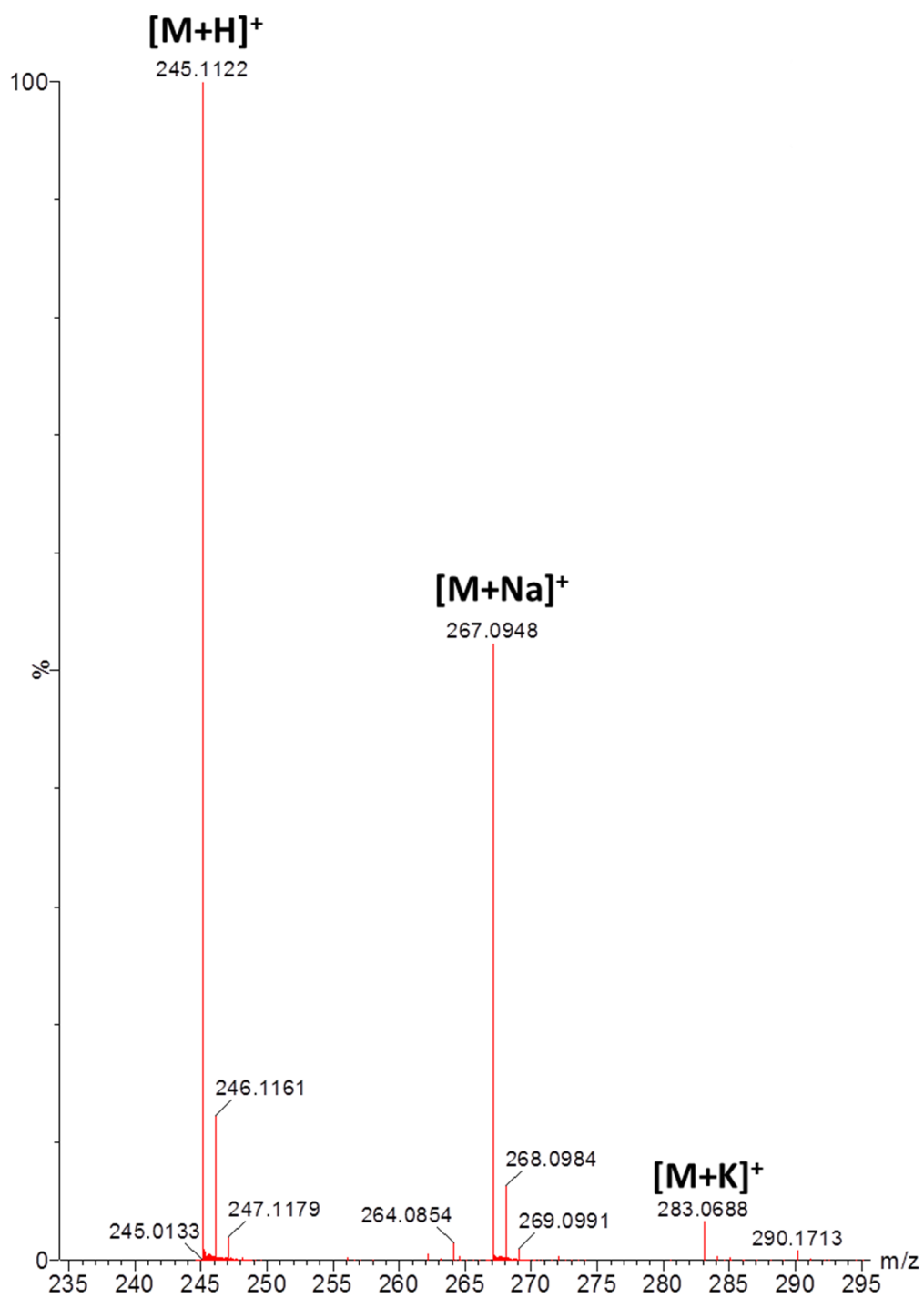


Figure 5. ESI-MS (acetonitrile) of HPMA-GA.

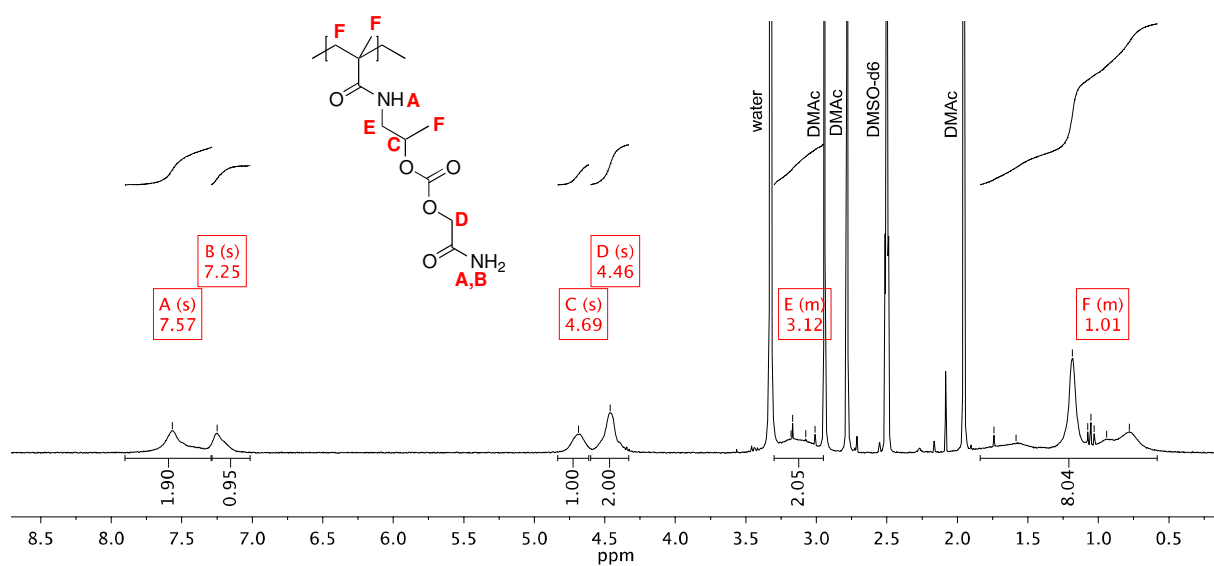


Figure 6. ¹H-NMR (300 MHz, DMSO-d₆) of poly(HPMA-GA).

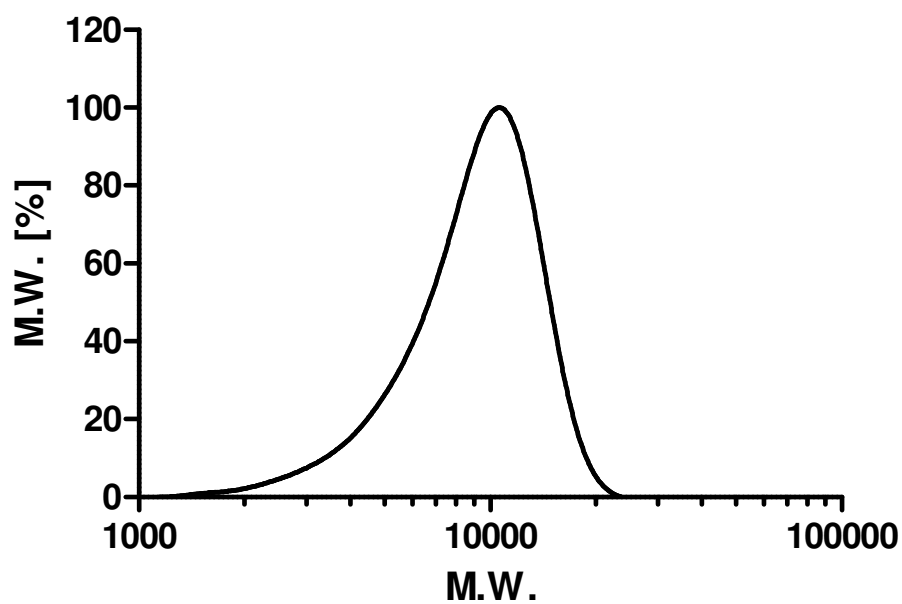


Figure 7. SEC elugram (DMAC, PMMA-St.) of poly(HPMA-GA)

To investigate the thermoresponsive properties of the polymer, aqueous solutions of the polymer were prepared at a concentration of 5 mg/mL. At first instance, we observed that heating to elevated temperatures was required to solubilize the polymer, whereas lowering of the temperature resulted in the solution to become hazy again – a phenomenon that could be repeatedly cycled as evidenced both by visual interrogation (**Figure 8.A1**), as well as by dynamic light scattering (DLS) (**Figure 8.A2**). These observations clearly evidence the UCST-behavior of poly(HPMA-GA) in water. DLS was used to study the thermal phase transition behavior of the polymer in more detail. To limit degradation of the carbonate ester linkages in the polymer backbone, these experiments were performed in a 50 mM acetate buffer at a PH of 5. The polymer solution was heated to 60°C and cooled to 25 °C at a cooling rate of 1K per 8 min to ensure that the UCST phase transition is thermodynamic and not a kinetic phenomenon. As evidenced by **Figure 8.B**, upon cooling of the polymer solution, a sharp transition from low to high light scattering intensity occurs at 42 °C. This indicates aggregate formation by the polymer in aqueous solutions when sur passing the UCST cloud point temperature. This is further evidenced when measuring the size of the aggregates, which are 820 nm below the UCST phase transition whereas soluble unimers (3.5 nm) are measured above the UCST phase transition (**Figure 8.C**). As a control, we also synthesized a HPMA homopolymer and a random copolymer of HPMA and HPMA-GA containing 15% of unmodified HPMA. Both polymers were found to be fully solubilize in water between 0 and 100 °C. Apparently, the presence of a minor fraction of hydrophilic HPMA moieties interferes with the molecular attractions of HPMA-GA and alleviates the UCST behavior, providing a good basis for the hypothesized transient solubility of poly(HPMA-GA).

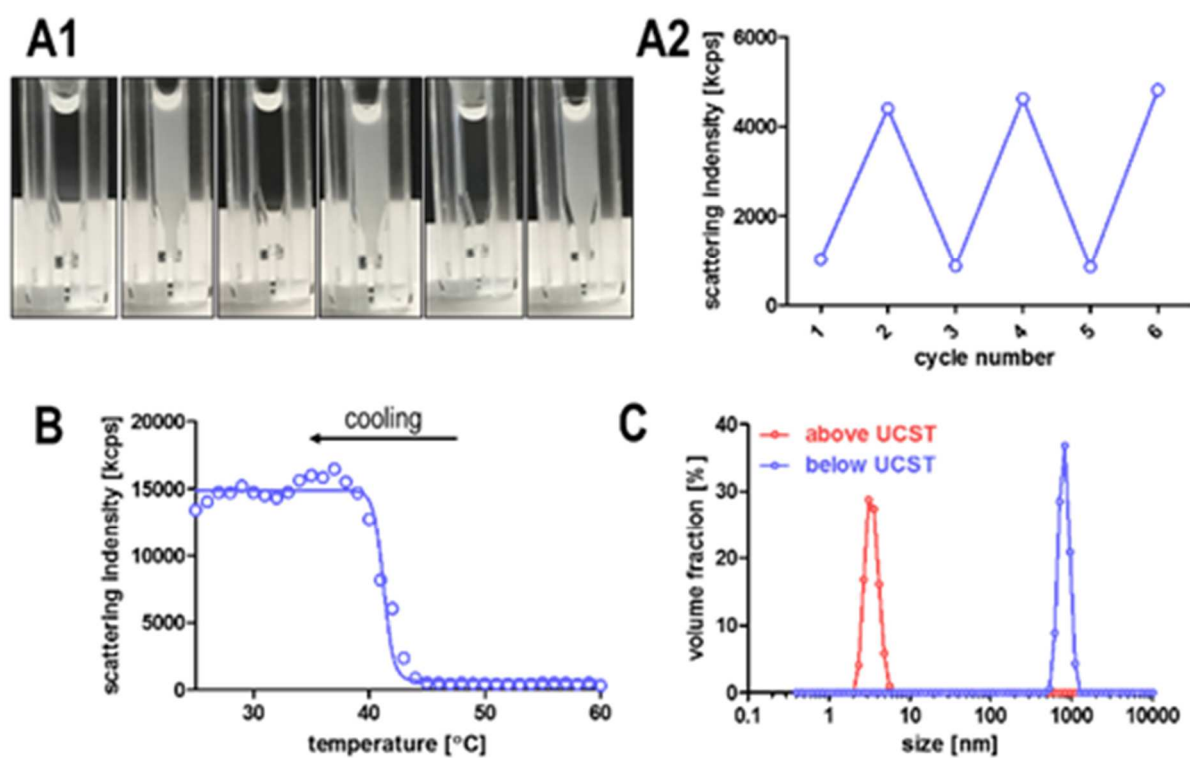


Figure 8. UCST behavior. (A1) Photographs of poly(HPMA-GA) solutions upon repeated heating and cooling and (A2) corresponding light scattering intensity measured by DLS. (B) Evolution of the light scattering intensity as function of temperature upon cooling of a 5 mg/mL poly(HPMA-GA) solution solubilized at 60°. (C) Aggregate size below and above the UCST measured by DLS.

Proof of hydrolytic instability of the poly(HPMA-GA) was gained by incubating both the monomer and the polymer in water at PH 7.4 and 37 °C, with intermittent sampling and subsequent ¹H-NMR spectroscopic analysis to measure the hydrolysis kinetics (**Figure 9.**). As depicted in **Figure 10.A**, both HPMA-GA and the corresponding polymer undergo hydrolysis under the applied conditions. Interestingly, we observed that the polymer degrades faster than the monomer. Although not yet fully understood, it may be speculated that the presence of hydroxyl groups in the partially hydrolyzed polymer may auto-catalyze the hydrolysis of neighboring HPMA-GA units as we recently demonstrated for acetal containing transiently soluble LCST polymers.^[30] To assess the effect of polymer hydrolysis on the UCST behavior, we solubilized the polymer in HEPES buffer at PH 7.4 by heating it above the UCST followed by cooling to 37 °C where it remained in the globular agglomerated state. This mixture was then monitored in time by DLS (**Figure 10.B**) and showed within a few hours a gradual transition of the polymer from the aggregated state to a solution of unimers, which we ascribe to gradual a gradual decrease of the UCST transition temperature upon hydrolysis of the polymer side chains until it becomes lower than 37°C leading to solubilization of the polymer. This is an interesting finding as it indicates that despite the relatively slow degradation of the polymer, a rather rapid phase transition takes place at physiological temperature and PH. This we ascribe to the strong influence of the presence of hydrolyzed HPMA residues on the UCST behavior of the resulting polymer. Altogether, these data suggest that when the temperature is maintained at the physiological values of 37 °C, the polymer will be able to undergo a globule-to-coil transition upon hydrolytic cleavage of the carbonate ester moieties in the polymer side chain.

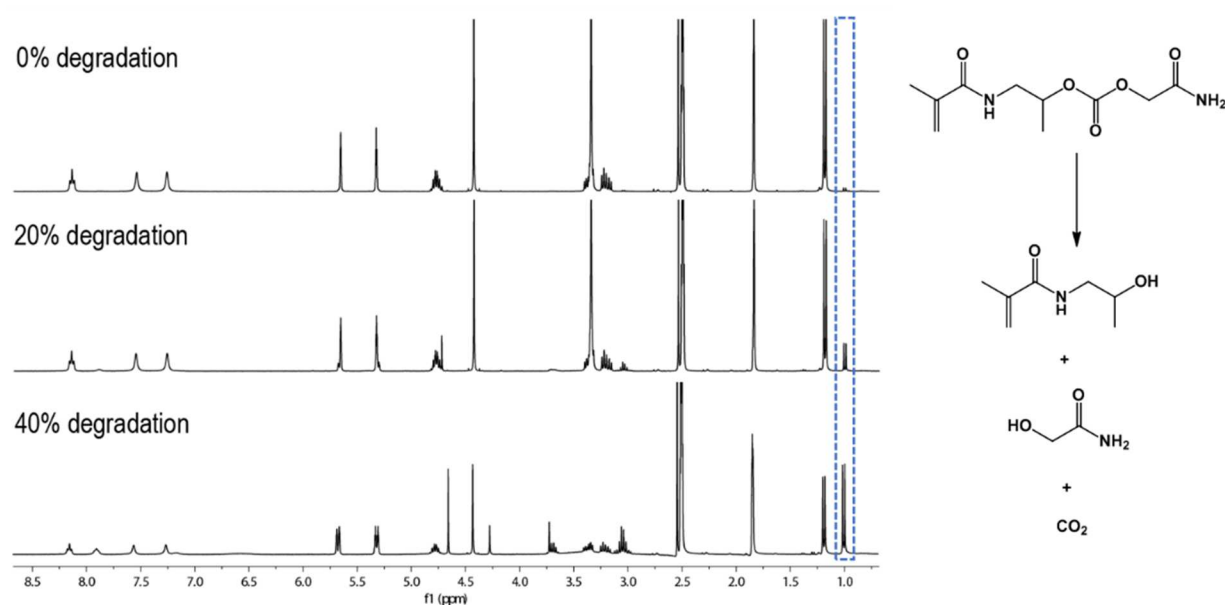


Figure 9. ¹H-NMR spectra of HPMA-GA during hydrolysis of the carbonate ester.

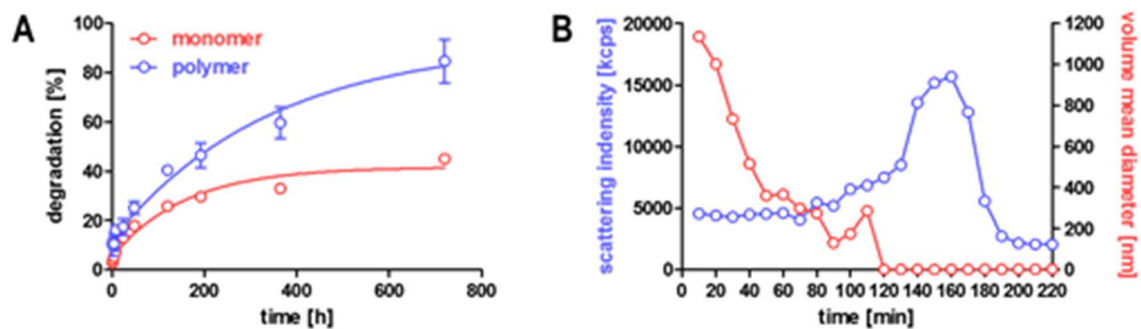


Figure 10. (A) Hydrolysis kinetics of HPMA-GA and poly(HPMA-GA) measured by appearance of the peak at 1 ppm in the ¹H-NMR spectrum. (B) Evolution of the light scattering intensity and aggregate size as function of time upon incubation of poly(HPMA-GA) at 37 °C in HEPES buffer at PH 7.4.

As final part of this study, we explored the possibility to accelerate the polymer hydrolysis by means of an external trigger. In this regard near infrared (NIR) light is attractive as it has a high penetration depth in living tissue and is relatively harmless.^[31, 32] Moreover, NIR light can be converted into thermal energy by gold nanorods (AuNRs) that show – owing to their high aspect ratio – two plasmonic peaks, including one in the NIR region. This prompted us to investigate whether poly(HPMA-GA) hydrolysis could be accelerated fostered by the heat generated by NIR irradiation of AuNRs, pushing the temperature of the medium beyond the UCST and hence induce hydration and faster hydrolysis of poly(HPMA-GA). AuNRs stabilized by CTAB were synthesized according to literature^[33] and transferred to the aqueous phase by extensive dialysis. The AuNRs were characterized by transmission electron microscopy (TEM; **Figure 11.A1**) and UV-vis spectroscopy (**Figure 11.A2**), which confirmed the successful formation of rod-shaped nanoparticles with plasmon peaks at 510 nm and 806 nm. Irradiation of an aqueous AuNRs solution with an NIR laser (808nm, 380mW) resulted in heating of the solution up to 50°C which could be cycled back to ambient temperature upon alternated on/off switching of the NIR laser light (**Figure 12.**). Control experiments in which NIR laser light was applied in absence of AuNRs only yielded a minor heating of the solution (**Figure 13.**). We also confirmed that an aqueous solution of poly(HPMA-GA) could be heated upon NIR laser irradiation in presence of AuNRs (**Figure 11.B**). Subsequently, AuNR were mixed with poly(HPMA-GA) in aqueous medium buffered at a PH of 7.4, followed by NIR laser irradiation. In parallel, the experiment was repeated in absence of AuNRs. After 1, 2 and 3h of irradiation samples were collected and analyzed by ¹H-NMR spectroscopy to determine the extent of polymer hydrolysis. These measurements (**Figure 11.C**) revealed a much faster hydrolysis of the polymer in presence of AuNRs and NIR laser irradiation, thereby demonstrating a proof-of-concept that hydrolysis of poly(HPMA-GA) can be triggered by an externally applied physical source.

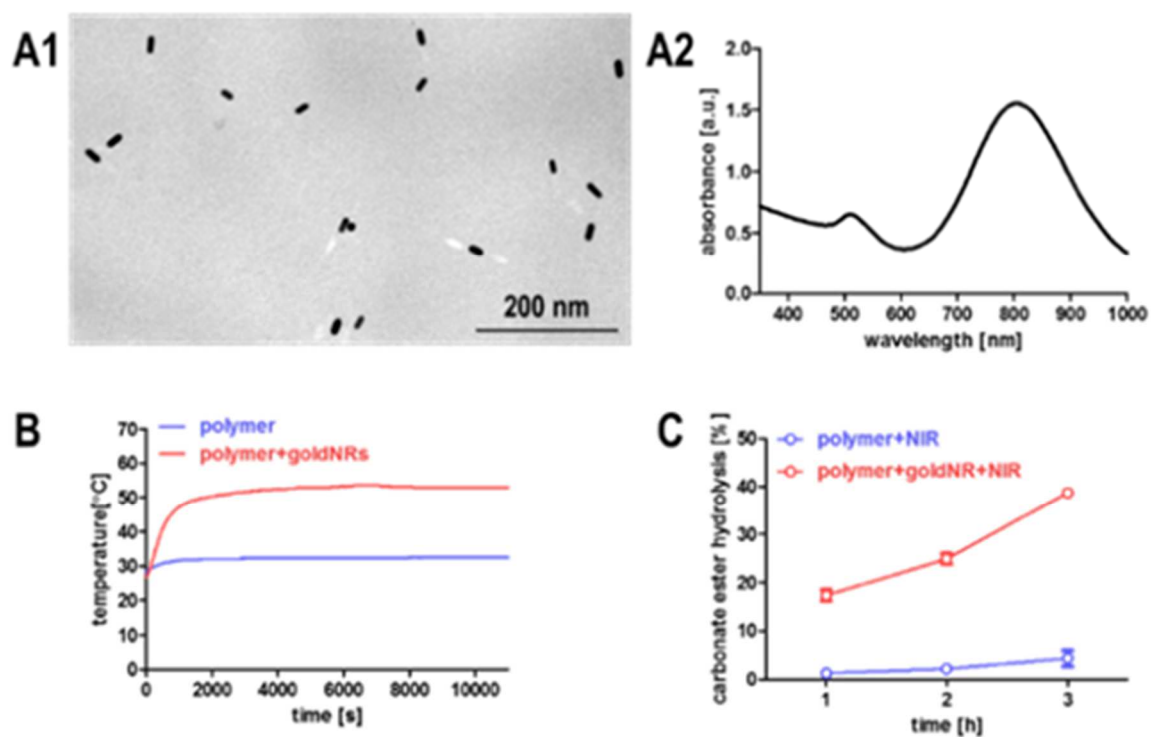


Figure 11. (A1) TEM image of AuNR and (A2) corresponding UV-Vis spectrum. (B) Temperature of an aqueous poly(HPMA-GA) solution in absence (blue) or presence (red) of AuNRs in response to NIR irradiation. (C) NIR-induced degradation of poly(HPMA-GA) in absence (blue) and presence of AuNRs (red).

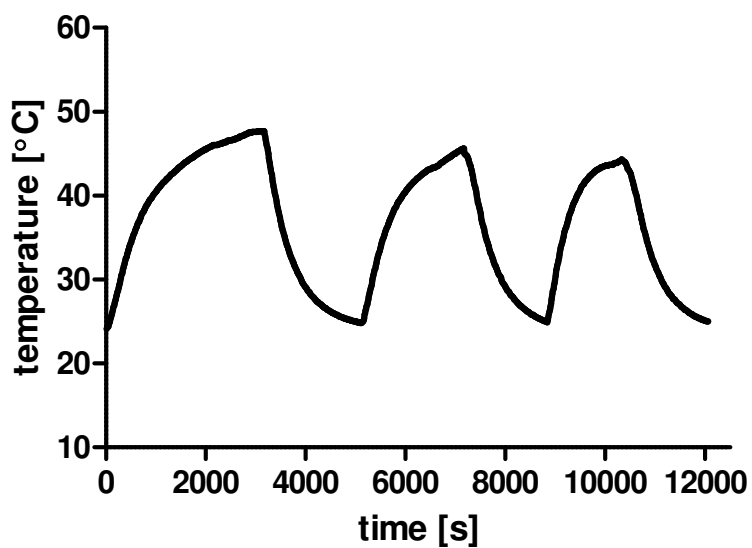


Figure 12. Change in temperature of an aqueous solution containing gold nanorods upon alternated ON/OFF switching of the laser light.

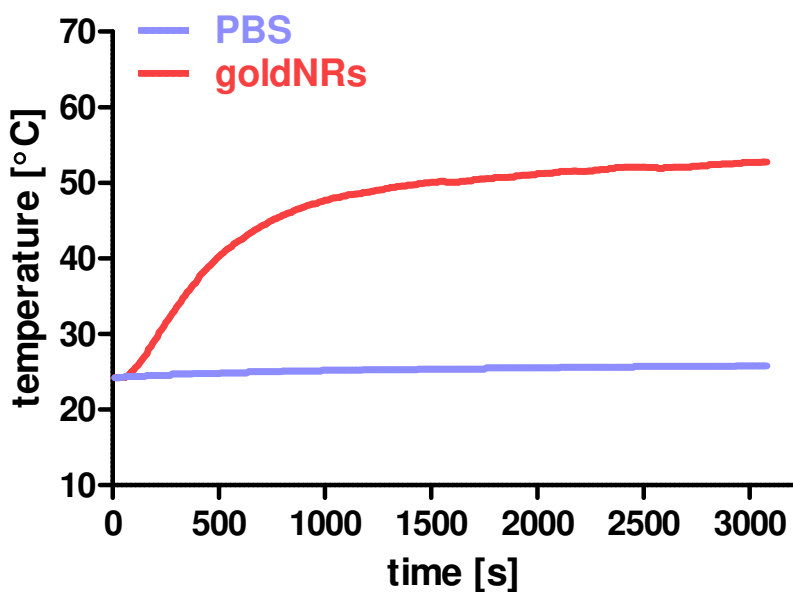


Figure 13. Change in temperature of aqueous solution with/without gold nanorods upon laser irradiation.

CONCLUSIONS

In conclusion, we reported a transiently thermoresponsive UCST polymer that is operational within a physiologically relevant window in terms of temperature, ionic strength and PH. These polymers are obtained through modification of a well-established biocompatible polymer, i.e. poly(HPMA), through a degradable hydrolysis-sensitive carbonate linker. Carbonate hydrolysis alleviated the UCST behavior of the polymers, which could also be accelerated by addition of AuNRs and NIR laser irradiation. Taken together we believe that our findings represent a valuable addition to the armory of degradable responsive materials that form self-assembled structures at and below the physiological temperature and gradually go into solution upon spontaneous hydrolysis or by a noninvasive external stimulus.

EXPERIMENTAL SECTION

Materials

Monomer of N-(2-Hydroxypropyl) methacrylamide (HPMA) was purchased from polysciences, the inhibitor of hydroquinon-monomethylether was obtained from Fluka. All other chemicals were purchased from Sigma Aldrich of at least ACS grade, and used as received.

Instrumentations

Nuclear magnetic resonance (NMR) spectra were recorded on a Bruker 400MHz FT-NMR spectrometer using d6-DMSO as solvents. Chemical shifts (δ) are given in ppm relative to TMS.

Electron spray ionization-mass spectroscopy (ESI-MS) was performed on a Waters LCT Premier XETM TOF mass spectrometer with a ZsprayTM source and ESI and modular LocksprayTM interface, coupled to a Waters alliance HPLC system.

Size exclusion chromatography (SEC) was performed on a Shimadzu 20A system, equipped with a 20A ISO-pump and a 20A refractive index detector (RID). Measurements were executed in N,N-dimethylacetamide (DMAc) containing 50mM LiBr at 50°C with a flow rate of 0.700mL/min. Calibration of the 2 PL 5 μ m Mixed-D columns was done with polymethylmethacrylate (PMMA standards) obtained from PSS (Mainz).

Ultraviolet-visible spectroscopy(UV-Vis) was performed on a Shimadzu UV-1650PC spectrophotometer. Gold nanorods were placed in plastic cuvettes, and spectral analysis was performed in the 350-1000nm range at room temperature.

Methods

Synthesis of HPMA-GA monomer

The synthesis of monomer of HPMA-GA contains two steps. HPMA was firstly activated with CDI as reported previously.¹ Briefly, 3.42g of 1,1'-carbonyldiimidazole (CDI) was dissolved in 20mL of anhydrous DCM in a 100mL of round-bottom flask, and then 2.148g of HPMA was added into the obtained solution and kept reaction at room temperature under N₂ atmosphere for 2.5h. Afterwards, the organic phase was separated and washed with 50ml of water twice and dried over Na₂SO₄. Pure HPMA-Cl was obtained as yellow oil by removing the solvents under reduced pressure. (yield 90%)

The obtained activated monomer of HPMA-Cl was mixed with excess of glycolamide (2 molar eqa.) and then dissolved in 20mL of anhydrous DMF under a nitrogen atmosphere. Prior to the reaction at 80°C for 24h under stirring, a small piece of inhibitor (hydroquinone monomethyl ether) was added into the solution to avoid auto-polymerization during this process. The solvent was evaporated under reduced pressure and the pure monomer of HPMA-GA was obtained via passing through column with eluent of chloroform containing 3% of methanol (v/v). (yield 85%)

¹H NMR (DMSO-d₆, 400 MHz), δ[PPM]= 8.08 (t, J = 5.8 Hz, 1H, NH-C=O), 7.37 (d, J = 81.5 Hz, 2H, NH₂-C=O), 5.64 (dt, 1H, C=CH₂), 5.33 (dt, J = 3.0, 1.5 Hz, 1H, C=CH₂), 4.78 (pd, 1H, CH-CH₃), 4.42 (s, 2H, CH₂C=O), 3.37 (m, 8H, CH-NH-), 3.21 (ddd, 1H, CH-NH-), 1.86 (dd, 3H, CH-CH₃), 1.17 (d, J = 20.1, 6.3 Hz, 3H, CH₃-C=CH₂).

¹³C NMR (DMSO-d₆, 400MHz), δ[PPM]= 168.41 (-CO-NH₂); 167.93 (-CO-NH-); 153.85 (-COO-), 139.72 (C=CH₂); 119.29 (C=CH₂); 73.66 (-CH-CH₃); 64.62 (-CH₂-CONH₂); 42.91 (-CH₂-NH-); 18.60 (-CH-CH₃); 17.34 (CH₃-C=CH₂).

ESI-MS(acetonitrile): m/z=245.1122 [M+H]⁺; 267.0948 [M+Na]⁺; 283.0688 [M+K]⁺

RAFT polymerization of HPMA-GA

A Schlenk tubes with a stir bar was loaded with monomer of HPMA-GA, CTA and AIBN with molar ratio of 50:1:0.2. All compounds were dissolved in anhydrous DMAc with final monomer concentration of 1M. Then the obtained solution was degassed via 4 cycles of freeze-pump-thaw, and then put into pre-heated oil bath at 70°C for 70h under vacuum. A 1H-NMR sample of the reaction mixture dissolved in DMSO-d6 was analyzed showing 75% monomer conversion. The resulting polymer was isolated by precipitation in acetone and centrifugation. After re-dissolving in few mL of DMAc, this process was repeated three times. The precipitated polymer was dried for 12h at room temperature under vacuum, affording poly(HPMA-GA).

UCST behavior of poly(HPMA-GA)

The UCST behavior of poly(HPMA-GA) in aqueous solution was investigated by DLS. Briefly, the polymer was dissolved in preheated 50mM acetated buffer with a PH of 5 at a concentration of 5mg/mL. The sample was then cooled from 60 to 25°C using a 1 °C interval. During cooling, the size and scattering intensity were measured. The cloud point of the polymer was estimated as the onset on the X-axis obtained by extrapolation of the scattering intensity-temperature curve to intensity baseline.

Hydrolysis of HPMA-GA

1) hydrolysis of HPMA-GA monomer

100mg of monomers were first dissolved in 0.5mL DMSO, followed by being added dropwise into 10mL of PBS at 37°C under stirring. At different time intervals (1h, 2h, 4h, 8h, 12h, 24h, 96h,192h, 364h, 720h), 1mL of solution was taken out to be freeze-dried and then re-dissolved in DMSO-d6 for 1H-NMR measurement.

2) hydrolysis of HPMA-GA polymer

100mg of polymers, synthesized by RAFT polymerization as reported earlier, were first dissolved in 0.5mL DMSO, followed by being added dropwise into 10mL of PBS at 37°C under stirring. At different time intervals (1h, 2h, 4h, 8h, 12h, 24h, 96h,192h, 364h, 720h), 1mL of

solution was taken out to be freeze-dried and then re-dissolved in DMSO-d6 for 1H-NMR measurement.

Hydrolysis effect on UCST behavior

To assess the effect of polymer hydrolysis on the UCST behavior of the polymer, the polymer was dissolved in 25mM Heppes buffer with pH7.4 at a concentration of 5mg/mL by heating it above the UCST. Followed by cooling to 37°C, the size and scattering intensity as a function of time was then monitored by DLS.

Synthesis of CTAB@AuNR

The gold nanorods (AuNRs) were synthesized as described before with a little modification.² All glass vials were first cleaned by aqua regia (3:1 of HNO₃: HCl) and then rinsed with MilliQ water several times prior to the synthesis. Firstly, 5mL of 1mM HAuCl₄ was mixed with 5mL of 0.2M CTAB aqueous solution, and the color turned orange immediately. 290μl of 4.0mM AgNO₃ was added into the solution above and vortexed for 5 seconds, and then 8μl of 37% HCl was added and gently shaken for 5 seconds. 70μl of 78.8mM ascorbic acid aqueous solution was added and the solution became colorless during 10s under gently shaken. Afterwards, 15μl of fresh prepared ice-cold 0.01M NaBH₄ aqueous solution was added into the colorless solution without shaking and put into water bath at 30°C for 6h, allowing for the growth of gold nanorods. Excess of CTAB in AuNRs solution was removed by 3 cycles of centrifugation at 15000rpm for 20min at room temperature, and the precipitated AuNRs were dispersed in MilliQ water and stored in fridge. The resulting gold nanorods had dimension of 27×5 nm, with an aspect ratio of ~5, and longitudinal plasmon absorption at 806nm.

Near infrared radiation(NIR)- induced Hydrolysis of poly(HPMA-GA)

120mg of poly(HPMA-GA) was dissolved in 0.6mL DMSO, and then 50uL of polymer DMSO solution was added into 1mL of PBS solution containing 66.7uL of gold nanorods stock solution with a concentration of 1mg/mL, followed by NIR irradiation (wavelength: 808nm, power: 380mW) for 1h, 2h, and 3h, respectively. The change in temperature of the solution during NIR

irradiation was monitored. Afterwards, samples were freeze-dried and then re-dissolved in DMSO-d₆ for ¹H-NMR measurement.

REFERENCES

1. Stuart, M.A., et al., *Emerging applications of stimuli-responsive polymer materials*. Nat Mater, 2010. **9**(2): p. 101-13.
2. de Las Heras Alarcon, C., S. Pennadam, and C. Alexander, *Stimuli responsive polymers for biomedical applications*. Chem Soc Rev, 2005. **34**(3): p. 276-85.
3. Hoffman, A.S., *Stimuli-responsive polymers: biomedical applications and challenges for clinical translation*. Adv Drug Deliv Rev, 2013. **65**(1): p. 10-6.
4. Mura, S., J. Nicolas, and P. Couvreur, *Stimuli-responsive nanocarriers for drug delivery*. Nat Mater, 2013. **12**(11): p. 991-1003.
5. Cheng, R., et al., *Dual and multi-stimuli responsive polymeric nanoparticles for programmed site-specific drug delivery*. Biomaterials, 2013. **34**(14): p. 3647-57.
6. Matricardi, P., et al., *Interpenetrating Polymer Networks polysaccharide hydrogels for drug delivery and tissue engineering*. Adv Drug Deliv Rev, 2013. **65**(9): p. 1172-87.
7. Cobo, I., et al., *Smart hybrid materials by conjugation of responsive polymers to biomacromolecules*. Nat Mater, 2015. **14**(2): p. 143-59.
8. Theato, P., et al., *Stimuli responsive materials*. Chem Soc Rev, 2013. **42**(17): p. 7055-6.
9. Custers, J.P., et al., *Reversible Calcium(II)-Ion Binding through an Apparent pKa Shift of Thermosensitive Block-Copolymer Micelles*. Angew Chem Int Ed Engl, 2015. **54**(47): p. 14085-9.
10. Vanparijs, N., L. Nuhn, and B.G. De Geest, *Transiently thermoresponsive polymers and their applications in biomedicine*. Chem Soc Rev, 2017. **46**(4): p. 1193-1239.
11. Schmaljohann, D., *Thermo- and pH-responsive polymers in drug delivery*. Advanced Drug Delivery Reviews, 2006. **58**(15): p. 1655-1670.
12. Roy, D., W.L.A. Brooks, and B.S. Sumerlin, *New directions in thermoresponsive polymers*. Chem Soc Rev, 2013. **42**(17): p. 7214-7243.
13. Zhang, Q.L., et al., *Thermoresponsive polymers with lower critical solution temperature: from fundamental aspects and measuring techniques to recommended turbidimetry conditions*. Materials Horizons, 2017. **4**(2): p. 109-116.
14. Gibson, M.I. and R.K. O'Reilly, *To aggregate, or not to aggregate? considerations in the design and application of polymeric thermally-responsive nanoparticles*. Chem Soc Rev, 2013. **42**(17): p. 7204-13.

15. Gibson, M.I., D. Paripovic, and H.A. Klok, *Size-dependent LCST transitions of polymer-coated gold nanoparticles: cooperative aggregation and surface assembly*. *Adv Mater*, 2010. **22**(42): p. 4721-5.
16. Aseyev, V., H. Tenhu, and F.M. Winnik, *Non-ionic Thermoresponsive Polymers in Water. Self Organized Nanostructures of Amphiphilic Block Copolymers* li, 2011. **242**: p. 29-89.
17. Li, W., et al., *Antitumor drug delivery modulated by a polymeric micelle with an upper critical solution temperature*. *Angew Chem Int Ed Engl*, 2015. **54**(10): p. 3126-31.
18. Zhang, Q.L. and R. Hoogenboom, *Polymers with upper critical solution temperature behavior in alcohol/water solvent mixtures*. *Progress in Polymer Science*, 2015. **48**: p. 122-142.
19. Seuring, J. and S. Agarwal, *Polymers with Upper Critical Solution Temperature in Aqueous Solution: Unexpected Properties from Known Building Blocks*. *Acs Macro Letters*, 2013. **2**(7): p. 597-600.
20. Shimada, N., et al., *Design of UCST polymers for chilling capture of proteins*. *Biomacromolecules*, 2013. **14**(5): p. 1452-7.
21. Shimada, N., et al., *Ureido-derivatized polymers based on both poly(allylurea) and poly(L-citrulline) exhibit UCST-type phase transition behavior under physiologically relevant conditions*. *Biomacromolecules*, 2011. **12**(10): p. 3418-22.
22. Zhang, H., X. Tong, and Y. Zhao, *Diverse thermoresponsive behaviors of uncharged UCST block copolymer micelles in physiological medium*. *Langmuir*, 2014. **30**(38): p. 11433-41.
23. Boustta, M., et al., *Versatile UCST-based thermoresponsive hydrogels for loco-regional sustained drug delivery*. *J Control Release*, 2014. **174**: p. 1-6.
24. Seuring, J., et al., *Upper Critical Solution Temperature of Poly(N-acryloyl glycinamide) in Water: A Concealed Property*. *Macromolecules*, 2012. **45**(1): p. 374-384.
25. Gupta, A., B. Mohanty, and H.B. Bohidar, *Flory temperature and upper critical solution temperature of gelatin solutions*. *Biomacromolecules*, 2005. **6**(3): p. 1623-1627.
26. Wolf, T., et al., *Reversible Self-Assembly of Degradable Polymersomes with Upper Critical Solution Temperature in Water*. *Journal of the American Chemical Society*, 2017. **139**(32): p. 11064-11072.
27. Zhang, Z., et al., *Influenza-binding sialylated polymer coated gold nanoparticles prepared via RAFT polymerization and reductive amination*. *Chemical Communications*, 2016. **52**(16): p. 3352-3355.

28. Scales, C.W., et al., *Corona-stabilized interpolyelectrolyte complexes of SiRNA with nonimmunogenic, hydrophilic/cationic block copolymers prepared by aqueous RAFT polymerization*. *Macromolecules*, 2006. **39**(20): p. 6871-6881.
29. Kasmi, S., et al., *Transiently Responsive Block Copolymer Micelles Based on N-(2-Hydroxypropyl)methacrylamide Engineered with Hydrolyzable Ethylcarbonate Side Chains*. *Biomacromolecules*, 2016. **17**(1): p. 119-27.
30. Zhang, Q.L., et al., *Acid-Labile Thermoresponsive Copolymers That Combine Fast pH-Triggered Hydrolysis and High Stability under Neutral Conditions*. *Angewandte Chemie-International Edition*, 2015. **54**(37): p. 10879-10883.
31. Liu, Q., et al., *Strong Two-Photon-Induced Fluorescence from Photostable, Biocompatible Nitrogen-Doped Graphene Quantum Dots for Cellular and Deep-Tissue Imaging*. *Nano Letters*, 2013. **13**(6): p. 2436-2441.
32. Matousek, P., *Deep non-invasive Raman spectroscopy of living tissue and powders*. *Chem Soc Rev*, 2007. **36**(8): p. 1292-1304.
33. Ali, M.R.K., B. Snyder, and M.A. El-Sayed, *Synthesis and Optical Properties of Small Au Nanorods Using a Seedless Growth Technique*. *Langmuir*, 2012. **28**(25): p. 9807-9815.

Broader International Context, Relevance and Future Perspectives

High-aspect ratio nanomaterials, owing to their unique electrical, optical and mechanical properties, especially their large surface areas, are intensively investigated for their interaction with biological systems.^[1-4] Such anisotropic nanomaterials also hold opportunities in an immune-oncological context, owing to their relatively efficient internalization by cancer cells, which often exhibit increased phagocytotic behaviour, and antigen presenting cells.^[5-8]

However, an important challenge that arises when envisioning the use of such nanomaterials as drug carriers is to keep the formulation simple and scalable, involving a minimum of steps and to avoid reactive chemistry and toxic organic solvents.^[9, 10] Additionally, clinical applications of high-aspect ratio nanomaterials are still in their infancy. Therefore, there is still much work to be done.

Different structures, sizes, charges, shapes and surface chemistry determine different biological activity of nanomaterials.^[11] As a growth area in nanotechnology, high-aspect ratio carbon nanotubes (CNTs),^[6, 12-15] since the first discovery in 1991,^[16] have stimulated intense interest in their unique optical, electrical, magnetic anisotropy and biological properties which has offered exciting opportunities for a variety of applications.^[17-22]

Bare CNTs are hydrophobic and trend to self-associate into micro-scale aggregates. Therefore, the goal of **Chapter 1**, was to devise a simple strategy for the debundling and bio-functionalization of CNT. For this purpose, three different batches of carboxylic acid functionalized carbon nanotubes (CNTs-COOH) from different commercial sources were tested.

There are two distinct approaches that have been reported in the literatures for dispersing carbon nanotubes: mechanical methods (ultra-sonication, refluxing and high shear mixing)^[23-26] and processing methods to alter the surface energy, i.e. physically (non-covalent adsorption)^[23, 24, 26] and/or chemically (covalent treatment).^[25, 27-29] However, mechanical dispersion methods could not only separate nanotubes from each other, but also slice them and decrease their aspect ratio.^[23, 24, 30, 31]

Chemical treatments, aiming at surface functionalization of CNTs side wall or opening their ends to enhance the chemical compatibility and reduce their tendency to agglomerate.^[23, 25, 28, 32-36] Nanotube-polymer composite is a good example,^[37-39] such as SWCNT-polystyrene composites made by latex technology,^[40] SWCNT-polyimide^[41, 42] and poly(phenyleneethynylene) functionalized SWCNT-polystyrene composites^[43]. However, chemical methods often introduce structural defects (reduction in average length and sidewall disordering). Alternatively, non-covalent approaches by wrapping of surfactants or polymers is particularly attractive, without disturbing the π - π structure of CNT and preserving their intrinsic properties.^[44-47] Hereto, we have chosen a mild mechanical method based on ultra-sonication and non-covalent adsorption of tannic acid to unbundle CNT and, at the same time, to minimize the tubes shortening. The obtained dispersions are stable, without precipitation, upon prolonged their storage(months) under ambient conditions.

Thanks to the vehicle structure of CNT, they have been proven to possess the ability to pierce the cytoplasmic membrane and nuclear membrane of cells.^[48-53] Moreover, partly due to the EPR effect, CNT appears much more accumulation in cancerous tumour tissue than in normal tissues.^[48] Given that, owing to their high surface area and rich electronic polyaromatic structure, CNTs are able to conjugate with a wide variety of ligands (drugs, proteins, peptides, polysaccharides, enzymes, etc.).^[54-58] Bio-conjugation is a future tendency

on cancer treatment research. For example, SWNTs can be efficiently burdened with aromatic chemotherapy drug doxorubicin (DOX) via supramolecular π - π stacking.^[57, 58] Meanwhile, the antibody Herceptin that is specifically over-expressed on a wide range of human breast cancer cells,^[59] was first thiolated by Traut's reagent to produce active thiol groups for bio-conjugation with CNTs.^[60, 61] Also for siRNA, CNTs are first reacted with a bifunctional linker, Sulfosuccinimidyl 6-(3'-[2-pyridyldithio]-propionamido) hexanoate (Sulfo-LC-SPDP) and then bio-conjugated with thiolated siRNA via a cleavable disulfide bond.^[62-64] Additionally, the most common strategy for the bio-conjugation is still the protocol with the help of EDC/Sulfo-NHS,^[58, 65-70] which could destroy the stability of CNT dispersions. Therefore, in this thesis, we directly used the obtained water-soluble CNT~TA to couple with model proteins (BSA and OVA) in absence of other linker strategies.

Confocal microscopy showed that protein-adsorbed CNT were efficiently internalized by dendritic cells. This is in accordance to earlier reports by the Kotov's group,^[71] that CNTs showed fast and deep permeation into the tissue, which is often difficult to realize with anticancer agents. For the treatment of cancer and other diseases, understanding the transport of carbon nanotubes (CNTs) as nanocarriers within tissues and cells is essential for biomedical imaging and drug delivery.^[72-74] Further controlling the subcellular delivery of CNTs is also important for the realization of safe and effective cellular therapies.^[75-77] We postulate that the bio-conjugation of CNTs and proteins will open new possibilities to utilize their properties for multifunctional subcellular targeting applications. Xing-Jie Liang and co-workers provided evidence that SWCNTs may be useful for the treatment of methamphetamine addiction.^[21] Therefore, these nanotubes are expected to be further developed as a new approach for the treatment of drug abuse and addiction. Additionally, their environmental behaviour and ecological risk (toxicological studies) are also attracting great attentions.^[78, 79] In future, more studies are required to address these issues.

Besides these, due to the magnetic anisotropy, carbon nanotubes (CNTs) could be used as an improved contrast agent relative to other spherical nanomaterials for magnetic resonance imaging (MRI) applications^[80, 81] and also hold promise for the construction of high-efficiency solar cells.^[82, 83]

Graphene oxide (GOx) stands out among the graphene derivatives^[84] and is generating great interest, not only from the point of view of academic curiosity, but also considering its potential applications in a wide range of areas.^[85-87] This water-soluble material is highly transparent and combines high-aspect ratio dimension with hydrophilic functional groups such as epoxide, hydroxyl and carboxyl groups.^[88-91] Due to these oxygen functional groups which are linked to the hexagonal carbon structure, the chemical versatility of GOx makes it relatively easy to be further modified with organic molecules or biological structures.^[92, 93] In addition, GOx could also be reduced into graphene typically by chemical or thermal methods as intermediate species.^[92, 93] Contrary to several other linker strategies which were reported to bind therapeutic molecules to GOx with the help of Tannic Acid,^[94-97] gold or silver nanoparticles, etc.^[96, 98-103], in **Chapter 2** of this thesis a facile method was elucidated to formulate vaccine antigens with GOx without the requirement of additional reagents. Confirmed by different techniques, we observed that GOx can be coupled to proteins spontaneously without the need for introducing specific linker strategies. The nature of these interactions, however, remains elusive. Owing to the random distribution of the oxygen-containing functional groups, the precise atomic structure of GOx is still uncertain and yet remains to be fully elucidated.

It was observed that, due to the high aspect ratio and surface area of GOx, which has been reported to pierce or destabilize lipid bilayer membranes of living cells and bacteria,^[5, 104, 105] GOx nanosheet with adsorbed proteins could strongly promote DCs to secrete effector cytokines and antigen cross-presentation to CD8 T cells.^[104, 105] The later one is a hallmark in the induction of potent cellular antigen-specific immune responses against intracellular pathogens (e.g. HIV, malaria, tuberculosis) and cancer. These features could render GOx an attractive nanocarrier for intracellular delivery of therapeutic molecules and enhance vaccine delivery efficiency.

However, it is also important to highlight the current challenges regarding the use of GOx for biomedical applications. The large scale production of standardizing GOx,^[106, 107] especially with reproducible dimensions, are still far from the criteria that are required for industry or commercialization with the satisfactory precision and reproducibility.^[108] Furthermore, one hurdle preventing the widespread use of GOx is the lack of miscibility of the nanoplatelets

with functional polymer matrixes. Besides these, the uncertainty on the long-term fate of GOx and possible nanotoxicity issues are also restricting their potential applications. Bearing all of the aforementioned unique features and challenges of GOx in mind, in particular its planar ultra-thin morphology and protein-binding capacity, we do believe GOx merits the effort of being further investigated for intracellular delivery applications.

To date, cancer is still a leading cause of death. Although a large number of drugs and methods to relieve the negative impacts by cancer have been developed, off-target side effects are continuing disturbing the patients' quality of life.^[109] So there is a clear need for more efficient strategies for the delivery of anti-cancer drugs which should only be internalized by cancer cells and would not affect healthy cells and tissues.^[110, 111] This has prompted the development of stimuli-responsive polymer-based delivery systems that can respond to a specific trigger and release a drug payload, preferably inside a cancer cell. Among the stimuli-responsive polymers which are also called 'smart polymers'^[112-114] and responding to chemical or physical changes by the change in solution behaviour, transiently thermoresponsive polymers exhibit a soluble-insoluble switch in response to temperature,^[115, 116] but gradually lose this property in response to a hydrolysis reaction in the polymer backbone or side-chain, are attractive biomaterials for the drug delivery.

Compared to a rather common phenomenon lower critical solution temperature (LCST) behaviour which means the polymers are soluble at low temperature but become insoluble above LCST,^[117-121] upper critical solution temperature (UCST)^[122] behaviour is the inverse of LCST behaviour. This means that a polymer is insoluble below a critical temperature but becomes soluble above this temperature, which is a relative rare phenomenon in aqueous media. This unique property has fuelled the interest in these materials for a number of applications, including drug delivery, tissue engineering, separation, catalysis, bio-sensing etc..^[123-125] For example, gelatine is a degradable natural macromolecular UCST system,^[126, 127] whereas degradable synthetic UCST systems that operate within a physiological window are extremely rare and limited to only a few examples. Very recent work by the Wurm group introduced an interesting class of phosphonate based copolymers which show UCST behavior in acid condition and degradability in alkaline condition.^[128] However, due to the presence of ionisable groups these polymers did not exhibit UCST behaviour at physiological pH.

Therefore, in **Chapter 3**, we chose poly(N-(2-hydroxypropyl)methacrylamide), owing to the biocompatible and non-immunogenic nature, as a polymeric scaffold to obtain a biocompatible and biodegradable transiently thermoresponsive homo-polymer,^[129, 130] Poly(HPMA–glycolamide), through a degradable hydrolysis-sensitive carbonate ester linkage.^[131] Most examples of UCST polymers operating within a physiologically relevant context are based on hydrogen bond formation between amide- or urea-based repeating units in the polymer backbone. Poly(HPMA–glycolamide) possesses upper critical solution temperature (UCST) behavior at 42°C in aqueous medium. Additionally, at a physiological pH, this polymer could undergo a globule-to-coil transition and gradually lose its UCST behaviour upon the hydrolytic cleavage of the carbonate ester moieties in the polymer backbone.

AuNRs, owing to their high-aspect ratio, have two plasmonic peaks at 510 nm and 806 nm and can convert the irradiation NIR laser into thermal energy. Near infrared (NIR) light is attractive as it has a high penetration depth in living tissue and is relatively harmless^[132, 133]. AuNRs with poly(HPMA-glycolamide) in aqueous subjected to NIR laser irradiation could be heated and work as an external trigger to accelerate the hydrolysis of poly(HPMA-glycolamide). Equally important, irradiating these AuNRs with NIR light could generate heat and induce a phase transition to release the payload drug.^[134, 135] Meanwhile, the generated heat can also increase the efficacy of drug molecules which have been localized to the certain area.^[122, 124]

It is certainly interesting to investigate in future endeavours the influence of anisotropy on the interactive properties of polymer-functionalized gold nanoparticles. However, it is worth to point out that each material has its own disadvantages (such as issues of dosage, toxicity and potential risks to human health and the environment). Furthermore, our investigation on the biological interaction between polymer-functionalized gold nanoparticles and living cells were limited to *in vitro* settings. The behaviour of these systems *in vivo* still needs to be explored and recent findings by the Parak group have suggested that the presence of enzymes can strongly alter the *in vivo* fate of polymer coated gold nanoparticles.^[136]

REFERENCES

1. Oberdörster, G., V. Stone, and K. Donaldson, *Toxicology of nanoparticles: a historical perspective*. *Nanotoxicology*, 2007. **1**(1): p. 2-25.
2. Ji, Z., et al., *Designed synthesis of CeO₂ nanorods and nanowires for studying toxicological effects of high aspect ratio nanomaterials*. *ACS nano*, 2012. **6**(6): p. 5366-5380.
3. Meng, H., et al., *Aspect ratio determines the quantity of mesoporous silica nanoparticle uptake by a small GTPase-dependent macropinocytosis mechanism*. *ACS nano*, 2011. **5**(6): p. 4434-4447.
4. Poland, C.A., et al., *Carbon nanotubes introduced into the abdominal cavity of mice show asbestos-like pathogenicity in a pilot study*. *Nature nanotechnology*, 2008. **3**(7): p. 423-428.
5. Li, H., et al., *Spontaneous protein adsorption on graphene oxide nanosheets allowing efficient intracellular vaccine protein delivery*. *ACS applied materials & interfaces*, 2016. **8**(2): p. 1147-1155.
6. Bauer, L.A., N.S. Birenbaum, and G.J. Meyer, *Biological applications of high aspect ratio nanoparticles*. *Journal of Materials Chemistry*, 2004. **14**(4): p. 517-526.
7. Chou, L.Y., K. Ming, and W.C. Chan, *Strategies for the intracellular delivery of nanoparticles*. *Chemical Society Reviews*, 2011. **40**(1): p. 233-245.
8. Wang, J., et al., *The complex role of multivalency in nanoparticles targeting the transferrin receptor for cancer therapies*. *Journal of the American Chemical Society*, 2010. **132**(32): p. 11306-11313.
9. Reddy, L.H., et al., *Magnetic nanoparticles: design and characterization, toxicity and biocompatibility, pharmaceutical and biomedical applications*. *Chemical reviews*, 2012. **112**(11): p. 5818-5878.
10. Buzea, C., I.I. Pacheco, and K. Robbie, *Nanomaterials and nanoparticles: Sources and toxicity*. *Biointerphases*, 2007. **2**(4): p. MR17-MR71.
11. Mu, Q., et al., *Protein binding by functionalized multiwalled carbon nanotubes is governed by the surface chemistry of both parties and the nanotube diameter*. *The Journal of Physical Chemistry C*, 2008. **112**(9): p. 3300-3307.
12. Zhu, L., et al., *Growth and electrical characterization of high-aspect-ratio carbon nanotube arrays*. *Carbon*, 2006. **44**(2): p. 253-258.

13. Jensen, K., et al., *Buckling and kinking force measurements on individual multiwalled carbon nanotubes*. Physical Review B, 2007. **76**(19): p. 195436.
14. Wang, X., et al., *Fabrication of ultralong and electrically uniform single-walled carbon nanotubes on clean substrates*. Nano letters, 2009. **9**(9): p. 3137-3141.
15. Jia, W., B. Tang, and P. Wu, *Novel Composite PEM with Long-Range Ionic Nanochannels Induced by Carbon Nanotube/Graphene Oxide Nanoribbon Composites*. ACS applied materials & interfaces, 2016. **8**(42): p. 28955-28963.
16. Iijima, S., *Helical microtubules of graphitic carbon*. nature, 1991. **354**(6348): p. 56-58.
17. Feazell, R.P., et al., *Soluble single-walled carbon nanotubes as longboat delivery systems for platinum (IV) anticancer drug design*. Journal of the American Chemical Society, 2007. **129**(27): p. 8438-8439.
18. Liu, Z., et al., *Drug delivery with carbon nanotubes for in vivo cancer treatment*. Cancer research, 2008. **68**(16): p. 6652-6660.
19. Münzer, A.M., Z.P. Michael, and A. Star, *Carbon nanotubes for the label-free detection of biomarkers*. ACS nano, 2013. **7**(9): p. 7448-7453.
20. Singh, R., et al., *Tissue biodistribution and blood clearance rates of intravenously administered carbon nanotube radiotracers*. Proceedings of the National Academy of Sciences of the United States of America, 2006. **103**(9): p. 3357-3362.
21. Xue, X., et al., *Aggregated single-walled carbon nanotubes attenuate the behavioural and neurochemical effects of methamphetamine in mice*. Nature nanotechnology, 2016. **11**(7): p. 613-620.
22. Kam, N.W.S., et al., *Carbon nanotubes as multifunctional biological transporters and near-infrared agents for selective cancer cell destruction*. Proceedings of the National Academy of Sciences of the United States of America, 2005. **102**(33): p. 11600-11605.
23. Vaisman, L., H.D. Wagner, and G. Marom, *The role of surfactants in dispersion of carbon nanotubes*. Advances in colloid and interface science, 2006. **128**: p. 37-46.
24. Wang, Y., Z. Iqbal, and S. Mitra, *Rapidly functionalized, water-dispersed carbon nanotubes at high concentration*. Journal of the American Chemical Society, 2006. **128**(1): p. 95-99.
25. Paredes, J. and M. Burghard, *Dispersions of individual single-walled carbon nanotubes of high length*. Langmuir, 2004. **20**(12): p. 5149-5152.

26. Dassios, K.G., et al., *Optimization of sonication parameters for homogeneous surfactant-assisted dispersion of multiwalled carbon nanotubes in aqueous solutions*. The Journal of Physical Chemistry C, 2015. **119**(13): p. 7506-7516.
27. Haggemueller, R., et al., *Comparison of the quality of aqueous dispersions of single wall carbon nanotubes using surfactants and biomolecules*. Langmuir, 2008. **24**(9): p. 5070-5078.
28. Stankovich, S., et al., *Graphene-based composite materials*. nature, 2006. **442**(7100): p. 282-286.
29. Xie, X.-L., Y.-W. Mai, and X.-P. Zhou, *Dispersion and alignment of carbon nanotubes in polymer matrix: a review*. Materials Science and Engineering: R: Reports, 2005. **49**(4): p. 89-112.
30. Chen, J., et al., *Solution properties of single-walled carbon nanotubes*. Science, 1998. **282**(5386): p. 95-98.
31. Lu, K., et al., *Mechanical damage of carbon nanotubes by ultrasound*. Carbon, 1996. **34**(6): p. 814-816.
32. Hirsch, A., *Functionalization of single-walled carbon nanotubes*. Angewandte Chemie International Edition, 2002. **41**(11): p. 1853-1859.
33. Bahr, J.L. and J.M. Tour, *Covalent chemistry of single-wall carbon nanotubes*. Journal of Materials Chemistry, 2002. **12**(7): p. 1952-1958.
34. Sun, Y.-P., et al., *Functionalized carbon nanotubes: properties and applications*. Accounts of chemical research, 2002. **35**(12): p. 1096-1104.
35. Banerjee, S., M.G. Kahn, and S.S. Wong, *Rational chemical strategies for carbon nanotube functionalization*. Chemistry-A European Journal, 2003. **9**(9): p. 1898-1908.
36. Khan, M.U., et al., *Polymer brush synthesis on surface modified carbon nanotubes via in situ emulsion polymerization*. Colloid and Polymer Science, 2016. **294**(10): p. 1599-1610.
37. Yue, L., et al., *Epoxy composites with carbon nanotubes and graphene nanoplatelets—Dispersion and synergy effects*. Carbon, 2014. **78**: p. 268-278.
38. Mohamed, A., et al., *Enhanced dispersion of multiwall carbon nanotubes in natural rubber latex nanocomposites by surfactants bearing phenyl groups*. Journal of colloid and interface science, 2015. **455**: p. 179-187.

39. Shokrieh, M., A. Saeedi, and M. Chitsazzadeh, *Evaluating the effects of multi-walled carbon nanotubes on the mechanical properties of chopped strand mat/polyester composites*. *Materials & Design*, 2014. **56**: p. 274-279.
40. Grossiord, N., J. Loos, and C.E. Koning, *Strategies for dispersing carbon nanotubes in highly viscous polymers*. *Journal of Materials Chemistry*, 2005. **15**(24): p. 2349-2352.
41. Ounaies, Z., et al., *Electrical properties of single wall carbon nanotube reinforced polyimide composites*. *Composites Science and Technology*, 2003. **63**(11): p. 1637-1646.
42. McLachlan, D.S., et al., *AC and DC percolative conductivity of single wall carbon nanotube polymer composites*. *Journal of Polymer Science Part B: Polymer Physics*, 2005. **43**(22): p. 3273-3287.
43. Ramasubramaniam, R., J. Chen, and H. Liu, *Homogeneous carbon nanotube/polymer composites for electrical applications*. *Applied Physics Letters*, 2003. **83**(14): p. 2928-2930.
44. Richard, C., et al., *Supramolecular self-assembly of lipid derivatives on carbon nanotubes*. *Science*, 2003. **300**(5620): p. 775-778.
45. Samanta, S.K., et al., *Conjugated polymer-assisted dispersion of single-wall carbon nanotubes: the power of polymer wrapping*. *Accounts of chemical research*, 2014. **47**(8): p. 2446-2456.
46. Gilman, J.W., et al., *A Comparison of Quality of Dispersion of Single Wall Carbon Nanotubes Using Different Surfactants and Biomolecules*. NIST Interagency/Internal Report (NISTIR)-, 2017.
47. Ferguson, G.A. and J. Nielsen, *Optimizing the Dispersion of Single-Walled Carbon Nanotubes in Sodium Dodecylbenzene Sulfonate*. 2017.
48. Tavakolifard, S. and E. Biazar, *Modification of carbon nanotubes as an effective solution for cancer therapy*. *Nano Biomed. Eng*, 2016. **8**(3): p. 144-160.
49. Hirlekar, R., et al., *Carbon nanotubes and its applications: a review*. *Asian Journal of Pharmaceutical and Clinical Research*, 2009. **2**(4): p. 17-27.
50. Singh, B., et al., *Carbon nanotubes. A novel drug delivery system*. *International Journal of Research in Pharmacy and Chemistry*, 2012. **2**(2): p. 523-532.
51. Usui, Y., et al., *Carbon nanotubes innovate on medical technology*. *Medicinal Chemistry*, 2012. **2**(1): p. 1-6.

52. Zhang, Y., Y. Bai, and B. Yan, *Functionalized carbon nanotubes for potential medicinal applications*. Drug discovery today, 2010. **15**(11): p. 428-435.
 53. He, H., et al., *Carbon nanotubes: applications in pharmacy and medicine*. BioMed research international, 2013. **2013**.
 54. Kateb, B., et al., *Multi-walled carbon nanotube (MWCNT) synthesis, preparation, labeling, and functionalization*. Immunotherapy of Cancer: Methods and Protocols, 2010: p. 307-317.
 55. Zhang, W., Z. Zhang, and Y. Zhang, *The application of carbon nanotubes in target drug delivery systems for cancer therapies*. Nanoscale research letters, 2011. **6**(1): p. 555.
 56. Bekyarova, E., et al., *Applications of carbon nanotubes in biotechnology and biomedicine*. Journal of biomedical nanotechnology, 2005. **1**(1): p. 3-17.
 57. Liu, Z., et al., *Supramolecular chemistry on water-soluble carbon nanotubes for drug loading and delivery*. ACS nano, 2007. **1**(1): p. 50-56.
 58. Liu, Z., et al., *Preparation of carbon nanotube bioconjugates for biomedical applications*. Nature protocols, 2009. **4**(9): p. 1372-1381.
 59. Ross, J.S. and J.A. Fletcher, *The HER-2/neu Oncogene in Breast Cancer: Prognostic Factor, Predictive Factor, and Target for Therapy*. Stem cells, 1998. **16**(6): p. 413-428.
 60. Welsher, K., et al., *Selective probing and imaging of cells with single walled carbon nanotubes as near-infrared fluorescent molecules*. Nano letters, 2008. **8**(2): p. 586-590.
 61. Liu, Z., et al., *Multiplexed multicolor Raman imaging of live cells with isotopically modified single walled carbon nanotubes*. Journal of the American Chemical Society, 2008. **130**(41): p. 13540-13541.
 62. Anderson, J., et al., *Potent suppression of HIV type 1 infection by a short hairpin anti-CXCR4 siRNA*. AIDS research and human retroviruses, 2003. **19**(8): p. 699-706.
 63. Liu, Z., et al., *siRNA delivery into human T cells and primary cells with carbon-nanotube transporters*. Angewandte Chemie International Edition, 2007. **46**(12): p. 2023-2027.
 64. Kam, N.W.S., Z. Liu, and H. Dai, *Functionalization of carbon nanotubes via cleavable disulfide bonds for efficient intracellular delivery of siRNA and potent gene silencing*. Journal of the American Chemical Society, 2005. **127**(36): p. 12492-12493.
 65. Ziegler, K.J., et al., *Controlled oxidative cutting of single-walled carbon nanotubes*. Journal of the American Chemical Society, 2005. **127**(5): p. 1541-1547.
-

66. Asuri, P., et al., *Structure, function, and stability of enzymes covalently attached to single-walled carbon nanotubes*. Langmuir, 2007. **23**(24): p. 12318-12321.
67. Cuatrecasas, P. and I. Parikh, *Adsorbents for affinity chromatography. Use of N-hydroxysuccinimide esters of agarose*. Biochemistry, 1972. **11**(12): p. 2291-2299.
68. Lomant, A.J. and G. Fairbanks, *Chemical probes of extended biological structures: synthesis and properties of the cleavable protein cross-linking reagent [35S] dithiobis (succinimidyl propionate)*. Journal of molecular biology, 1976. **104**(1): p. 243-261.
69. Staros, J.V., R.W. Wright, and D.M. Swingle, *Enhancement by N-hydroxysulfosuccinimide of water-soluble carbodiimide-mediated coupling reactions*. Analytical biochemistry, 1986. **156**(1): p. 220-222.
70. Grabarek, Z. and J. Gergely, *Zero-length crosslinking procedure with the use of active esters*. Analytical biochemistry, 1990. **185**(1): p. 131-135.
71. Wang, Y., et al., *Anomalously fast diffusion of targeted carbon nanotubes in cellular spheroids*. ACS nano, 2015. **9**(8): p. 8231-8238.
72. Harrison, B.S. and A. Atala, *Carbon nanotube applications for tissue engineering*. Biomaterials, 2007. **28**(2): p. 344-353.
73. Bianco, A., K. Kostarelos, and M. Prato, *Applications of carbon nanotubes in drug delivery*. Current opinion in chemical biology, 2005. **9**(6): p. 674-679.
74. Misra, R., S. Acharya, and S.K. Sahoo, *Cancer nanotechnology: application of nanotechnology in cancer therapy*. Drug Discovery Today, 2010. **15**(19): p. 842-850.
75. Boyer, P.D., et al., *Delivering Single-Walled Carbon Nanotubes to the Nucleus Using Engineered Nuclear Protein Domains*. ACS applied materials & interfaces, 2016. **8**(5): p. 3524-3534.
76. Muthu, M.S., et al., *Nanotheranostics- application and further development of nanomedicine strategies for advanced theranostics*. Theranostics, 2014. **4**(6): p. 660.
77. Duncan, R. and S.C. Richardson, *Endocytosis and intracellular trafficking as gateways for nanomedicine delivery: opportunities and challenges*. Molecular pharmaceutics, 2012. **9**(9): p. 2380-2402.
78. Ge, C., et al., *Binding of blood proteins to carbon nanotubes reduces cytotoxicity*. Proceedings of the National Academy of Sciences, 2011. **108**(41): p. 16968-16973.
79. Alshehri, R., et al., *Carbon Nanotubes in Biomedical Applications: Factors, Mechanisms, and Remedies of Toxicity: Miniperspective*. Journal of medicinal chemistry, 2016. **59**(18): p. 8149-8167.

80. Lu, A.H., E.e.L. Salabas, and F. Schüth, *Magnetic nanoparticles: synthesis, protection, functionalization, and application*. Angewandte Chemie International Edition, 2007. **46**(8): p. 1222-1244.
81. Ananta, J.S., et al., *Single-walled carbon nanotube materials as T 2-weighted MRI contrast agents*. The Journal of Physical Chemistry C, 2009. **113**(45): p. 19369-19372.
82. Yang, Z., et al., *Carbon nanotubes bridged with graphene nanoribbons and their use in high-efficiency dye-sensitized solar cells*. Angewandte Chemie International Edition, 2013. **52**(14): p. 3996-3999.
83. Li, G.r., et al., *Carbon Nanotubes with Titanium Nitride as a Low-Cost Counter-Electrode Material for Dye-Sensitized Solar Cells*. Angewandte Chemie International Edition, 2010. **49**(21): p. 3653-3656.
84. Humers, W. and R. Offeman, *Preparation of graphitic oxide [J]*. J Am Chem Soc, 1958. **80**(6): p. 1339.
85. Kim, H.W., et al., *Selective Gas Transport Through Few-Layered Graphene and Graphene Oxide Membranes*. Science, 2013. **342**(6154): p. 91-95.
86. Zhu, Y., et al., *Graphene and graphene oxide: synthesis, properties, and applications*. Advanced materials, 2010. **22**(35): p. 3906-3924.
87. Liu, Y., et al., *Biocompatible graphene oxide-based glucose biosensors*. Langmuir, 2010. **26**(9): p. 6158-6160.
88. Nakajima, T., A. Mabuchi, and R. Hagiwara, *A new structure model of graphite oxide*. Carbon, 1988. **26**(3): p. 357-361.
89. Dreyer, D.R., et al., *The chemistry of graphene oxide*. Chemical Society Reviews, 2010. **39**(1): p. 228-240.
90. Titelman, G., et al., *Characteristics and microstructure of aqueous colloidal dispersions of graphite oxide*. Carbon, 2005. **43**(3): p. 641-649.
91. Sydlik, S.A., et al., *In vivo compatibility of graphene oxide with differing oxidation states*. ACS nano, 2015. **9**(4): p. 3866-3874.
92. Park, S. and R.S. Ruoff, *Chemical methods for the production of graphenes*. Nature nanotechnology, 2009. **4**(4): p. 217-224.
93. Compton, O.C. and S.T. Nguyen, *Graphene oxide, highly reduced graphene oxide, and graphene: versatile building blocks for carbon-based materials*. small, 2010. **6**(6): p. 711-723.

94. Ontiveros-Ortega, A., et al., *Effect of tannic acid on the surface free energy of polyester dyed with a cationic dye*. Journal of colloid and interface science, 1998. **199**(1): p. 99-104.
 95. Ariga, K., et al., *Forming nanomaterials as layered functional structures toward materials nanoarchitectonics*. NPG Asia Materials, 2012. **4**(5): p. e17.
 96. Lin, D. and B. Xing, *Tannic acid adsorption and its role for stabilizing carbon nanotube suspensions*. Environmental science & technology, 2008. **42**(16): p. 5917-5923.
 97. Wang, H., et al., *Graphene oxide-peptide conjugate as an intracellular protease sensor for caspase-3 activation imaging in live cells*. Angewandte Chemie International Edition, 2011. **50**(31): p. 7065-7069.
 98. Tang, X.-Z., et al., *Synthesis of graphene decorated with silver nanoparticles by simultaneous reduction of graphene oxide and silver ions with glucose*. Carbon, 2013. **59**: p. 93-99.
 99. Zhang, L., et al., *Functional graphene oxide as a nanocarrier for controlled loading and targeted delivery of mixed anticancer drugs*. Small, 2010. **6**(4): p. 537-544.
 100. Hu, W., et al., *Graphene-based antibacterial paper*. ACS nano, 2010. **4**(7): p. 4317-4323.
 101. Liu, J., et al., *Toward a universal "adhesive nanosheet" for the assembly of multiple nanoparticles based on a protein-induced reduction/decoration of graphene oxide*. Journal of the American Chemical Society, 2010. **132**(21): p. 7279-7281.
 102. Hung, A.H., et al., *Graphene oxide enhances cellular delivery of hydrophilic small molecules by co-incubation*. ACS nano, 2014. **8**(10): p. 10168-10177.
 103. Sun, X., et al., *Nano-graphene oxide for cellular imaging and drug delivery*. Nano research, 2008. **1**(3): p. 203-212.
 104. Tu, Y., et al., *Destructive extraction of phospholipids from Escherichia coli membranes by graphene nanosheets*. Nature nanotechnology, 2013. **8**(8): p. 594-601.
 105. Akhavan, O. and E. Ghaderi, *Toxicity of graphene and graphene oxide nanowalls against bacteria*. ACS nano, 2010. **4**(10): p. 5731-5736.
 106. Dreyer, D.R., R.S. Ruoff, and C.W. Bielawski, *From conception to realization: an historical account of graphene and some perspectives for its future*. Angewandte Chemie International Edition, 2010. **49**(49): p. 9336-9344.
 107. Chung, C., et al., *Biomedical applications of graphene and graphene oxide*. Accounts of chemical research, 2013. **46**(10): p. 2211-2224.
-

108. Gómez-Navarro, C., et al., *Electronic transport properties of individual chemically reduced graphene oxide sheets*. Nano letters, 2007. **7**(11): p. 3499-3503.
 109. Bernhardson, B.-M., C. Tishelman, and L.E. Rutqvist, *Chemosensory changes experienced by patients undergoing cancer chemotherapy: a qualitative interview study*. Journal of pain and symptom management, 2007. **34**(4): p. 403-412.
 110. Brigger, I., C. Dubernet, and P. Couvreur, *Nanoparticles in cancer therapy and diagnosis*. Advanced drug delivery reviews, 2002. **54**(5): p. 631-651.
 111. Sinha, R., et al., *Nanotechnology in cancer therapeutics: bioconjugated nanoparticles for drug delivery*. Molecular cancer therapeutics, 2006. **5**(8): p. 1909-1917.
 112. Stuart, M.A., et al., *Emerging applications of stimuli-responsive polymer materials*. Nat Mater, 2010. **9**(2): p. 101-13.
 113. de Las Heras Alarcon, C., S. Pennadam, and C. Alexander, *Stimuli responsive polymers for biomedical applications*. Chem Soc Rev, 2005. **34**(3): p. 276-85.
 114. Hoffman, A.S., *Stimuli-responsive polymers: biomedical applications and challenges for clinical translation*. Adv Drug Deliv Rev, 2013. **65**(1): p. 10-6.
 115. Talelli, M. and W.E. Hennink, *Thermosensitive polymeric micelles for targeted drug delivery*. Nanomedicine, 2011. **6**(7): p. 1245-1255.
 116. Yang, M., et al., *Novel thermosensitive polymeric micelles for docetaxel delivery*. Journal of Biomedical Materials Research Part A, 2007. **81**(4): p. 847-857.
 117. Roy, D., W.L.A. Brooks, and B.S. Sumerlin, *New directions in thermoresponsive polymers*. Chem Soc Rev, 2013. **42**(17): p. 7214-7243.
 118. Zhang, Q.L., et al., *Thermoresponsive polymers with lower critical solution temperature: from fundamental aspects and measuring techniques to recommended turbidimetry conditions*. Materials Horizons, 2017. **4**(2): p. 109-116.
 119. Gibson, M.I. and R.K. O'Reilly, *To aggregate, or not to aggregate? considerations in the design and application of polymeric thermally-responsive nanoparticles*. Chem Soc Rev, 2013. **42**(17): p. 7204-13.
 120. Gibson, M.I., D. Paripovic, and H.A. Klok, *Size-dependent LCST transitions of polymer-coated gold nanoparticles: cooperative aggregation and surface assembly*. Adv Mater, 2010. **22**(42): p. 4721-5.
 121. Zhang, Q.L., et al., *Acid-Labile Thermoresponsive Copolymers That Combine Fast pH-Triggered Hydrolysis and High Stability under Neutral Conditions*. Angewandte Chemie-International Edition, 2015. **54**(37): p. 10879-10883.
-

122. Aseyev, V., H. Tenhu, and F.M. Winnik, *Non-ionic Thermoresponsive Polymers in Water*. Self Organized Nanostructures of Amphiphilic Block Copolymers II, 2011. **242**: p. 29-89.
123. Zhang, Q.L. and R. Hoogenboom, *Polymers with upper critical solution temperature behavior in alcohol/water solvent mixtures*. Progress in Polymer Science, 2015. **48**: p. 122-142.
124. Li, W., et al., *Antitumor drug delivery modulated by a polymeric micelle with an upper critical solution temperature*. Angew Chem Int Ed Engl, 2015. **54**(10): p. 3126-31.
125. Seuring, J. and S. Agarwal, *Polymers with Upper Critical Solution Temperature in Aqueous Solution: Unexpected Properties from Known Building Blocks*. ACS Macro Letters, 2013. **2**(7): p. 597-600.
126. Coelho, J.F., et al., *Drug delivery systems: Advanced technologies potentially applicable in personalized treatments*. EPMA journal, 2010. **1**(1): p. 164-209.
127. Gupta, A., B. Mohanty, and H.B. Bohidar, *Flory temperature and upper critical solution temperature of gelatin solutions*. Biomacromolecules, 2005. **6**(3): p. 1623-1627.
128. Wolf, T., et al., *Reversible Self-Assembly of Degradable Polymersomes with Upper Critical Solution Temperature in Water*. Journal of the American Chemical Society, 2017. **139**(32): p. 11064-11072.
129. Zhang, Z., et al., *Influenza-binding sialylated polymer coated gold nanoparticles prepared via RAFT polymerization and reductive amination*. Chemical Communications, 2016. **52**(16): p. 3352-3355.
130. Scales, C.W., et al., *Corona-stabilized interpolyelectrolyte complexes of siRNA with nonimmunogenic, hydrophilic/cationic block copolymers prepared by aqueous RAFT polymerization*. Macromolecules, 2006. **39**(20): p. 6871-6881.
131. Kasmi, S., et al., *Transiently Responsive Block Copolymer Micelles Based on N-(2-Hydroxypropyl)methacrylamide Engineered with Hydrolyzable Ethylcarbonate Side Chains*. Biomacromolecules, 2016. **17**(1): p. 119-27.
132. Liu, Q., et al., *Strong Two-Photon-Induced Fluorescence from Photostable, Biocompatible Nitrogen-Doped Graphene Quantum Dots for Cellular and Deep-Tissue Imaging*. Nano Letters, 2013. **13**(6): p. 2436-2441.
133. Matousek, P., *Deep non-invasive Raman spectroscopy of living tissue and powders*. Chem Soc Rev, 2007. **36**(8): p. 1292-1304.

134. Zhang, Z., et al., *Near infrared laser-induced targeted cancer therapy using thermoresponsive polymer encapsulated gold nanorods*. Journal of the American Chemical Society, 2014. **136**(20): p. 7317-7326.
135. Guerrero, A.R., et al., *Gold nanoparticles for photothermally controlled drug release*. Nanomedicine, 2014. **9**(13): p. 2023-2039.
136. Kim, D., et al., *Antibiofouling polymer-coated gold nanoparticles as a contrast agent for in vivo X-ray computed tomography imaging*. Journal of the American Chemical Society, 2007. **129**(24): p. 7661-7665.

Summary and General Conclusions

This PhD dissertation explores potential biomedical applications of three different high-aspect ratio nanomaterials in three chapters, which are summarized below.

In **Part I**, a general introduction was provided to discuss the importance of materials science to our lives, especially regarding biomedical applications of high-aspect ratio nanomaterials such as carbon-derived multi-dimensional nanomaterials (zero-dimensional fullerene; one-dimensional carbon nanotubes; two-dimensional graphene and graphene oxide nanosheets; three-dimensional graphite and diamond) and polymer-functionalized inorganic metal nanoparticles, i.e. gold-nanorods.

In **Part II** and **Part III**, three experimental chapters were presented. Structure, size, charge, shape and surface chemistry play key roles with respect to the bioactivity of nanomaterials.

Carbon nanotubes (CNTs) are hydrophobic and trend to aggregate in aqueous media due to the high Van der Waals interaction forces along their length axis. Hence, for biomedical applications, CNTs must be functionalized to afford water solubility and biocompatibility. Furthermore, an ideal functional CNT should exhibit minimal damage of nanotube structure and have availability of functional groups for further bio-conjugation.

In **Chapter 1**, three different batches of carboxylic acid functionalized carbon nanotubes from different commercial sources were chosen, with different diameters, length and number of walls. Ultra-sonication and tannic acid were used to render these CNTs dispersible in water. It

was found that tannic acid could efficiently stabilize CNTs, even in absence of sonication. ATR-FTIR proved that all of these CNTs had been covered by tannic acid.

Next, we investigated the protein coupling ability of these CNT-TA and found that all of them could successfully spontaneously adsorb the model proteins, i.e. BSA and OVA.

The aim of **Chapter 2** was to investigate the potential of graphene oxide (GOx) nanosheets for intracellular delivery of proteins. GOx nanosheets were prepared by a modified Hummers' method, and ATR-FTIR and AFM gave further proof of successful formation of monomolecular layered GOx nanosheets which were highly transparent and combined high-aspect ratio dimension (sheet-like structures) with hydrophilic functional groups such as epoxide, hydroxyl and carboxylic acids.

Contrary to several other linker strategies which were reported to bind therapeutic molecules to GOx, we aimed in **Chapter 2** to elucidate a facile method to formulate vaccine antigens with GOx without the requirement of additional reagents. Confirmed by ATR-FTIR, SDS-PAGE and fluorescence spectroscopy and microscopy, we observed that GOx nanosheets can be spontaneously coupled to proteins which were used as model protein antigens without the need for introducing specific linker strategies. When bound to GOx, we further investigated the interaction between protein (i.e. OVA) loaded GOx and dendritic cells *in vitro*. The obtained GOx~OVA could still be internalized by dendritic cells and promote antigen cross-presentation to CD8 T cells. The latter is a hallmark in the induction of potent cellular antigen-specific immune responses against intracellular pathogens and cancer.

Apart from the carbon-derived multi-dimensional nanomaterials, in **Chapter 3**, we also elaborated on another type of high-aspect ratio nanomaterials, i.e. gold nanorods (AuNRs) as an external trigger in combination with a polymer that exhibits upper critical solution temperature (UCST) behaviour. In particular we were interested in developing a transiently thermoresponsive UCST polymer. Such polymer should exhibit a soluble-insoluble switch in response to temperature, but gradually lose this property in response to a hydrolysis reaction in the polymer backbone or side-chain. In **Chapter 3**, we developed a fully synthetic approach to obtain a biodegradable transiently thermoresponsive homo-polymer, i.e.

poly(HPMA–glycolamide), which possesses upper critical solution temperature (UCST) behaviour in aqueous medium.

Hereto we have chosen a well-established biocompatible polymer poly(N-(2-hydroxypropyl)methacrylamide) as a polymeric scaffold and modified the hydroxyl-position with glycolamide through a degradable carbonate ester linkage, thereby yielding HPMA-GA. Polymerization of HPMA-GA by reversible addition-fragmentation chain transfer (RAFT) polymerization resulted in a polymer with an UCST at 42° C, and that could be repeatedly cycled when alternately raising/lowering the temperature. Furthermore, at a physiological pH, when the temperature is maintained at the physiological values of 37 °C, the polymer undergoes a globule-to-coil transition upon hydrolytic cleavage of the carbonate ester moieties in the polymer backbone.

AuNRs stabilized by CTAB were prepared via a one-step seedless method and transferred to the aqueous phase by extensive dialysis. Owing to their high-aspect ratio, these AuNRs have two plasmonic peaks, i.e. at 510 nm and 806 nm. These AuNRs can convert NIR light into thermal energy. Hence, mixed AuNRs with poly(HPMA-GA) in aqueous medium buffered at a pH of 7.4 and followed by NIR laser irradiation (808nm, 380mW) could accelerate the hydrolysis of poly(HPMA-GA). In other words, a much faster hydrolysis of poly(HPMA-GA) could be triggered in presence of AuNRs and NIR laser irradiation within a physiologically relevant window in terms of temperature and pH.

Samenvatting en Algemene Conclusies

Dit proefschrift handelt over potentiële biomedische toepassingen van drie verschillende *high aspect ratio* nanomaterialen in drie hoofdstukken, die hieronder worden samengevat.

In Deel I werd een algemene inleiding gegeven om het belang van materiaalwetenschap m.b.t. ons dagelijkse leven te bespreken. Hierbij werd voornamelijk de focus gelegd op biomedische toepassingen van nanomaterialen met *high aspect ratio* zoals van koolstof afgeleide nanomaterialen (fullerenen, zero-dimensie, *carbon nanotube*, één -dimensie; *graphene* en *graphene oxide*, tweedimensionaal; grafiet, driedimensionaal) en polymeer-gefunctionaliseerde anorganische metaalnanodeeltjes, dwz *gold nanorods*.

In Deel II and Deel III werden drie experimentele hoofdstukken gepresenteerd. Structuur, grootte, lading, vorm en oppervlaktechemie spelen een sleutelrol m.b.t. de bioactiviteit van nanomaterialen.

Carbon nanotubes (CNTs) zijn hydrofoob en aggregeren makkelijk in waterige media als gevolg van de sterke Van der Waals interactiekrachten langs hun lengteas. Vandaar dat voor biomedische toepassingen CNT's moeten worden gefunctionaliseerd om wateroplosbaarheid en biocompatibiliteit te verschaffen. Verder zou een ideale functionele CNT minimale schade aan de CNT-structuur moeten vertonen en over voldoende functionele groepen moeten beschikken voor verdere bio-conjugatie.

In Hoofdstuk I werden drie verschillende batches CNT's van verschillende commerciële bronnen gekozen, met verschillende diameter, lengte en aantal *walls*. Ultra-sonicatie en tanninezuur werden gebruikt om deze CNT's dispergeerbaar in water te maken. Er werd

gevonden dat tanninezuur efficiënt CTN kon stabiliseren, zelfs in afwezigheid van sonicatie. ATR-FTIR bewees dat al deze CNT's waren bedekt met tanninezuur.

Vervolgens onderzochten we het eiwitkoppelingsvermogen van deze CNT-TA en ontdekten dat al deze CNT-TA spontaan de modelproteïnen BSA en OVA konden binden.

Het doel van **Hoofdstuk 2** was om het potentieel van *graphane oxide* (GOx) *nanosheets* voor intracellulaire levering van eiwitten te onderzoeken. GOx *nanosheets* werden bereid volgens een gemodificeerde Hummers-methode en ATR-FTIR en AFM gaven verder bewijs van succesvolle vorming van monomoleculaire gelaagde GOx *nanosheets* die een transparante oplossing in water gecombineerden met een *high aspect ratio* en met hydrofiele functionele groepen zoals epoxide, hydroxyl en carbonzuren.

In tegenstelling tot verschillende andere linker-strategieën waarvan gerapporteerd werd dat ze therapeutische moleculen binden aan GOx, hebben we in **Hoofdstuk 2** getracht een eenvoudige methode te ontwikkelen om vaccinantigenen met GOx *nanosheets* te formuleren zonder de behoefte aan extra reagentia. Bevestigd door ATR-FTIR, SDS-PAGE en fluorescentiespectroscopie en microscopie, hebben we waargenomen dat GOx *nanosheets* spontaan kunnen eiwitten kunnen adsorberen. Wanneer gebonden aan GOx *nanosheets*, onderzochten we verder de interactie tussen eiwit (nl. OVA) geladen GOx en dendritische cellen *in vitro*. De verkregen GOx:OVA kan nog steeds worden geïnternaliseerd door dendritische cellen en *antigen cross-presentation* aan CD8 T-cellen bevorderen. Het laatste is een kenmerk van de inductie van krachtige cellulaire antigeen-specifieke immuunresponsen tegen intracellulaire pathogenen en kanker.

Afgezien van koolstof-afgeleide multidimensionele nanomaterialen, hebben we in **Hoofdstuk 3** ook met een ander type nanomaterialen met een *high aspect ratio*, namelijk *gold nanorods* als een externe trigger in combinatie met een polymeer dat *upper critical solution temperature* (UCST) gedrag vertont. In het bijzonder waren we geïnteresseerd in het ontwikkelen van een *transiently thermoresponsive* UCST-polymeer. Een dergelijk polymeer zou een *soluble-insoluble switch* moeten vertonen als reactie op temperatuur, maar geleidelijk aan deze eigenschap verliezen ten gevolgd van een hydrolysereactie in het polymeer *backbone* of in de polymeer zijketen. In **Hoofdstuk 3** hebben we een volledig

synthetische benadering ontwikkeld om een bio-degradeerbaar *transiently thermoresponsive* UCST-homopolymeer te synthetiseren, nl. poly (HPMA-glycolamide).

Hiertoe hebben we een geked biocompatibel polymeer, nl. poly(N-(2-hydroxypropyl) methacrylamide) als een *scaffold* gekozen en de hydroxyl-positie te modificeren met glycolamide d.m.v. een afbreekbare carbonaatester verbinding, waardoor HPMA-GA werd verkregen. Polymerisatie van HPMA-GA door *reversible addition-fragmentation chain transfer* (RAFT) polymerisatie resulteerde in een polymeer met een UCST van 42 °C. Verder ondergaat, bij een fysiologische pH, wanneer de temperatuur wordt gehandhaafd op de fysiologische waarde van 37 °C, het polymeer een overgang van *soluble-to-coil* ten gevolge van hydrolyse van de carbonaatester groepen in de polymeer zijketen.

Gold nanorods gestabiliseerd door CTAB werden bereid via een *one-step seedless* methode en overgebracht naar de waterige fase d.m.v. dialyse. Vanwege hun *high aspect ratio* hebben deze *gold nanorods* twee plasmonische pieken, nl. bij 510 nm en 806 nm. Deze AuNR's kunnen NIR-licht omzetten in thermische energie. Daarom konden AuNR's gemengd met poly(HPMA-GA) in waterig medium gebufferd bij een pH van 7.4 en in combinatie met NIR laserbestraling de hydrolyse van poly(HPMA-GA) versnellen. Met andere woorden, een veel snellere hydrolyse van poly (HPMA-GA) kon worden verkregen in aanwezigheid van AuNR's en NIR laserbestraling binnen een fysiologisch relevant venster in termen van temperatuur en pH.

Curriculum Vitae

PERSONALIA

Name	LI
First Name	Hui
Gender	Female
Citizenship	P.R. China
Date of birth	8 th , June, 1987
Place of birth	Nei Mongol, P.R. China
Address	Laboratory of Pharmaceutical Technology, Department of Pharmaceutics, Ghent University, Ottergemsesteenweg 460, B-9000, Ghent, Belgium
E-mail	lihui0476@hotmail.com
Telephone	0032 486 25 89 48

EDUCATIONS

2018	Faculty of Pharmaceutical Science, Ghent University, Belgium PhD in Pharmaceutical Science
Thesis	High-Aspect-Ratio Nano-Materials For Biomedical Applications
2013	Pharmacy of Chinese Materia Medica, School of Pharmaceutical Sciences, Shandong University of Traditional Chinese Medicine Master in Medicine
Thesis	Comparative study of targeting HCS liposomes and nanoparticles
2009	School of Marine, Shandong University, P.R. China Bachelor in Science

PUBLICATIONS

1. **Hui Li**, Kaat Fierens, Zhiyue Zhang, Nane Vanparijs, et al., Bruno G. De Geest*. Spontaneous protein adsorption on graphene oxide nanosheets allowing efficient intracellular vaccine protein delivery. *ACS applied materials & interfaces*, 2016. 8(2): p. 1147-1155. (IF₂₀₁₆: 7.504)
2. Yang Shi, Xiuli Bi, **Hui Li**, Guihua Huang*. Study on the tissue distribution of joint that articular cavity injection of Ligustrazine PLGA microspheres. *Journal of Shandong University*, 2010, 48(1), 154-158
3. Zhiyue Zhang, Xiuli Bi, **Hui Li**, Guihua Huang*. Enhanced targeting efficiency of PLGA microspheres loaded with Lornoxicam for intra-articular administration. *Drug Delivery*, 2011, 18(7): 536-544. (IF₂₀₁₆: 6.4019)
4. **Hui Li**, Zhiyue Zhang, Ping Sun*. Solid lipid nanoparticles (SLN) research progress of parcel of cytotoxic chemotherapy. *China Pharmacy*, 2013(09)

ATTENDED CONFERENCES

1. **Hui Li**, Selective a suitable targeting dosage form of HCS from liposomes and nanoparticles.
Biopharmacy Day 2013, December 18, 2013. Ghent, Belgium, Poster.
2. **13th European Symposium on Controlled Drug Delivery**, April 16-18, 2014. Egmond Aan Zee, The Netherlands.
3. **Biopharmacy Day 2014**, December 12, 2014. Unilever R&D Vlaardingen, Netherlands,
4. **Hui Li**, Zhiyue Zhang, Bruno G. De Geest. Protein Spontaneously Adsorbed On Graphene Oxide Nanosheets For Intracellular Vaccine Protein Delivery.
249th ACS National Meeting& Exposition, March 22-26, 2015. Denver CO, USA, Oral presentation.
5. **Biopharmacy Day 2015**, November 23, 2015. Leuven, Belgium.
6. **Biopharmacy Day 2017**, December 08, 2017. Brussels, Belgium.

AWARDS

1. Chinese Scholarship Council for the PhD scholarship
2. Ghent University for BOF co-funding

